



**HAL**  
open science

## Current status and challenges of plasma and plasma-catalysis for methane coupling: A review

Valeriia Maslova, Raluca Nastase, Gleb Veryasov, Nikolai Nesterenko, Elodie Fourré, Catherine Batiot-Dupeyrat

### ► To cite this version:

Valeriia Maslova, Raluca Nastase, Gleb Veryasov, Nikolai Nesterenko, Elodie Fourré, et al.. Current status and challenges of plasma and plasma-catalysis for methane coupling: A review. *Progress in Energy and Combustion Science*, 2024, 101 (4), pp.101096. 10.1016/j.pecs.2023.101096 . hal-04426383

**HAL Id: hal-04426383**

**<https://hal.science/hal-04426383v1>**

Submitted on 18 Jul 2024

**HAL** is a multi-disciplinary open access archive for the deposit and dissemination of scientific research documents, whether they are published or not. The documents may come from teaching and research institutions in France or abroad, or from public or private research centers.

L'archive ouverte pluridisciplinaire **HAL**, est destinée au dépôt et à la diffusion de documents scientifiques de niveau recherche, publiés ou non, émanant des établissements d'enseignement et de recherche français ou étrangers, des laboratoires publics ou privés.

# **Current status and challenges of Plasma and Plasma-catalysis for methane coupling: A review**

*Valeriia Maslova<sup>1</sup>, Raluca Nastase<sup>1</sup>, Gleb Veryasov<sup>2</sup>, Nikolai Nesterenko<sup>2</sup>, Elodie Fourré<sup>1\*</sup>,  
Catherine Batiot-Dupeyrat<sup>1\*</sup>*

<sup>1</sup>Université de Poitiers, UMR CNRS 7285 – IC2MP, ENSIP- bat B1, 1 rue Marcel Doré, TSA41105, 86073 Poitiers Cedex 9, France

<sup>2</sup>TotalEnergies One Tech Belgium, Zone Industrielle Feluy C, 7181, Seneffe, Belgium

*\*[elodie.fourre@univ-poitiers.fr](mailto:elodie.fourre@univ-poitiers.fr) ; [catherine.batiot.dupeyrat@univ-poitiers.fr](mailto:catherine.batiot.dupeyrat@univ-poitiers.fr)*

Abstract:

Non-thermal plasma appears as a promising alternative technology to develop the electrification of the petrochemical industry. Non-thermal plasma has the advantage of operating at atmospheric pressure and room temperature in "on/off" mode. The high-energy electrons generated are able to activate many reactants allowing thermodynamically unfavorable reactions to occur. Methane coupling is particularly important to produce C<sub>2</sub> hydrocarbons, especially ethylene known as a platform chemical for the synthesis of many products. In this review, the state-of-the-art of plasma and plasma-catalysis for methane coupling is described. Focus is given on plasma chemistry and the influence of different parameters related to plasma reactors and gas composition are discussed. The role of a catalyst coupled with plasma is detailed and synergies are explained for various catalytic compositions.

## **List of abbreviations**

bcm: billion cubic meter

NTP : non-thermal plasma

OCM : oxidative coupling of methane

Non-OCM: non-oxidative coupling of methane

Te: electron temperature

Th: heavy particle temperature

DBD: dielectric barrier discharge

DC: direct current voltage

AC: alternative current voltage

IPC: in plasma catalysis

PPC: post plasma catalysis

SEI : Specific Energy Input

RGA : Rotating Gliding Arc

MW: Microwave

GA : gliding arc

SL min<sup>-1</sup>: Standard Liter per minute

IS: internal standard

Td: Townsend

AP: atmospheric pressure

Ca. : circa

i.e. : id est

OES: optical emission spectroscopy

eV: electron Volt

$E_T$ : Threshold Energy

$\epsilon_r$  : dielectric constant

wt% : weight percent

mol. : molar

## Table content

<b>1. Introduction</b> .....	<b>5</b>
<b>2. Plasma-alone for non- and oxidative coupling of methane</b> .....	<b>10</b>
<u>2.1. Plasma-alone for the non-oxidative coupling of methane</u> .....	<u>10</u>
2.1.1. Plasma chemistry.....	10
2.1.2. Influence of the plasma type and reactor geometry .....	15
2.1.3. Influence of the gap.....	19
2.1.4. Influence of the pressure .....	22
2.1.5. Influence of the specific energy input .....	23
2.1.5.1. <i>Effect of the input power</i> .....	23
2.1.5.2 <i>The effect of pulse repetition frequency and pulse duration</i> .....	25
2.1.5.3 <i>The effect of residence time</i> .....	26
2.1.6. Influence of the temperature .....	29
2.1.7. Influence of co-existing gases .....	30
2.1.7.1. <i>The addition of nitrogen</i> .....	30
2.1.7.2. <i>The addition of hydrogen</i> .....	34
2.1.7.3. <i>The addition of noble gases</i> .....	35
<u>2.2. Plasma-alone for the oxidative coupling of methane</u> .....	<u>38</u>
2.2.1. Effect of the oxidant nature: oxygen with methane .....	39
2.2.1.1. <i>Plasma chemistry</i> .....	39
2.2.1.2. <i>Influence of the oxygen-methane ratio</i> .....	42
2.2.2. Effect of the oxidant nature: carbon dioxide and methane.....	44

2.2.2.1. <i>Plasma chemistry</i> .....	44
2.2.2.2. <i>Influence of the specific input energy</i> .....	48
2.2.2.3. <i>Influence of methane/carbon dioxide ratio</i> .....	51
2.2.3. <i>Effect of the oxidant nature: water and methane</i> .....	54
<u>2.3. Comparison of plasma-alone non-oxidative and oxidative methane coupling</u> .....	<u>55</u>
<b>3. Plasma-catalysis for methane coupling</b> .....	<b>61</b>
<u>3.1. Influence of the particle size</u> .....	<u>63</u>
<u>3.2. Influence of the material shape</u> .....	<u>67</u>
<u>3.3. Influence of the dielectric constant</u> .....	<u>68</u>
<u>3.4. Catalysts in the plasma-assisted oxidative coupling of methane</u> .....	<u>71</u>
3.4.1. <i>Effect of alumina-based catalysts</i> .....	72
3.4.1.1. <i>Effect of alumina catalysts</i> .....	72
3.4.1.2. <i>Effect of the metal over alumina</i> .....	77
3.4.1.3. <i>The influence of oxides over alumina support</i> .....	88
3.4.2. <i>Effect of zeolite catalysts</i> .....	88
3.4.2.1. <i>Effect of coupling zeolites with plasma</i> .....	89
3.4.2.2 <i>Effect of coupling metal/zeolite with plasma</i> .....	91
3.4.3. <i>Effect of SBA-15 catalysts</i> .....	94
3.4.4 <i>Effect of other metal oxide</i> .....	96
<u>3.5. Post-plasma catalysts for the oxidative coupling of methane</u> .....	<u>101</u>
<b>4. Compiling plasma alone and plasma-catalysis results</b> .....	<b>102</b>
<b>5. Concluding remarks</b> .....	<b>107</b>
<b>References</b> .....	<b>111</b>

## 1. Introduction

Light olefins are key components in our societies that are in constant demand for chemicals to produce modern consumer goods. The International Energy Agency reported, in 2018, that petrochemical demand will consume an additional 56 billion cubic meters of natural gas by 2030, increasing to 83 bcm by 2050 [1]. Seven primary petrochemicals (ammonia, methanol, ethylene, propylene, benzene, toluene, and xylenes) provide the key building blocks on which most of the chemical industry is based. The global demand for ethylene, one of the target products for the plastic industry, was estimated to be 185 million tons in 2022 [2]. As an alternative process to naphtha steam cracking, the possible production of ethylene from the direct conversion of methane has led to vigorous industrial and academic research. However, the low natural gas price is currently not sufficient to overcome the process's high costs. A recent techno-economic analysis of the oxidative coupling of methane reported that to be competitive, the process must achieve at least 25-30 % C<sub>2</sub> yield to reach an ethylene cost below 1000 €/ton [3]. Considering the foreseen prices of oil and natural gas, combined with the development of efficient technologies for direct methane conversion, the process should become economically viable in around 20 years. In the range of nascent technologies, catalysis coupled to electro, photo and non-thermal plasma methane activation are the most widely investigated to offer reliable alternatives to traditional processes.

The attempts to break the methane C-H bond and lower its activation barrier energy using catalysts have led to the report of promising results. In fact, different catalytic processes involving a direct conversion of methane to C<sub>2</sub>, such as the oxidative coupling [4–9] and the non-oxidative coupling of methane [10–14] have been published in the literature. The thermal catalytic processes result in C<sub>2</sub> yields up to 25 % with low selectivity, mainly due to catalysts' surface contamination by carbon. In the context of high carbon dioxide emissions, the decarbonization of the chemical industry is a subject of great interest and the electrification of the petrochemical industry is at the center of extensive research work. Catalysis coupled to

electro, photo and non-thermal plasma has the advantage of being non-thermal through electrical activation, where the presence of an electric field promotes surface charges and their diffusion [15,16]. Furthermore, the low temperature reduces coke deposition, catalyst deactivation, and favors selectivity to products that would degrade under thermal activation. One advantage of non-thermal plasma resides in its reactivity zone, which is not limited to the contact surface of the electrodes (2D-like process) but is extended to the complete reactor volume as in thermal catalysis (3D-like process). Additionally, plasma can activate gases readily with just an on/off switch and thus can be adapted to time-varying renewable energy production. In this context, C<sub>2</sub> production from methane using non-thermal plasma is investigated as the process could become economically viable with the decrease in electricity prices [17]. Non-thermal plasmas are at non-thermodynamic equilibrium, where electrons can reach an average temperature of 1-10 eV ( $\sim 10^4$ - $10^5$  K) and surrounding gas remains close to ambient. Ionization processes are determined by the electrons' energy and lead to reactive free radicals, metastable and excited state atoms that rapidly undergo several chemical reactions [18,19]. When a high voltage is applied between two electrodes, an intense electric field is generated and the free electrons in the gas are accelerated. They will collide with the surrounding molecules and will give rise to ionization and excitation reactions, creating an electron avalanche, which leads to the propagation of a discharge and the formation of the plasma.

Various plasma processes have been proposed as alternative tools for methane conversion [20,21]. It was suggested that an appropriate design of discharge reactors can modify and improve the selectivity to the desired products. Different types of plasma such as corona [14,22–24], glidarc discharge [25–27], dielectric barrier discharge [28–31], micro DBD [32,33] and microwave plasmas [34,35] were developed. Dielectric barrier discharge is one of the most extensively investigated types of reactor. DBD, also called silent discharges, are generated between two electrodes of various shapes, e.g. planar, cylindrical or tip and are separated by an

insulating material (dielectric barrier) made either of glass, quartz or ceramics. The dielectric allows plasma diffusion in the whole discharge volume by dispersing the micro-filaments over the electrode surface. The dielectric surface charging reduces the field strength in the gap, preventing an arc formation after the breakdown. Various factors will affect the total charge transferred in a discharge, such as the gas properties, the discharge gap and the properties of the dielectric [21,36]. Among the advantages of DBD plasma reactors, scalability and ease of maintaining the non-thermal plasma offer good control of the process [21]. However, the principal disadvantages of DBD are the lack of homogeneity and the high energy cost. Even if, to the eye, it seems that all the gas in the inter-electrode space is ionized, this is not the case in practice. High-speed camera images show that the plasma is made up of very fine streamers (small gas threads). Moreover, the presence of a dielectric requires the use of alternating voltage with relatively high frequencies to avoid surface charging and extinction of the plasma. Any materials subject to alternating current will heat up and a non-negligible part of the injected power will not be used to generate plasma but will be lost upon heating.

Despite the large number of publications in this field, the C<sub>2</sub> yield in the methane coupling in plasma remains low (below 40 %), due to the high electron energy requirements to trigger ionization reactions [21]. Since advances in improving product selectivity are essential, the combination of non-thermal plasma with a catalyst was proposed, as described in “The 2020 plasma catalysis roadmap” [16]. Coupling catalysis to plasma can enhance the process in a manner that cannot be achieved by plasma alone or by catalysis, separately. There are two ways in which plasma and catalyst can be configured: either the catalyst is placed in the plasma discharge (IPC), or in the post-discharge (PPC). Some types of plasma reactors present particular difficulties in incorporating the catalyst directly in the discharge region (e.g. gliding arc).

The dielectric barrier discharge plasma is, once again, one of the most studied systems due to its configuration, facilitating the filling of the volume with catalyst particles. How the catalytic



materials are introduced in the plasma plays an important role in determining the nature of the plasma–catalyst interaction. When the catalyst is placed into the discharge volume, the electrons, ions, radicals and all the other plasma species will activate the catalyst, depending on its chemical nature and electrical properties. In the case of a post-discharge catalyst, only the long-lived species and stable intermediates will reach the catalyst [37]. In the same time, the catalyst in the plasma volume act as a dielectric material, reducing the gap width of the reactor and, consequently, enhancing the electric field strength and electron temperature [38].

The main benefit of combining plasma and a catalyst is the resulting synergistic effect: the whole process's performance is higher than both processes taken separately [37]. This synergistic effect comes with its share of issues as questions remain in assessing the benefits associated with the plasma versus those coming from the catalyst [39]. Moreover, the catalyst is not left unscathed by the plasma impact. Plasma changes the chemical and electronic properties of a surface [39,40]. For example, in the field of catalyst synthesis, non-thermal plasma treatment can enhance the stability and activity of catalysts [41]. Plasma activation can improve nanoparticle dispersion on surfaces, reduce particle sizes and strengthen the metal support interaction. Based on published work, Table 1 briefly summarizes the plasma catalytic interactions at stake in the process.

Table 1: Plasma-Catalyst interactions and synergy [39]

<b>Morphological changes</b>		
<b>Effects of the plasma on the catalyst</b>	Chemical and electronic changes	Change in catalyst work function
		Change in oxidation state
		Reduced coke formation
	Changes in surface process	Modification of the reaction pathways
		Lower activation barriers and higher pre-exponential factors
<b>Effects of the catalyst on the plasma</b>	Enhancement of the electric field	
	Formation of micro discharges in porous catalysts	
	Changes in discharge type	

If these synergistic effects showed improvements in terms of reactant conversion and energy efficiency, the process still suffers from technical issues. Coke formation remains a problem as it deactivates the catalyst and reduces the plasma discharge to its neutralization. In addition, the plasma electric field influences the catalyst surface in terms of surface diffusion. The electron impact alters the surface, which may create defects, thus modifying the catalyst's active phase and lowering its reactivity [21].

The review aims to evaluate the current state of the art in the coupling of methane by plasma alone and plasma-catalysis, with a focus on the effect of the reaction conditions and fixed parameters. The first part is dedicated to sole plasma and is presented in two sections on the non-oxidative and oxidative coupling of methane. The plasma chemistry is first described, followed by the description of the influence of different parameters. The effects of added gases such as N<sub>2</sub>, H<sub>2</sub> and noble gases, as well as the effects of oxidants (oxygen, carbon dioxide and water) on the reaction are reported. In the second part, the coupling of plasma with catalysis is

described with a focus on the chemistry at the surface of the material. The effects of catalyst particle size, shape and dielectric constant are reported.

## 2. Plasma-alone for non- and oxidative coupling of methane

### 2.1. Plasma-alone for the non-oxidative coupling of methane

One approach for the plasma valorization of methane in the non-oxidative conversion consisted in feeding pure methane into the plasma zone. Some studies also investigated the addition of non-oxidative gases (noble gases, hydrogen or nitrogen) in the methane effluent. The nature and distribution of products depend on the reaction parameters (specific energy input, type of plasma reactor, gap, temperature, pressure and residence time) which are also interrelated. The main products reported in the literature are acetylene, ethylene, ethane, hydrogen, carbon and higher hydrocarbons in much smaller amounts [21].

#### 2.1.1. Plasma chemistry

Plasma activation of methane leads to numerous elementary reactions. Homogeneous reactions will take place in the gas phase through heavy particle collision reactions and inelastic collisions with electrons (*Table 2*), while heterogeneous reactions will occur between the plasma-activated species and the catalyst surface [18]. These reactions are mainly valid for atmospheric pressure plasma (and above) where particle recombination takes place.

*Table 2: Elementary reactions in plasma [18,42]. M is a third body specie. \* denotes an excited state, which may be short-lived or metastable.*

<b>Excitation</b>	$e^- + A_2 \rightarrow A_2^* + e^-$	Leads to electronically excited state of atoms and molecules by energetic electron impact
<b>Dissociation</b>	$e^- + A_2 \rightarrow 2A + e^-$	Inelastic electron impact with a molecule causes its dissociation without ions
<b>Ionization</b>	$e^- + A_2 \rightarrow A_2^+ + 2e^-$	Energetic electrons ionize neutral species through electron

		detachment and positively charged particles are formed
<i>Attachment</i>	$e^- + A_2 \rightarrow A_2^-$	Negative ions can be produced by ionization reactions
<i>Dissociative attachment</i>	$e^- + A_2 \rightarrow A^- + A$	Negative ions can also be produced by dissociative ionization reactions
<i>De-excitation</i>	$e^- + A_2^* \rightarrow A_2 + e^- + h\nu$	Electronically excited state emits electromagnetic radiations on returning to the ground state
<i>Volume recombination</i>	$A^+ + A^- \rightarrow A^* + A$	Loss of charged particles from the plasma by recombination of opposite charges
<i>Penning dissociation</i>	$M^* + A_2 \rightarrow 2A + M$	Collision of energetic metastable species with neutral leads to ionization or dissociation
<i>Penning ionization</i>	$M^* + A_2 \rightarrow A_2^+ + M + e^-$	
<i>Charge transfer</i>	$A^\pm + B \rightarrow B^\pm + A$	Transfer of charge from incident ion to the target neutral between two identical or dissimilar partners
<i>ions recombination</i>	$A^- + B^+ \rightarrow AB$	Two colliding ions recombine to form a molecule
<i>Electron-ion recombination</i>	$e^- + A_2^+ + M \rightarrow A_2 + M$	Charge particles are lost from the plasma by recombination of opposite charges
<i>Ion-ion recombination</i>	$A^+ + B^- + M \rightarrow AB + M$	Ion-ion recombination can take place through three body collisions

As described in diverse publications (non-exhaustive list [20,21,43,44,26,45–47]), most of the energy is spent producing electrons that are accelerated in the electric field to form high-energy electrons. Electron impact reactions depend on the electron energy distribution function (or

electron temperature) and the electron collisional cross-section areas of a molecule. The electron energy is controlled by the reduced electric field strength, E/N. It is defined by the electric field (E, V cm<sup>-1</sup>), divided by the gas number density (N, cm<sup>-3</sup>).

Vibrational excitation will happen with low energy electrons following:



CH<sub>3</sub>, CH<sub>2</sub>, CH and H radicals will be produced from the electron's inelastic collisions with the methane molecules, at higher electron energy. The following mechanism for methane decomposition reaction were proposed:



Additionally, direct methane conversion can produce solid carbon and hydrogen following:



Ionization of methane is taking place following, with high energy electrons:

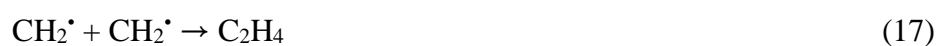


Ionization sustains the discharge and is a source of ions and electrons for further reactions.

Hydrogen radicals react quickly to form hydrogen and is unlikely to produce methyl radicals from methane dehydrogenation [45]:



C<sub>2</sub> - C<sub>3</sub> hydrocarbons will be generated by recombination of radicals. Methyl radical will initiate the recombination reaction:



Dissociation of higher hydrocarbon will also occur due to electronic impact [48]. The longer the residence time, the higher the formation of C<sub>2</sub>H<sub>5</sub> radicals and ethylene till a possible dissociation into lower hydrocarbons, and further to carbon and hydrogen.



Depending on the process parameters, potential higher hydrocarbons will be formed through radical recombination.



A 1D fluid model was developed for a cylindrical DBD plasma with pure methane. The simulation showed that methane activation starts mainly with the radical reaction (3) and, to a lesser extent, methane ionization (7) and (8) [49]. The radical reaction (3) is responsible for 79 % of the total electronic dissociation of methane, while the reaction (4) accounts for 15 % and (5) for 5 %. Methane ionization (7) accounts for 66 % and (8) for 33%. The recombination (and dissociation) reactions to various hydrocarbons were also depicted in their model. They did not take the vibrational excitation into account despite their importance, as they were only seen as energy loss reactions for the electrons. In their numerical simulation, Nozaki *et al.* [45] reported similar fragmentation patterns (CH<sub>3</sub>, CH<sub>2</sub>, CH and C) in pure methane using a microscale DBD plasma reactor and showed their dependence on the reduced electric field. From the simulated time evolution of a streamer, they showed that the density of the CH<sub>3</sub> radical was dominant. Methane hydrogen abstraction by CH<sub>4</sub><sup>+</sup> ion helped to produce methyl radicals. Ethane was the main product because coupling of methyl radicals is most likely to occur. From a simulated fragmentation pattern as a function of external electric field, the author showed that fragmentation into methyl radicals is maximum (60%) at an electric field of 80 Td, which corresponds to the breakdown field of methane. As the electric field increased (up to 500 Td), methane fragmentation pattern shifted from CH<sub>3</sub> radicals to CH<sub>2</sub>, CH and C, affecting the final product distribution.

### 2.1.2. Influence of the plasma type and reactor geometry

Many efforts have been made on the plasma type and reactor design in order to improve efficiency in methane coupling reaction, yielding different performances in terms of conversion, energy cost and selectivity towards hydrocarbons.

AC and pulsed discharges: They are the most common sources in the non-oxidative methane reaction as their low temperatures might be favorable for some reactions, due to their thermodynamics. Experiments using pure methane as a feed gas are resumed in *Table 3*. In the case of pulsed discharges, methane conversion is generally superior to 20 % at very low specific energy input ( $SEI < 1.44 \text{ kJ L}^{-1}$ ), while in the case of AC discharges, conversions superior to 20 % are achieved at much higher SEI, varying from 25 to  $150 \text{ kJ L}^{-1}$ . The product selectivities are highly dependent on the plasma source: very high selectivities of acetylene obtained in the pulse discharges as compared to AC discharges, where ethane is predominant. The generation of plasma from pulsed excitation ensures very high instantaneous energy and reduced electric field to produce highly energetic electrons promoting methane conversion, as well as acetylene and ethylene products [50].

Spark discharges: When comparing pulsed corona and pulsed spark discharges, Kangjun *et al.* [51] observed a methane conversion of 36.8% for corona against 60.2% for spark discharges. This effect was related to higher electron energy in spark than in corona pulsed discharges. In spark discharge,  $C_2$  selectivity was 93.1 % which included 95 % of acetylene.  $C_2$  selectivity with the pulsed corona discharge was only 59.2 % including 58.3 % of acetylene. Kado *et al.* [52] showed that independently of the reactant (methane, ethane, ethylene or propane), acetylene was the major reaction product in a pulsed spark discharge. From emission spectroscopy and isotope exchange reactions, they concluded that the very high electron density due to strong current (40A) in short time (500ns) of the spark contributed to the successive dehydrogenation of methane to  $CH_3$ ,  $CH_2$ ,  $CH$  radicals up to atomic carbon and hydrogen. They



also reported that carbon recombination into  $C_2$  and hydrogenation into CH radicals would be high, promoting ethylene formation.

Reactor geometry: The performance of two reactor geometries, namely coaxial and plate-to-plate, using  $CH_4 : H_2 = 1:1$  mixture (Table 3b) [53] was compared using nanosecond pulsed discharge. Methane conversion was favored in the coaxial configuration (45%) due to the higher energy channeling into the discharge, *i.e.* higher electron density and greater ionization rates, compared to plate-to-plate (35%), while the selectivity of the products (acetylene, ethylene and ethane) were not impacted. The authors attributed the differences in performance between the two reactors to the heating effects. The low reactor mass and stainless-steel cylindrical ground electrode of the coaxial reactor resulted in limited heat loss, thus thermal-driven cracking of methane was added to the electron impact. On the other hand, the high heat capacity of the plate-to-plate reactor resulted in greater heat loss and therefore, lower bulk gas temperature and lower methane conversion. Nevertheless, considering the power input, the energy-to-chemicals transfer occurred at a lower energy cost in plate-to-plate geometry, while the substantial amount of energy in the coaxial one was dissipated into gas heating. The reactor geometry affects the gas velocity and temperature within the discharge zone and thus methane conversion. However,  $C_2$  selectivity was not altered in the reported publications.

Modelling: Adding up to experimental investigations, numerical simulation of the reaction kinetics of a spark discharge at atmospheric pressure showed that accumulated  $CH_2$  radicals in the discharge channel react very rapidly with hydrogen radicals to form CH radicals ( $CH_2 + H^\bullet \rightarrow CH^\bullet + H_2$ ), precursors in the formation of acetylene [54]. Such reactivity is also linked to the temperature of spark discharges, which are considered warm plasmas ( $10^3$ - $10^4$  °C) as compared to DBD and corona which are cold plasmas (ambient temperatures up to 500°C).

In their studies using a 0D modeling approach, Heijkers *et al.* [55] gave possible reaction pathways of methane conversion into hydrocarbons (*i.e.* acetylene, ethylene and ethane) and hydrogen, in a DBD, a microwave and a gliding arc plasma. They compared their calculated

and experimental results according to fixed conditions and obtained satisfactory correlations between them. Additionally, they highlighted the beneficial effect of temperature on methane conversion in the gliding arc and in atmospheric pressure microwave plasmas. In both cases, neutral dissociation and dehydrogenation processes of the hydrocarbons take place, forming acetylene, hydrogen, and, to a lesser extent, ethylene. In cases of DBD and reduced pressure microwave plasmas, dissociation by electron impact and three-body recombination processes occurred, creating more saturated compounds. Ethane was the main product, but other hydrocarbons were detected such as propane and butane.

Table 3: Performances of different DBD plasmas for methane coupling from scientific literature in terms of methane conversion, selectivities and yields to C<sub>2</sub> products and H<sub>2</sub> yields. (a) methane alone and (b) in mixture with hydrogen. SEI in kJ L<sup>-1</sup> of methane

Plasma	SEI kJ L <sup>-1</sup>	CH <sub>4</sub> conversion %	C <sub>2</sub> selectivity %			C <sub>2</sub> yield %			H <sub>2</sub> yield %	Ref
			C <sub>2</sub> H <sub>2</sub>	C <sub>2</sub> H <sub>4</sub>	C <sub>2</sub> H <sub>6</sub>	C <sub>2</sub> H <sub>2</sub>	C <sub>2</sub> H <sub>4</sub>	C <sub>2</sub> H <sub>6</sub>		
<b>a. CH<sub>4</sub> alone</b>										
AC DBD	150	36.5	-			11			12	[56]
AC DBD	33	22	15		43	0.7	1.9		8	[44]
AC DBD	76.3	20.5	12		17	6			-	[57]
AC DBD	-	55	4.8	-	20.9	2.6	-	11.5	15	[58]
AC DBD	180	38	-	6.6	38.9	-	2.5	14.8	-	[59]
Nanosecond pulse discharge	1.4	32.4	54	10.3	1.9	17.3	3.3	0.6	-	[60]
Pulsed streamer discharge	26	31	74	4.8	4.2	23	1.5	1.3	18	[61]
Pulsed spark discharge		34	82	2.3	0	28	0.8	0	22	
Pulsed DBD		11	0	2.7	53.6	0	0.3	5.9	3	
AC DBD		5	0	6	50	0	0.3	2.5	0.5	
DC Pulse discharge	15	40.6	94.4	4.2	1.4	38	1.7	0.5	-	[62]
<b>b. CH<sub>4</sub> : H<sub>2</sub> (approximate values from figures)</b>										
Nanosecond pulse discharge (coaxial reactor) ratio 1:1	5	45	68	7	23	30.6	3.15	10.35	-	[53]
Nanosecond pulse discharge (plate to plate reactor) ratio 1 : 1	3	35	68	7	23	23.8	2.45	8.05	-	
Pulsed spark discharge ratio 1:2	57.6	60.2	88.4	4.5	0.1	53.2	2.7	0.06	-	[51]
Pulsed corona discharge 1:2	56.1	36.8	34.5	8.9	15.7	12.7	3.1	5.8	-	

### 2.1.3. Influence of the gap

Using a repetitive nanosecond pulsed plasma and by varying the gap from 3 to 8 mm width, Lotfalipour *et al.* [63] showed that 5 mm was the optimal gap for methane conversion in their process (Table 4). However, only small variations in selectivities to C<sub>2</sub>-C<sub>6</sub> with the electrode spacing were observed. The distance between the two electrodes impacts the plasma by modifying the average electron energy and reduced electric field, which drops with increased gap width. Despite the mean electron energy decrease, the authors suggested the importance of vibrational excitation reactions, reactions (1) and (2), and low momentum transfer cross section at a mean electron energy of around 0.3 eV to improve the conversion process. They concluded on the difficulty to relate average electron energy to conversion efficiencies when modifying the electrode gap because it also altered the pulse energy. Belouqui *et al.* [14] reported a maximum methane conversion with an electrode gap between 5 and 7 mm. At longer distances, the electric discharge would weaken or not be generated. The author concluded that in the case of electrodes having different geometries, not only the length but also the shape of the plasma volume changed with the electrode gap, resulting, in some cases, in variations in the product distribution, but without further investigation.

In a gliding arc reactor [26], methane conversion rate and C<sub>2</sub> hydrocarbon yield increased with the electrode gap distance from 2 to 4 mm. However, higher voltages were needed for larger gaps and over 4 mm, the discharge was unstable.

In the recent work by Delikonstantis *et al.*[53], using plate-to-plate configuration and nanosecond pulse of various frequencies, the optimum gap range for methane conversion was between 2.5 and 3.5 mm. At 3 kHz, the selectivity of acetylene reached a maximum at a 2.5 mm gap. At 10 kHz, acetylene selectivity was not only stable over the range of 2.5 to 3.5 mm but was also improved when compared to 3 kHz due to a higher concentration of active species with a longer lifetime. The greatest yield of acetylene in this range was due to the efficient load-impedance matching and subsequent high energy in the plasma.

Table 4: effect of the gap distance between the electrodes with different plasma sources from literature in terms of methane conversion, specific energy input (per Liter of input CH<sub>4</sub>), selectivities, yields to C<sub>2</sub> products and hydrogen selectivity (S<sub>H2</sub>). (-) no data.

Plasma	Feed, comments	Gap mm	SEI kJ L <sup>-1</sup>	CH <sub>4</sub> conversion %	C <sub>2</sub> Selectivity %			C <sub>2</sub> Yield %	S <sub>H2</sub> %	Ref	
					C <sub>2</sub> H <sub>2</sub>	C <sub>2</sub> H <sub>4</sub>	C <sub>2</sub> H <sub>6</sub>				
<i>Nanosecond pulse spark</i>	*SEI in term of energy per pulse in mJ ; flow rate: 400ml.min <sup>-1</sup>	3	3.4*	27	72.6	2.1	0.2	20.2	72.6	[63]	
		4	4.7*	39	74.4	2.2	0.2	29.9	74.4		
		5	4.8*	48	71.7	2.1	0.1	35.4	71.7		
		6	5*	50	72.6	2.5	0.2	37.6	72.6		
		7	5.3*	51	71.3	2.5	0.2	37.7	72.6		
		8	5.9*	53	72	2.3	0.1	39.5	72		
<i>corona</i>	CH <sub>4</sub> =36.6 mL min <sup>-1</sup> C <sub>2</sub> yield consist in only C <sub>2</sub> H <sub>2</sub>	2	164	2.1	38	-	-	0.8	-	[14]	
		4		2.3	42	-	-	0.9	-		
		6		3.2	62	-	-	2	-		
		7		3	66	-	-	2	-		
		8		2.1	65	-	-	1.3	-		
		10		0.1	32	-	-	0.3	-		
		12		0	12	-	-	0	-		
<i>Micro DBD</i>	CH <sub>4</sub> at residence time of 4.1 s	0.4	149.2	25.1	15	50	16.3	46	[57]		
		0.9		75.9	20.0	11	48	11.8		49	
<i>DBD</i>		1.9	44.4	13.8	17	48	8.9	48			
<i>Micro DBD</i>	CH <sub>4</sub> at 20±0.2 mL min <sup>-1</sup>	0.4	76	20.2	13	47	12.1	45	[57]		
		0.9		20.3	13	46	11.9	46			
<i>DBD</i>	6.94 s residence time	1.9		15.8	13	47	9.5	47			
<i>Gliding arc</i>	CH <sub>4</sub> =22 mL min <sup>-1</sup> , Ar=52 mL min <sup>-1</sup>	2	73	23.4	92			22	85	[26]	
		3	81	30	80			25	70		
		4	90	33.36	95			30	75		
		>4	INSTABILITY OF DISCHARGE								
<i>Pulsed spark</i>	H <sub>2</sub> /CH <sub>4</sub> =2 25 mL min <sup>-1</sup>	7	69	50	90	<5	-	-	-	[51]	
		10		55	90	<5	-	-			
		13		60	90	<5	-	-			
<i>Nanosecond pulse</i>	CH <sub>4</sub> : H <sub>2</sub> = 1:1 at 200 mL min <sup>-1</sup> SEI in term of energy per pulse	3 kHz (approximation from the figures)									
		1.5	~ 1.6 mJ/pulse	32.5	64.0	8.0	25.0	31.5	-	[53]	
		2.5		37.5	68.0	8.0	22.5	37.0	-		
		3.5		37.5	62.0	10.0	26.0	34.3	-		
		5		25.0	45.0	12.5	28.0	21.4	-		
		10 kHz (approximation from the figures)									
		1.5	~ 1.6 mJ/pulse	32.5	68.0	6.0	22.5	31.4	-		
		2.5		40	72.5	5.0	21.0	39.4	-		
		3.5		44.5	71.0	6.0	21.5	43.8	-		
		5.0		40	67.0	6.0	24	38.8	-		

The authors also observed several types of plasma regimes generated with different gaps. The spark regime (in the range of 2-3.5 mm) was the most advised for efficient plasma performances. At spark regime, corresponding to a high energy regime in the discharge, methane was cracked into C and C<sub>2</sub> via an electron-impact reaction (confirmed by optical

emission spectroscopy), generating acetylene *via* stepwise C<sub>2</sub> hydrogenation and leaving a high carbon content. At lower gaps ( $\leq 3$  mm), even when a spark regime was generated, the discharge did not propagate into streamers because of the reduced space. As a result, high bulk temperature and low energy input promoted methane thermal cracking into CH<sub>3</sub>, forming ethane *via* CH<sub>3</sub> coupling, and further resulting in acetylene *via* stepwise ethane dehydrogenation. Noteworthy, lower carbon deposition was produced in this case. At greater gaps, the spark discharge went into filamentary mode and further to diffuse regime, delivering low energy input and thus low performance.

In the experiments referenced in Table 4, the product selectivity was mostly independent of the electrode distance (except corona), indicating that the reaction pathways of methane conversion are not changed by varying the electrode distance. For example, in DBD and micro DBD experiments, for three discharge gaps (0.4, 0.9 and 1.9 mm), the applied voltage and current remained constant while the methane flow was varied to maintain the same residence time (4.1 s) for all configurations [57]. However, the SEI increased and methane conversion improvement was related to the SEI and not to the discharge gap. At constant SEI, a decrease of the methane conversion (15.8 %) was registered only when the gap was greater than 1 mm, which was the result of low plasma density and applied electric field intensity.

An important parameter in non-thermal plasma is the reduced electric field E/N which determines the mean electron energy in a plasma and is inversely proportional to the gap distance. Above a certain gap distance defined by the geometry of the reactor, the decrease in the reduced electric field and the mean electron energy leads to a decrease in methane conversion and C<sub>2</sub> yield (Figure 1).

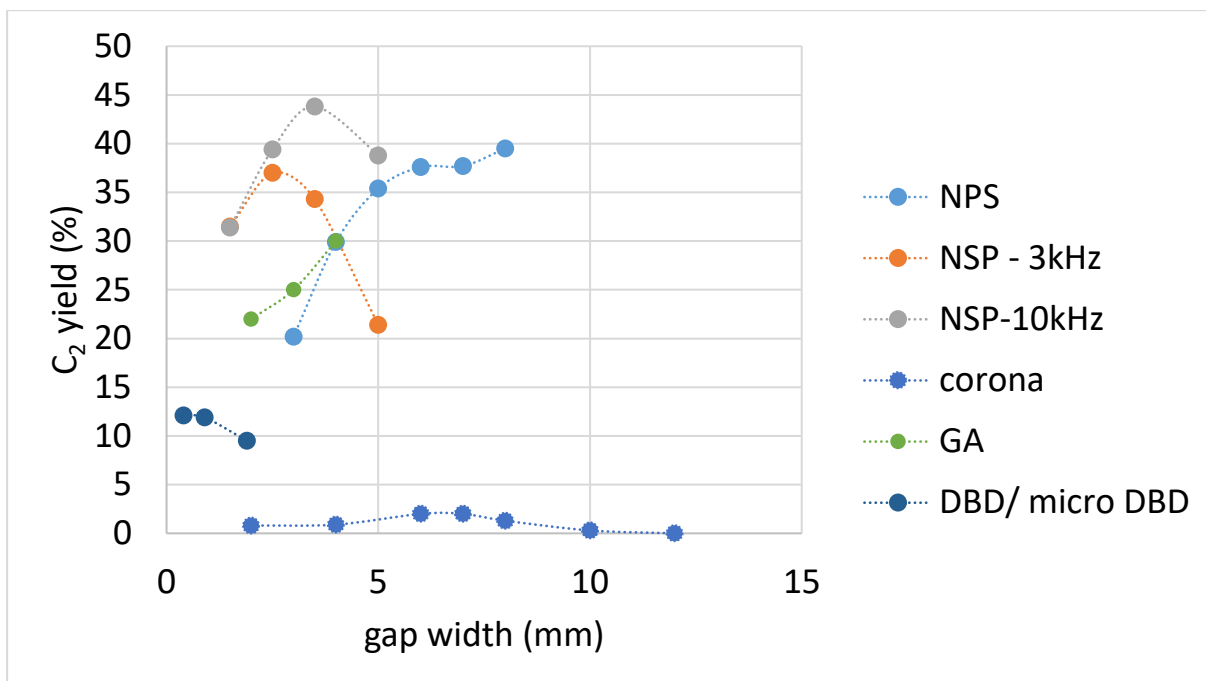


Figure 1:  $C_2$  yield as a function of gap width for different reactor type. NPS: nanosecond pulsed spark ( $SEI = 3,4$  to  $5,9 \text{ kJ L}^{-1}$ ) [63]; NSP- 3kHz nanosecond pulse plasma and NSP- 10kHz nanosecond pulse plasma [53]; Corona ( $SEI= 164 \text{ kJ L}^{-1}$ ) [14]; GA: glidarc ( $SEI= 73-90 \text{ kJ L}^{-1}$ ) [26]; DBD / micro DBD ( $SEI= 76 \text{ kJ L}^{-1}$ ) [57].

#### 2.1.4. Influence of the pressure

The pressure in the system is also an important parameter to be considered in the distribution of products. Taking into consideration the breakdown voltage, it is a function of the product of the discharge gap and discharge pressure, known as the Paschen curve. The pressure rise leads to a decrease in the electron mean free path due to higher molecular density, requiring a higher electric field to maintain the discharge. At constant power, the breakdown voltage increases with the increase in pressure [53,60,64].

In their nanosecond pulsed discharge reactor, Scapinello *et al.* [48] showed that acetylene or ethylene were major products depending on the pressure. At atmospheric pressure,  $CH_3$ ,  $CH_2$  and  $CH$  radicals were formed, with methyl radicals being the most abundant primary products, from electron impact dissociation and thermal cracking (due to high temperature). methyl radical recombination into ethane occurred in the first step, followed by successive dehydrogenation, through cracking or H abstraction. This led to a majority of acetylene following  $C_2H_6 \rightarrow C_2H_5 \rightarrow C_2H_4 \rightarrow C_2H_3 \rightarrow C_2H_2$ .

Above 3 bars, ethane was also the first product formed from methyl radical coupling. Concomitantly, a higher gas temperature was reached, enhancing methane conversion and concentration of methyl radicals. Stepwise ethane dehydrogenation to acetylene was the main mechanism of acetylene formation. Due to the high bulk gas temperature at 3 bars, methyl radicals were combined not only to ethane, but also to ethylene. Then, as under atmospheric pressure, thermal stepwise ethane dehydrogenation to acetylene occurred.

#### 2.1.5. Influence of the specific energy input

One essential parameter in plasma-assisted methane conversion is the specific energy input, which is defined as the plasma input power divided by the methane flow rate. It is usually expressed in  $\text{kJ L}^{-1}$  of feed flow or  $\text{kJ mol}^{-1}$  of input methane. SEI can be altered by either varying the input power, or the flow rate, *i.e.* residence time. Increasing the power (via the applied voltage or pulse frequency) increases the energy function of electrons and the frequency of electron-molecule collisions which then leads to higher methane conversion. On the other hand, high SEI favors carbon formation. The trick is to find a good balance between those parameters to promote both methane conversion and selectivity to desired products.

##### 2.1.5.1. Effect of the input power

Increasing the applied voltage increases the electric field strength, electron density, and energy brought to the system. Liu *et al.* [65] obtained an increase in methane conversion that was almost linear with the input power from 15 to 75 W, corresponding to SEI from 18 to 90  $\text{kJ L}^{-1}$  of pure methane in a DBD plasma. The maximum methane conversion reached 36 % at a discharge power of 75 W, which was also predicted by an artificial neural network model. In addition, increasing the discharge power decreased the selectivity of acetylene and ethylene by 30 % and simultaneously enhanced the selectivity of saturated hydrocarbons (ethane, propane and butane). A perfect match between the experimental and simulated data at discharge powers between 15-55 W was achieved. The authors suggested that increasing the plasma power



inhibits the generation of light hydrocarbons and converts them to saturated hydrocarbons and hydrogen.

The input energy showed a powerful but also antagonist effect on the conversion of methane, depending on the plasma configuration. Using a micro-plasma reactor (micro-DBD, below 1 mm) with pure methane flow, Wang *et al.* [57] showed that increasing the power, thus the average input energy from 31 J L<sup>-1</sup> to 76 kJ L<sup>-1</sup>, led to an increase in methane conversion (maximum at 20.5 %). They stated that the increase in the specific energy input (SEI) is linked to the enhanced electric field and to the increased average input energy per methane molecule. Ethane was the main product due to the low energy per pulse (1.3 mJ) and short period (< 52 μs) of the micro discharge. Moreover, selectivity to ethane (67.5 kJ mol<sup>-1</sup>) was favored due to its lower thermodynamics when compared to ethylene (202.6 kJ mol<sup>-1</sup>). Further increase of the SEI, above 90 kJ L<sup>-1</sup>, had negative results on the reaction, leading to an unstable plasma process and a 9 % selectivity to carbon. With that in mind, the increase in methane conversion was observed up to the limit where carbon formation and its deposition altered the discharge characteristics. A decrease in the ethane selectivity was equally observed. This was attributed to the more energetic plasma species and the reaction of ethane to form higher hydrocarbons or degradation to carbon.

Zhu *et al.* [24] found that methane conversion and C<sub>2</sub> yield were promoted when the input energy density was increased in a positive pulsed corona discharge, and more favorably than under a negative corona. They explained this difference based on the propagation of streamers. Positive pulse streamers can cross the electrode gap and activate a larger volume than negative pulse streamers which remain concentrated in the vicinity of the corona wire. They increased the SEI by increasing the input power and decreasing the residence time, favoring methane conversion and C<sub>2</sub> yield. At an input energy density of 1.8 kJ mol<sup>-1</sup>, the conversion of methane reached 44.6 % and 31.6 % C<sub>2</sub> yield with an acetylene yield of 30.1 %.

### 2.1.5.2 The effect of pulse repetition frequency and pulse duration

In their 2017 review, Scapinello *et al.* [21] cited a large number of authors who reported only a weak effect of frequency (below 10 kHz) on methane conversion and product selectivities, either from experimental or modeling studies with various DBD plasma reactors, due to their low energy density and low temperature. However, above 10 kHz, frequency leads to a different reactivity trend as the gas temperature increases. As cited by the authors, the memory effect and ionic remnants would also modify the chemical reactions and physical characteristics of the discharge and thus affect methane conversion. Jeong *et al.* [66] have shown that in a pulsed DC barrier discharge at atmospheric pressure, the selectivities of ethane and ethylene were not influenced by the change of pulse frequency, but by the change of energy input from applied voltage and methane flow rate. The increase in the pulse frequency led only to an increase in methane conversion but there was no significant change in the product selectivities.

Recently, the same group [53] looked at the influence of applied frequency on the conversion of methane and product selectivity using nanosecond pulse discharge in a plate-to-plate configuration. The methane conversion and acetylene yield were maximized in an optimal range of frequencies (3-10 kHz), where the discharge and bulk temperatures, as well as the concentration of active species with long lifetimes were high. Such effects would promote thermal cracking of methane instead of excitation and ionization of the gas. A further increase in the frequency (above 20 kHz) led to an even higher bulk gas temperature, reducing the plasma resistance and energy in the heating of the system instead of channeling it into the discharge. The drop in energy input in the discharge took over the thermal effect that led to the decrease in methane conversion and acetylene yield.

The methane conversion and product distribution dependence on pulse repetition and pulse duration in a microwave plasma was studied by Heintze *et al.* [35]. The results were plotted as a function of the energy input, *i.e.* pulse duration increase. At low frequency (200 Hz), increasing the pulse duration from 100 to 300  $\mu\text{s}$  (energy input from 2.2 to 9.8 eV molecule<sup>-1</sup>)

enhanced methane conversion (from 19 % to 68 %) and acetylene selectivity (from 48 % to 72 %). Ethylene and ethane selectivities remained below 20 % and tend to decrease slightly with increased SEI. A much different trend was observed at high frequency (1 kHz) with very short pulses (from 20 to 60  $\mu$ s), where the increase of input energy to 9 eV led to 90 % methane conversion and changed the profile of C<sub>2</sub> products selectivity. Increasing the energy input from 1.5 to 9 eV molecule<sup>-1</sup> increased the acetylene selectivity from 5 % to 80 %, while the ethane selectivity dropped considerably (from 75 % to nearly zero from 7 eV molecule<sup>-1</sup>).

The authors showed an increased concentration of atomic hydrogen with increasing energy density, thus increasing the dehydrogenation reaction. Additionally, they recorded the gas temperature time-averaged over the microwave pulse and observed a significant increase with the increase of input energy from 1477 K to 2551 K. In their process, the dissociation of methane to produce CH<sub>x</sub> and atomic hydrogen is greatly enhanced with energy input, either from pulse frequency or pulse duration increase. The increase in gas temperature with the energy input enhances the dehydrogenation of methane (whose rate is exponentially dependent on temperature) and reduces the energy requirements for the conversion. The selectivity to C<sub>2</sub> products also depends on the concentration of hydrogen atoms and temperature. From time resolved OES analysis, long pulses (100- 300  $\mu$ s) lead to a strong increase of hydrogen atoms, enhancing the reaction rate of atomic hydrogen and favoring acetylene production, while short pulses result in low concentration of hydrogen atoms and are selective to ethane. This conclusion is only valid for low energy inputs. At high energy input, the dehydrogenation of CH<sub>x</sub> and C<sub>2</sub>H<sub>x</sub> by hydrogen atoms and by the high gas temperature shifts the selectivity of ethane to acetylene for the short and long pulse durations.

### *2.1.5.3 The effect of residence time*

The residence time, by changing the gas flow rate, influences the SEI and thus the methane conversion [32,56]. Experiments were performed at the same deposited power while varying the total gas flow rate. Consequently, the specific energy input varied as a function of residence

time. Long residence times in the discharge volume increase the collision probability of the feed gas molecules with the plasma active species and increase the energy input, enhancing highly energetic electrons. Increasing the residence time in the plasma discharge zone can significantly enhance the conversion of methane, as seen in Table 5.

The increase in conversion of methane with prolonged residence time [44,56,57,67] resulted in high C<sub>2</sub> yields. However, it was difficult to draw a trend since, to double the value of the C<sub>2</sub> yield, the residence time had to be increased six times in reference [44] as compared to an increase of only three times in reference [32]. In the presence of helium, in stoichiometry with methane, the C<sub>2</sub> yield was less affected by the residence time: doubling the residence time from 12 to 24 s led to an increase in C<sub>2</sub> yield by only 5 %. The selectivity of ethane, however, decreased with the increased residence time, as was the case for the overall C<sub>2</sub> selectivities, suggesting carbon deposition even though no indication was given by the authors.

The residence time is an important parameter not only in DBD reactors but also in gliding arc reactors [26]. Increasing the flow rate above a certain value (66 mL min<sup>-1</sup> in this case) led to the formation of an intermittent discharge, caused by the carbon deposition. As the flow rate increased, the C<sub>2</sub> hydrocarbons selectivity fluctuated around 90 %, while C<sub>2</sub> and hydrogen yields decreased, indicating that the carbon balance was lower due to a more important carbon deposition.

Table 5: Literature review of the effect of residence time on methane conversion, C<sub>2</sub> selectivities and hydrogen yield (Comment: Y<sub>H2</sub>), when given with different plasma sources

Plasma	Feed	Flow (mL min <sup>-1</sup> )	Residence time (s)	SEI kJ L <sup>-1</sup>	CH <sub>4</sub> conv. (%)	C <sub>2</sub> selectivity (%)			C <sub>2</sub> yield (%)	Comment	Ref
						C <sub>2</sub> H <sub>2</sub>	C <sub>2</sub> H <sub>4</sub>	C <sub>2</sub> H <sub>6</sub>			
DBD	CH <sub>4</sub>	100	3.82	21	8.1	-			3.8	Y <sub>H2</sub> =3.3 %	[56]
		20	19.08	120	31.5	-			9.7	Y <sub>H2</sub> =12 %	
DBD	CH <sub>4</sub>	300	2.7	9	7	28		45	5.5	Y <sub>H2</sub> =1.7 %	[44]
		50	16.3	54	25	12		35	11	Y <sub>H2</sub> =9 %	
Micro DBD	CH <sub>4</sub>	59.75	1.39	-	9.6	15.5		48.8	6.2	-	[57]
		20.24	4.11	-	20.3	16.7		44.8	12.5	-	
DBD	He –CH <sub>4</sub> 1:1	64	12	262.5	17	0.9	7.9	81.5	15.3	T=100 °C	[67]
				262.5	20	3.4	11.2	73.0	17.5	T=350 °C	
		32	24	431.2	23.2	1.4	5.5	79.2	20	T=100 °C	
				431.2	30.1	3.2	7.8	72.4	25	T=350 °C	
DBD	Ar-CH <sub>4</sub> 3:1	32	0.7	39.4	33	20		35	18.1	-	[32]
		40	0.6	31.5	31	20		34.5	16.9	-	
		48	0.5	26.2	27.5	22		35	15.7	-	
		60	0.4	21	25	22		33.5	13.9	-	
		80	0.3	15.7	22	22.5		35	12.6	-	
Gliding arc	Ar –CH <sub>4</sub>	118	-	5.03	22	80			17.6	-	[26]
		57	-	10.4	45	90			40	-	

### 2.1.6. Influence of the temperature

As seen previously, the system reactivity can be influenced by the temperature evolution inside the plasma volume, either from Joule dissipation or from external heating (in the presence of an oxidant [68–70]).

An example illustrating this behavior is the increase in ethane selectivity with the decreased gas temperature of different plasma sources: hollow cathode = pulsed spark < pulsed DBD < AC DBD. AC and pulsed DBD were also the sources with the lowest electron density [20]. The same effect was observed by Li [61], when comparing pulsed streamer discharges, pulsed spark discharges, pulsed DC DBD and AC DBD. Acetylene yield was almost the same in pulsed streamer discharges as in pulsed spark discharges. The highest ethane yield (~6 % at 700 kJ mol<sup>-1</sup> of methane) was obtained in pulsed DC DBD. In all four electric discharges, the ethylene yield was less than 2 % and in the DBD the acetylene yield was less than 0.5 %.

One study [71] revealed, from a simulation, that endothermic reactions (*i.e.* homolytic scissions) occurred in the first few milliseconds of a non-thermal pulsed plasma discharge, when the local temperature rose rapidly (Figure 2).

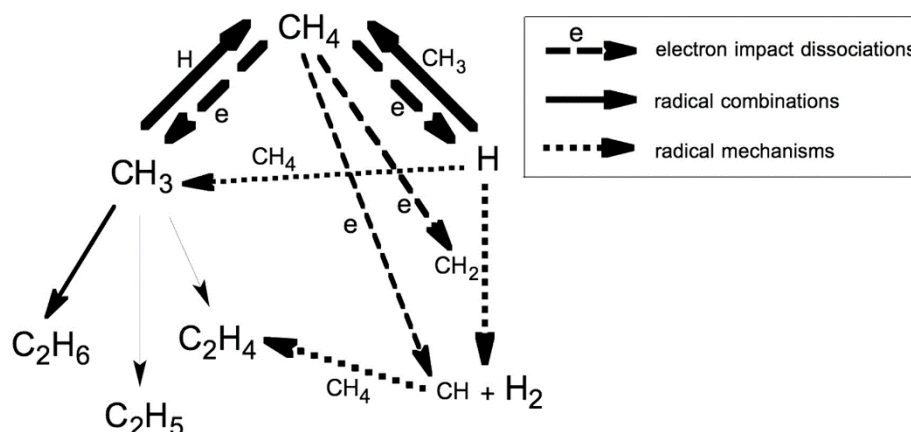


Figure 2: Main active reaction pathways in a micro-discharge [71]

The authors proposed reaction mechanisms, starting with an electronic impact generating radicals and ions from methane dissociation. Then, radical propagation and recombination led to exothermic reactions and an increase in the local gas temperature, which would noticeably

affect the energy efficiency. High energy efficiencies would be obtained if the local gas temperature allowed the thermal decomposition of ethane and methane, valorizing the thermal energy from exothermic reactions instead of losing it upon dissipation. They concluded that high energy efficiencies are linked to the plasma's high specific energies and to the formation of acetylene, which is thermodynamically stable at elevated local temperatures.

Tarverdi *et al.* [67] observed, in a DBD plasma, a synergistic effect of the reactor temperature on methane conversion, C<sub>2</sub> and C<sub>3+</sub> selectivities. Increasing the reactor temperature to 350°C led to higher methane conversion (from 18 to 26 % at CH<sub>4</sub>/He ratio = 1). C<sub>2</sub> selectivity was altered by the reactor temperature. The acetylene and ethylene selectivities increased, while the ethane selectivity decreased with the increased temperature.

#### 2.1.7. Influence of co-existing gases

##### 2.1.7.1. The addition of nitrogen

Using nitrogen appears to provide stability to the plasma discharge [72] and has been used in various applications such as air stream decontamination, combustion or hydrogen production, to name a few. The addition of nitrogen as a co-feed for methane coupling is not very common and, to our knowledge, only a very few studies have treated this subject (Table 6). Despite its elevated dissociation energy (9.7 eV), nitrogen can dissociate and react to produce hydrogen cyanide and ammonia in low concentrations.

The experimental and computational studies performed by Snoeckx *et al.* [73] revealed that increasing nitrogen content led to an increase in methane conversion and hydrogen yield. The authors reported a decrease in electron density with rising nitrogen content, lowering the impact probabilities with methane molecules. This effect was counteracted by the lower reaction rate constant of three-body reactions with nitrogen (instead of methane) as the third body, reducing the generation of methane from recombination reactions. Finally, a non-symmetric change of the dominant three-body reaction occurred at 90 % nitrogen content (methane as the third body

is three times more efficient than nitrogen). With increasing nitrogen content, penning dissociation became the dominant reaction and favored methane dissociation and hydrogen yield. However, the overall decrease of methane content with rising nitrogen content impacted the overall methane conversion (*i.e.*  $\text{CH}_4 \text{ loss (\%)} = \text{CH}_4 \text{ content (\%)} \times \text{CH}_4 \text{ conversion (\%)}$ ) and hydrogen yield, which decreased with increasing nitrogen content. Only small yields of hydrogen cyanide or ammonia were predicted from calculations (ppm and ppb levels) due to the low nitrogen ionization (low electron energy), knowing that nitrogen metastable species are precursors for their formation.

However, one of these two studies provided results only in the presence of nitrogen, so no comparison could be made with the reaction under pure methane. Nevertheless, the presence of nitrogen in excess (95 %) in the feed resulted in good methane conversion, reaching 80 % depending on the plasma source [20]. As seen in previous sections, the plasma source has a significant effect on the product selectivities: low-density plasmas such as DBD, which have low electron energy, will favor the formation of ethane, while high-density plasma (with a high electron density and a higher bulk gas temperature) will favor dehydrogenation to acetylene.

In the case of excess methane in the feed [56], the addition of 10 % nitrogen did not result in a significant improvement in methane conversion (36.5 to 37.6 %). The  $\text{C}_2$  yield slightly decreased from 11 % to 9 % when nitrogen was present as a co-feed gas. An interesting feature was the increase in carbon balance from 71 % to 93 % when nitrogen was added as an additive due to the presence of metastable excited species. Based on Snoeckx *et al.* [73] work, the author implied that the addition of nitrogen led to active nitrogen metastable species. The methane dissociation then occurred via Penning dissociation reactions due to the collision of methane with those metastable species.

Interestingly, the addition of nitrogen to methane was also used as a precursor for ammonia and  $\text{C}_2$  synthesis [74], but only in the presence of a cobalt supported on  $\gamma$ -alumina catalyst. The authors showed improved conversion of methane and an increased production rate of ammonia



under microwave plasma as compared to microwave only. However, catalyst deactivation by black carbon limited the process.

Table 6: The effect of nitrogen as a co-feed for non-oxidative methane coupling

Type of discharge	Feed	SEI kJ L <sup>-1</sup>	CH <sub>4</sub> conversion %	C <sub>2</sub> Selectivity %			C <sub>2</sub> Yield %			H <sub>2</sub> Yield %	Ref
				C <sub>2</sub> H <sub>2</sub>	C <sub>2</sub> H <sub>4</sub>	C <sub>2</sub> H <sub>6</sub>	C <sub>2</sub> H <sub>2</sub>	C <sub>2</sub> H <sub>4</sub>	C <sub>2</sub> H <sub>6</sub>		
AC DBD	95 % N <sub>2</sub> – 5 % CH <sub>4</sub>	45.6	14.8	2.2	1.9	28.7	0.3	0.3	4.2	0.5	[20]
Pulsed DBD		9.4	12.4	1.0	0.9	21.0	0.1	0.1	2.6	0.2	
AC spark		7.2	82.9	41.5	1.1	0	34.4	0.9	0	1.4	
Pulsed Spark		13.4	49.4	37.2	2.5	2.1	18.4	1.2	1.0	2.9	
Rotating arc		2.6	42.2	39.8	1.0	0.2	16.8	0.4	0.07	0.8	
Gliding arc		3	23.7	45.9	-	-	10.9	-	-	1.8	
Hollow cathode		1.2	25.8	41.9	2.3	2.2	10.8	0.6	0.5	1.3	
DBD	10 % N <sub>2</sub> - 90 % CH <sub>4</sub>	150	37.6	-	-	-	9			14	[56]
DBD	100% CH <sub>4</sub>	150	36.5	-	-	-	11			12	

Table 7: The effect of H<sub>2</sub> as a co-feed for non-oxidative methane coupling. \* Approximated from the figure

Type of discharge	Feed	SEI kJ L <sup>-1</sup>	CH <sub>4</sub> conversion %	C <sub>2</sub> Selectivity %			C <sub>2</sub> Yield %			H <sub>2</sub> Yield %	Ref
				C <sub>2</sub> H <sub>2</sub>	C <sub>2</sub> H <sub>4</sub>	C <sub>2</sub> H <sub>6</sub>	C <sub>2</sub> H <sub>2</sub>	C <sub>2</sub> H <sub>4</sub>	C <sub>2</sub> H <sub>6</sub>		
DBD	90 % CH <sub>4</sub> -10 % H <sub>2</sub>	150	33.2	-	-	-	10			11*	[56]
DBD	100% CH <sub>4</sub>	150	36.5	-	-	-	11			12*	
Nanosecond pulse	100% CH <sub>4</sub>	-	32.4	54	10.3	1.9	17.3	3.3	0.6	-	[60]
	1:1 CH <sub>4</sub> : H <sub>2</sub>	-	36.7	1.9	53	3.3	0.7	19.5	1.2	-	
	1 :3 CH <sub>4</sub> : H <sub>2</sub>	-	36.8	6	43.6	6.1	2.2	16.5	2.3	-	
Pulsed streamer	33 % CH <sub>4</sub> - 67 % H <sub>2</sub>	24	46	97.8			45			-	[61]
DC Pulse	CH <sub>4</sub> + 50 % H <sub>2</sub>	-	46.3	94.2	4.4	1.1	46.2			-	[62]
	CH <sub>4</sub> + 67 % H <sub>2</sub>	-	57.4	92.7	5.7	1.2	57.1			-	
	CH <sub>4</sub> + 80 % H <sub>2</sub>	-	47	88.2	8.1	2.9	46.6			-	
	CH <sub>4</sub> + 90 % H <sub>2</sub>	-	11.8	63.7	15.2	17.7	11.4			-	

### 2.1.7.2. *The addition of hydrogen*

Hydrogen is generally added to the feed either to hydrogenate acetylene or its precursor, or for carbon black suppression [60,75]. The addition of hydrogen as a diluting gas stabilizes the discharge, improving methane dissociation. This enhancement was explained by the exceptional thermal conductivity of hydrogen (0.18 W/mK), which provides a large volume of heat energy. In addition, the slightly lower dissociation energy of the H-H bond (4.52 eV) compared to the CH<sub>3</sub>-H bond (4.55 eV), led to the reaction of the H radical (from the H-H bond) with the hydrogen in methane, enhancing methane activation and conversion [76,77].

The effect of hydrogen was examined in different types of plasma and the results are presented in Table 7. In the case of DBD plasma, the addition of 10 % hydrogen led to a small increase in methane conversion from 33.2 to 36.5 %, and a slight change of C<sub>2</sub> product yield. The overall results were not improved as compared to pure methane, suggesting that there is an optimum proportion at which hydrogen will have a positive effect. As a matter of fact, simulation analysis showed that there is an optimal value of the CH<sub>4</sub>/H<sub>2</sub> ratio to maximize methane conversion [78]. With an initial ratio <25 %, the collisions between electrons and methane are insignificant, therefore, minimal consumption of methane is expected due to the low methane density and high recombination rate of CH<sub>3</sub> and H radicals. The highest methane consumption was observed at 50 % methane, which was attributed to a higher energy amount channeled into the plasma due to the maximum collisions. At ratios >50 %, hydrogen was formed *via* collisions of electrons with ethane. As a result, ethylene production increased, and its dehydrogenation was slowed down in the presence of hydrogen. The same effect was observed in a non-equilibrium pulsed discharge, where contents up to 50 % hydrogen had no marked effect on methane conversion and product selectivity [75]. However, as the hydrogen concentration increased further, the state of discharge became more stable and methane conversion increased. Over 80 % hydrogen, the process lost its interest due to the severe reduction of the possible electron's collision with methane.

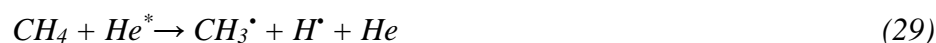
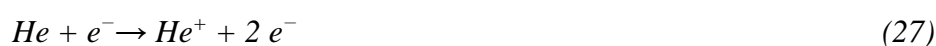
In a nanosecond pulsed discharge at atmospheric pressure, the addition of hydrogen decreased the carbon lack [60]. Carbon lack was defined as carbon balance with carbon deposited on the reactor walls and heavier species (C<sub>3</sub>-C<sub>6</sub>) inputs. At a pressure of 5 bar, by increasing the amount of hydrogen, product selectivity shifted from acetylene to ethylene. The ratio CH<sub>4</sub>:H<sub>2</sub> of 1:1 led to the highest ethylene yield (19.5 %) and an acetylene yield below 1 %. However, the increase in pressure also resulted in the intensification of carbon deposition and heavier species formation. The authors referred to the fundamentals related to pressure modification to explain their results. As mentioned previously, the pressure rise leads to a decrease in the electron mean free path due to higher molecular density, hence increasing the breakdown voltage. The direct consequence is the need for a stronger electric field to generate and maintain the plasma discharge. Additionally, as the pressure increases, a thermal effect leads to thermal equilibrium and a decrease in energetic collisions. By combining hydrogen content and pressure rise, it is then possible to shift the selectivity from acetylene to ethylene.

Heintze [35] investigated the effect of atomic hydrogen on methane conversion and product distribution in a pulsed microwave plasma. At low energy (2eV/molecule) with 17 % hydrogen, ethane was the most abundant product but with a much lower selectivity (45 %) than without hydrogen (~80 %). Conversely, ethylene (15 %) and acetylene (25 %) selectivities were three times higher than in the absence of hydrogen. The increase of energy, hence local temperature, led to the dehydrogenation of CH<sub>x</sub> and C<sub>2</sub>H<sub>x</sub> entities and to the shift of product distribution from ethane to acetylene.

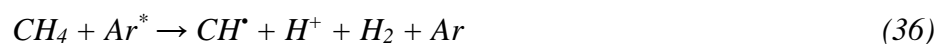
#### *2.1.7.3. The addition of noble gases*

Plasma discharge initiation, propagation and reactivity are modified in the presence of noble gases. A majority of published work accordingly agreed that CH<sub>3</sub> radicals are formed *via* homolytic hydrogen abstraction of methane, either catalytically or by electronic impact. In the presence of noble gases, the formation of methyl radicals can also be a result of direct methane collisions with excited noble gas species. Even though noble gases own a higher ionization

energy compared to methane, their breakdown voltage is much lower. This phenomenon is attributed to the small size of noble gas atoms, resulting in longer electron mean free path, greater electron acceleration and an increase in their temperature [78]. Compared to argon or nitrogen, activated helium is a much better charge and energy transfer body [67]. The “Penning dissociation” phenomenon, identified as an energy transfer from excited entities to others in the ground state, explains the improved methane reactivity in helium [79]:



Argon as diluent is also involved in some extra reactions in the plasma zone [26]. The argon atom in its ionic or excited state act as an energy carrier. The ionized species in the plasma can be involved in the charge-exchange and electro-ion recombination reactions:



The conversion of methane can be considerably affected by the nature of the noble gases, as it can be seen in Table 8. Regrettably, the studies did not provide results under pure methane for comparison.

Table 8: The effect of noble gases addition for the non-oxidative methane coupling

Type of discharge	Feed	T °C	SEI kJ L <sup>-1</sup>	CH <sub>4</sub> conversion %	C <sub>2</sub> Selectivity %			C <sub>2</sub> Yield %			H <sub>2</sub> Yield %	Ref
					C <sub>2</sub> H <sub>2</sub>	C <sub>2</sub> H <sub>4</sub>	C <sub>2</sub> H <sub>6</sub>	C <sub>2</sub> H <sub>2</sub>	C <sub>2</sub> H <sub>4</sub>	C <sub>2</sub> H <sub>6</sub>		
DBD	He 50 % – CH <sub>4</sub> 50%	100	262.5	17	0.93	7.93	81.47	0.15	1.34	13.84	-	[67]
		350	262.5	20	3.41	11.18	73.01	0.68	2.23	14.60	-	
DBD	He 90 % – CH <sub>4</sub> 10%	-	2.26	5	9	8	49	0.45	0.40	2.45	-	[47]
Gliding arc	Ar 70 % – CH <sub>4</sub> 30 %	-	7.81	35	95			37.83			35.27	[26]
Micro DBD	Ar 75 % – CH <sub>4</sub> 25 %	-	9.84	29.2	20.1		35	5.86		10.22	-	[32]
DBD	Ar 90 % – CH <sub>4</sub> 10 %	-	-	6.9	4.9	8.7	37.5	0.33	0.60	2.58	-	[79]
DBD	Ar 90 % – CH <sub>4</sub> 10 %	-	2.46	13	8	6	31	1.04	0.78	4.03	-	[47]
DBD	Kr 90 % – CH <sub>4</sub> 10 %	-	2.57	23	4	4.5	33	0.92	1.03	7.59	-	
DBD	Xe 90 % – CH <sub>4</sub> 10 %	-	2.51	22	10	6	35	2.20	1.32	7.70	-	
DBD	Ne 90 % – CH <sub>4</sub> 10 %	-	1.55	7	10	7	31	0.7	0.49	3.1	-	

The ratio of methane/noble gas is an important parameter and can have adverse effects on the plasma reaction. In their study, Wang *et al.* [32] showed a decrease in both methane conversion and selectivities to acetylene and ethylene while ethane selectivity increased when the CH<sub>4</sub>/Ar ratio increased in a micro DBD plasma. High content of methane in the feed favors its dissociation into methyl radicals and recombination in ethane. Under low CH<sub>4</sub>/Ar ratio, Penning dissociation phenomenon is favored and methane dissociates to CH<sub>3</sub> and further to CH<sub>2</sub> and CH radicals, promoting recombination into acetylene and ethylene.

In their glidarc reactor [26], Hu S. *et al.* also reported a decrease in methane conversion (from ~45 % to ~28 %) and total C<sub>2</sub> selectivities with the increase in CH<sub>4</sub>/Ar ratio. They observed deposited carbon on the electrodes, whose amount increased with the reaction time. At low carbon content, an increase in C<sub>2</sub> selectivity was observed. The authors suggested that the reaction mechanisms involved an equilibrium between the following species: C<sub>2</sub>H<sub>2x</sub> ↔ 2CH<sub>x</sub>• ↔ 2C• + 2xH•, depending on the carbon content.

Noble gases do not undergo chemical transformation, they mostly act like energy carriers for the reaction and they will modify the methane activation mechanism during the plasma treatment. Generally, a noble gas can affect methane conversion by increasing the electron temperature and the density of electrons and active species. Atomic hydrogen plays a key role in the methane plasma chemistry, with hydrogen abstraction by H atoms being an important channel for further dehydrogenation.

## 2.2. Plasma-alone for the oxidative coupling of methane

Within the vast literature involving the partial oxidation of methane, oxygen, carbon dioxide and water have been used as additives to promote the efficiency of the process and selectivity to end products. In this section, publications that reported the production of C<sub>2</sub> compounds are reported. In the production of C<sub>2</sub> hydrocarbons, the DBD plasma reactors present both

advantages and drawbacks. When pure methane is used as a feed, a major issue is the coke formation and the carbon deposition on the surface of the electrode and/or dielectric, which will impact the power. In this case, the number of discharge streamers is reduced, thus limiting the number of energetic electrons that interact with the feed gas in the discharge zone, which consequently lowers the methane conversion. For this reason, several studies [47,59,62] have attempted to reduce the coke formation by adding an oxidant to the discharge feed. Despite the low improvements in yield of C<sub>2</sub> compounds, mostly ethylene, hindering a cost-effective upscaling, active research in this field has resulted in reliable mechanisms understanding [8].

## 2.2.1. Effect of the oxidant nature: oxygen with methane

### 2.2.1.1. Plasma chemistry

C-H bond dissociation is the rate determining step in methane activation. One advantage of plasma reactivity comes from its electronic activation of molecules. The process, though, requires a large amount of energy to trigger inelastic electron collisions, which is partially lost *via* molecular collisions, which is responsible for the low energy efficiency of the methane dissociation [33]. The high activation energy (440 kJ mol<sup>-1</sup> at 298 K) makes electronic methane dissociation a slow reaction. This can be counteracted by adding oxygen which, even if present in traces, can induce exothermic reactions. The presence of oxygen in a plasma results in the formation of ionic species (O<sup>+</sup>, O<sub>2</sub><sup>+</sup>, O<sup>-</sup>, O<sub>2</sub><sup>-</sup>, O<sub>3</sub><sup>-</sup>), excited neutrals (O<sup>\*</sup>, O<sub>2</sub><sup>\*</sup>, O<sub>3</sub><sup>\*</sup>) and ozone [80].

O<sup>-</sup> formation occurs via dissociation followed by electron attachment reaction [42,81]:



Ionisation reaction provides O<sub>2</sub><sup>+</sup> species:



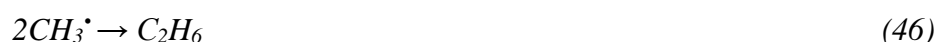


Kogelschatz *et al.* [42,80] showed that in oxygen plasma in micro DBD, about 80 % of the electron energy went into the dissociation process in E/N range of 100-200 Td. In their publication, Liu *et al.* [22] specified that in corona discharge at low input voltages, *i.e.* low reduced electric field, O<sup>-</sup> formation reaction is the determining step. Increasing the voltage will enhance the reduced electric field and mean electron energy, increasing in consequence the concentration of O<sup>-</sup> and dissociated radicals, promoting succeeding reactions. The authors suggested a “saturation” ionization rate in their corona system that may limit the rate of conversion. They reported the following reactions:

Methane radical formation:



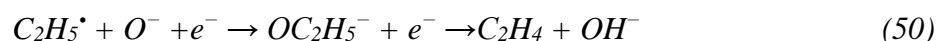
Ethane formation:



Ethylene formation:



Oxidative dehydrogenation of ethane:



Formaldehyde formation:



Higher hydrocarbons formation (M is a third body):



H<sub>2</sub>O formation:





CO<sub>x</sub> formation:



Based on optical emission spectroscopy results and kinetic data of combustion modeling, it was proposed that the reaction  $O(^1D) + CH_4 \rightarrow OH^{\bullet} + CH_3^{\bullet}$  plays a key role in plasma methane conversion [82]. Moreover, the authors showed that the activation degree of oxygen was increased by using a single dielectric plasma reactor and an arc discharge plasma reactor. Zhang *et al.* [68] studied in an AC DBD reactor the effect of an external temperature on the partial oxidation of methane in excess of nitrogen. Not only did they confirmed the electron-induced chemistry, but they also include thermal activation (up to a limit) for methane and oxygen conversion. From their results, they suggested that methane partial oxidation is mainly governed by the electron density at a given temperature and E/N, the reaction rate of the electron impact dissociation being proportional to the electron density. Once external heat was brought to the system, methane and oxygen conversion increased up to a temperature limit (773 K) then dropped. At this temperature, the plasma shifted from a filamentary discharge mode to a resistive power loss mode (from Lissajous observation). Selectivity to product was only linked to thermo-chemistry since it remained unchanged with the increase in energy input or E/N intensity. The increase in the background temperature from 273 K to 773 K improved carbon

monoxide and carbon dioxide selectivities, while hydrogen and C<sub>2</sub> selectivities dropped, due to the change in plasma resistance at high temperatures.

#### *2.2.1.2. Influence of the oxygen-methane ratio*

The addition of oxygen at different concentrations in the gas mixture affects the conversion and selectivities to C<sub>2</sub>, oxygenated compounds and syngas. The low energy threshold for oxygen dissociation produces reactive atomic oxygen species which improve methane conversion and reduce carbon deposition. The heat released from exothermic oxidation reactions also promotes thermo-chemical reactions. However, these reactions are only beneficial at low ratios where they supplement the electron/methane dissociation reactions. At high levels of oxygen, the reduction of the average electron temperature and reaction of oxygen with carbon favor syngas and carbon dioxide selectivities at the expense of C<sub>2</sub>.

The effect of the methane-oxygen ratio was reported in a study using negative DC glow discharge for ethylene production [83]. At relatively low oxygen content (20-25%), the conversion of methane reached a maximum at ~20 % with 46 % selectivity in acetylene and ethylene (Table 9). A complete suppression of carbon filaments that were observed in the absence of oxygen was achieved. At high oxygen content (above 30 %), the methane conversion dropped due to the increased collisions between energetic electrons with oxygen rather than methane. The C<sub>2</sub> selectivity also dropped and a shift of acetylene and ethylene selectivity to ethane was observed. The authors suggested that, under high oxygen content, the energy of the free electrons would be lower than under low oxygen content, at the same energy input. Methane dissociation into methyl radicals would be favored with subsequent dimerization in ethane. While, at low oxygen content, the higher electron collision with methane would favor its conversion into CH<sub>2</sub> radicals and increase ethylene production.

Methane-oxygen activation using DBD plasma was investigated [47] in the presence of noble gases. The oxidative methane conversion experiments were performed with either 1 % or 5 % oxygen in 10 % methane diluted in argon, at a constant applied voltage of 5 kV.

Table 9: The oxygen concentration effect on methane conversion and product distribution

Type of plasma	Gas	SEI (kJ L <sup>-1</sup> )	CH <sub>4</sub> conversion (%)	Selectivity (%)						CB (%)	Ref
				*C <sub>2</sub> H <sub>2</sub>	*C <sub>2</sub> H <sub>4</sub>	*C <sub>2</sub> H <sub>6</sub>	CO	CO <sub>2</sub>	H <sub>2</sub>		
DC glow discharge	CH <sub>4</sub> /O <sub>2</sub> =1:1	#2.25	**17	26	46	-	<5	■0.2	-	[83]	
	CH <sub>4</sub> /O <sub>2</sub> =2:1		**12	27	47			■0.3			
	CH <sub>4</sub> /O <sub>2</sub> =3:1		**21	37	48	<1	■0.6				
	CH <sub>4</sub> /O <sub>2</sub> =4:1		**21	46	44		■0.8				
	CH <sub>4</sub> /O <sub>2</sub> =1:0		**10	41	49	0	■0.4				
DBD	CH <sub>4</sub> -Ar	1.53	7.5	**4.5	**5.5	**45	-	-	65	77	[47]
	CH <sub>4</sub> -Ar-O <sub>2</sub> (1 %)	1.77	11	**2.5	**2.8	**13	65	20	40	100	
	CH <sub>4</sub> -Ar-O <sub>2</sub> (5 %)	1.92	10.5	**2.5	**2.8	**1	80	20	18	100	

# SEI was calculated as a product of voltage and current considering the total flow rate [83]

\* Selectivity was calculated considering the results of conversion and yield reported in the figure.

■ yield of hydrogen (%)

\*\* Approximate from the figure

The addition of oxygen (1 %) slightly enhanced methane conversion, which decreased to 5 %.

A small amount of oxygen improved methane conversion *via* electron impact dissociation reactions and reactions with reactive atomic oxygen. Thermo-chemical reactions also took place due to the heat released by the exothermic oxidation reactions. However, at higher oxygen content, methane conversion was limited by the reduction of the average electron temperature. The introduction of oxygen did reduce carbon formation (improved carbon balance) but, at high content, the selectivity to C<sub>2</sub> species, especially ethane was shifted to syngas formation (Table 9). The drop in hydrogen selectivity was due to its reaction with oxygen to form water.

Aghamir *et al.* [84] studied the effect of the methane-oxygen ratio diluted in helium on the methanol and C<sub>2</sub> selectivities in a DBD reactor. The methane flow rate was kept constant, while oxygen flow rate was adjusted with helium to maintain a total flow rate of 100 ml min<sup>-1</sup>. The conversion of methane improved slightly from 7 % to 12 % when the O<sub>2</sub>/CH<sub>4</sub> ratio increased from 0.1 to 1. The highest methanol and ethylene selectivities were obtained at low oxygen

content ( $O_2/CH_4 = 0.05$ ), while (surprising result) neither ethane nor acetylene were detected (Figure 3 **Erreur ! Source du renvoi introuvable.**). The authors based their argumentation on the production of  $O_2^-$  and  $O^-$  active species from electron impact reactions. On one, side the active oxygen species improved methane dissociation into methyl radicals and the production of ethylene, while on the other side,  $OH^-$  from  $O^-$  reaction with hydrogen would promote methanol production.

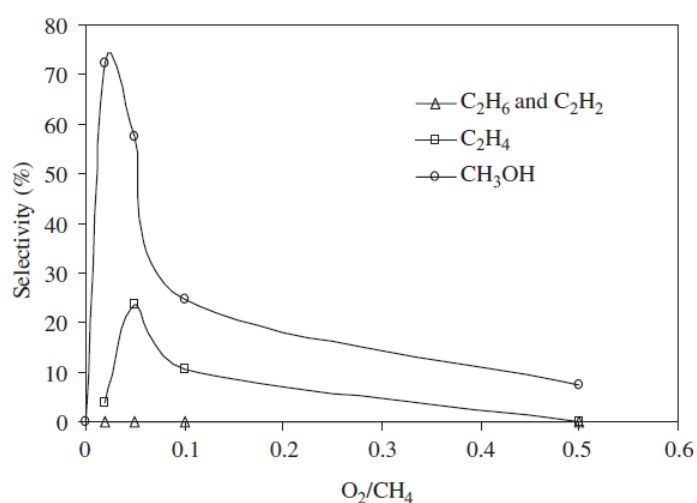


Figure 3: Effect of oxygen/methane ratio on product selectivity. Feed: methane, helium and oxygen, Methane flow rate:  $44.3 \text{ ml min}^{-1}$ . Applied voltage: 23 kV [84]

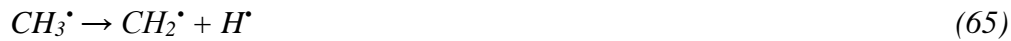
## 2.2.2. Effect of the oxidant nature: carbon dioxide and methane

### 2.2.2.1. Plasma chemistry

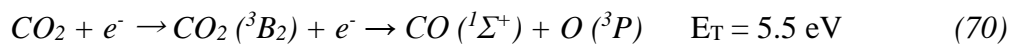
The use of carbon dioxide as a milder oxidant can, in some cases, be preferable to favor the desired end products, as summarized in different reviews [36,85,86]. Puliyalil *et al.* [36] discussed the fundamentals behind methane and carbon dioxide activation in non-thermal plasmas, as well as the ensuing mechanistic routes of excited species recombination to valuable products. Methane dissociation into methyl radicals requires electron energies of 4.45 eV [87]. To lose more than one hydrogen, higher electron energy is needed to produce  $CH_2$  and  $CH$  radicals ( $\sim 10$  eV), while the oxidants have lower dissociation energies (5.5 eV for carbon dioxide and 5.1 eV for oxygen). Non-equilibrium plasmas can provide electrons with energies

up to 10 eV [36], but they are scarce and it is most likely that methane further dissociation will occur *via* thermal dehydrogenation or reaction with excited species of carbon dioxide. Methane conversion increases under the influence of the reactive oxygen species arising from carbon dioxide. A mechanism proposed by Istadi *et al.* [85] relates the removal of H atom from methane to generate methyl radicals that subsequently react with excited species from carbon dioxide in the plasma zone. Co-feeding methane and carbon dioxide favor their respective conversion.

Ozkan *et al.* [88] described the reaction pathways for the formation and consumption of intermediates and value-added products from methane and carbon dioxide. Hydrogen is produced from numerous reactions, *via* radical or electron-induced dissociation of hydrocarbon species.



Carbon monoxide formation comes from carbon dioxide electron-induced excitation, which is the most important reactions in carbon dioxide splitting. Electron attachment, dissociation and ionization of carbon dioxide are others activation reactions that take place in a plasma [89] :



The dissociative recombination of  $CO_2^+$  ions can produce carbon monoxide and oxygen radical, but it requires first to overcome a high energy barrier for  $CO_2^+$  formation [89–91]:



It can also lead to carbon and oxygen or simply return back to carbon dioxide :



In presence of methane radicals, oxygen and methyl radicals as well as hydrogen will be consumed to produce carbon monoxide:

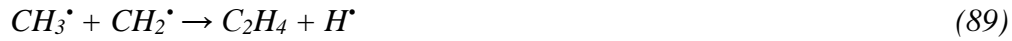


Ethane is generated from different pathways. The most probable is the recombination of two  $CH_3$  radicals (reaction 83). Ethane can also be formed *via*  $C_2H_5$  radicals (reactions 84 and 85). However, another study with an atmospheric DBD source has shown that the density of  $C_2H_5$  radicals is lower than the density of  $CH_3$  radicals, thus the formation of ethane is less probable [73].



The electron-induced dissociation of ethane into  $C_2H_5$  and H radicals, followed by a second electron collision with  $C_2H_5^*$  results in a hydrogen loss and the production of ethylene.

Additionally, ethylene can be produced from hydrocarbon species reaction with oxygen radicals or from recombination reactions.



The addition of noble gases (e.g. argon and helium) in methane-carbon dioxide plasmas provides a dilution degree and the new active species formed may speed up the reactions, as observed in non-oxidative processes. They will act as third body molecules, providing charge transfer to carbon dioxide and methane, improving their conversion. Moreover, the rather low breakdown potential of argon and helium increases the density of micro-discharges and electrons in the plasma and may improve oxygenates yield [86].

Janeco *et al.* [92] evaluated the role of helium in a kinetic model study of a DBD plasma. They showed that the addition of helium to CH<sub>4</sub>/CO<sub>2</sub> mixture led to significant changes in the electron kinetics. The elastic collisions in helium induced a shift of the electron velocity distribution function and led to an increase in the electronic excitation and ionization frequencies in methane and carbon dioxide. Moreover, the ionization reactions involved collisions between methane, carbon dioxide and their products, but not helium.

Changes in electron kinetics were also illustrated by Goujard *et al.* [79] in a coaxial DBD reactor, who showed that the addition of helium to a methane and carbon dioxide feed modified the physical parameters (discharge energy) and the chemical reactivity (reactants and products selectivity) of the plasma discharge. At a fixed contact time, the conversions of methane and carbon dioxide increased with the amount of helium in the gas mixture. The dilution with



helium greatly enhanced the selectivity to syngas, while the selectivities for higher hydrocarbons decreased significantly.

The overall spatially and time-averaged mean electron energy was calculated in a one-dimensional fluid model on a cylindrical DBD reactor for pure methane (2 eV), oxygen (1.6 eV) and carbon dioxide (2.1 eV) [93]. The calculations of the mean electron energy and ion (positive and negative) densities showed that methane with oxygen plasma possesses the highest density of negative ions and is more electronegative than with carbon dioxide. It resulted in a change in selectivity to products. Hydrogen peroxide, methanol, ethanol, methyl hydroperoxide (CH<sub>3</sub>OOH), and ethyl hydroperoxide (C<sub>2</sub>H<sub>5</sub>OOH) were the highest with oxygen. When the gas was switched to carbon monoxide, hydrogen, formaldehyde, acetaldehyde, ketene or ethenone (CH<sub>2</sub>CO) and higher hydrocarbons (C<sub>x</sub>H<sub>y</sub>) were favored.

Within the published data, only a few models have been proposed due to the complexity of linking discharge characteristics (in terms of small volume and extremely short time frame) to the chemical kinetics occurring in the whole reactor in a wider time range [92].

#### 2.2.2.2. Influence of the specific input energy

As already reported, a high SEI results in an increased probability of the collision of reactant molecules with highly energetic electrons and active species, resulting in increased conversion. In their review, Istadi *et al.* [85] reported the effect of input energy in various DBD reactors, including power and residence time modifications. At low discharge power, carbon dioxide conversion is higher than methane due to its lower dissociation threshold energy. By increasing the discharge power, electrons with higher energy are produced, improving the methane conversion and altering the selectivity to hydrocarbons. The authors reported several publications where high power led to a temperature increase in the discharge channel, shifting the selectivity of C<sub>2</sub>-C<sub>3</sub> hydrocarbons and oxygenates to C<sub>4</sub>-C<sub>5</sub> hydrocarbons, via thermal reactions. High power resulted also in a lower energy efficiency of the process and in coke

formation, which is a critical problem. Moreover, some publications were ambiguous when looking at products distribution, in particular the H<sub>2</sub>/CO ratio and hydrocarbons selectivity. As example, Liu *et al.* [94] reported an increase of the H<sub>2</sub>/CO ratio, with constant carbon monoxide selectivity, implying a decrease of the H/C ratio of hydrocarbons with increased power, while Song *et al.* [95] reported constant hydrocarbons selectivity and H<sub>2</sub>/CO ratio. In their review, Istadi *et al.* [85] reported that the change in residence time does not affect the H<sub>2</sub>/CO ratio, that would depend mainly on the CH<sub>4</sub>/CO<sub>2</sub> ratio.

Similarly to their study on partial oxidation, Zhang *et al.* [69] studied the dry reforming reaction on the same AC DBD reactor with the addition of external heat. They reported the same effects, i.e. the electron induced chemistry for methane and carbon dioxide dissociation, while selectivity to products was dictated by thermo-chemistry. Methane and carbon dioxide conversion increased with the SEI (increased input power), while selectivities to carbon monoxide, hydrogen, ethane and propane were not altered. When the temperature was increased to 773 K, the selectivity to syngas dropped as the selectivity to hydrocarbons rose. CH<sub>2</sub> and CH species are assumed to be produced by thermal dehydrogenation. The same effects on methane and carbon dioxide conversion and hydrocarbons selectivity were observed on a nanosecond pulsed DBD plasma by Mei *et al.* [96], except that the H<sub>2</sub>/CO ratio decreased with power.

The influence of the specific energy input was also studied in a gliding arc reactor by varying the input power (Table 10) [27]. The increase in the SEI led to an increase in both methane and carbon dioxide conversions, while the acetylene and ethylene selectivities decreased. The selectivity to acetylene was always higher than the selectivity to ethylene, which was explained by the lower bond dissociation energy of CH<sub>2</sub>CH-H (4.76 eV) [97] compared to CHC-H (5.71 eV) [98], thus leading to further dehydrogenation. No ethane was reported, due to the higher temperature of GAD compared to DBD or pulsed glow reactor, which led to a rapid dehydrogenation of ethane.

Table 10: Influence of the SEI on the methane and carbon dioxide conversions and main product selectivities.  $CH_4/CO_2$  ratio = 2/1. \*Approximated values from the graph; \*\* SEI in  $kJ L^{-1}$  (based on feed flow rate)

P (W)	SEI** $kJ L^{-1}$	Conversion ( $mol h^{-1}$ )		Selectivity (%)				
		CH <sub>4</sub>	CO <sub>2</sub>	CO	H <sub>2</sub>	C <sub>2</sub> H <sub>2</sub>	C <sub>2</sub> H <sub>4</sub>	Coke
205.3	0.96	* 1.8	* 0.5	26.41	72.76	37.81	20.39	15.38
315.0	1.48	* 2.2	* 1.2	20.41	62.99	26.46	14.37	38.76
418.8	1.97	* 3	* 1.6	20.34	57.91	23.33	13.20	43.13
531.8	2.51	* 4.2	* 1.8	18.44	44.83	18.26	10.80	52.50

The coke deposition on the electrodes was high at elevated power and in excess of methane. The coke deposition inhibited the insulating properties of the Teflon plates covering the gliding arc electrodes. This not only led to plasma instability but also to a discharge between the Teflon and the electrodes, ensuing safety issues (arc).

Uytendhouwen *et al.* [99] carried out a systematic study on the effect of the DBD reactor geometry on the methane coupling reaction by varying the shape and size of the reaction zone and the gas flow direction in a mixture of carbon dioxide and methane. They reported that a short and wide configuration with seven inlets - seven outlets placed in front of each other performed better than a traditional configuration with a long and narrow geometry. They also stated that in a one inlet-one outlet reactor with a flow from the bottom to the top, the traditional long configuration resulted in methane conversion of 13.7%. With the same residence time but in a shorter and wider reactor configuration methane conversion increased slightly to 14.9%. This was explained by the reduced gas velocity in short but wide reactor, allowing a better diffusion and mixing of reactants and products. As expected, methane conversion was found to be dependent on the input power and the residence time. In the pursuit of investigating the effect of SEI, it was found that increasing the residence time favored methane and carbon dioxide conversion since SEI increased.

### 2.2.2.3. Influence of methane/carbon dioxide ratio

The hydrocarbons selectivity was found to be strongly dependent on the molar ratio, as it was observed with oxygen (Table 11). In a study by Pham *et al.* [100], the production of syngas was favored, the carbon monoxide selectivity being equal to ~70 %, when a stoichiometric mixture of methane and carbon dioxide was used in a DBD reactor (Figure 4).

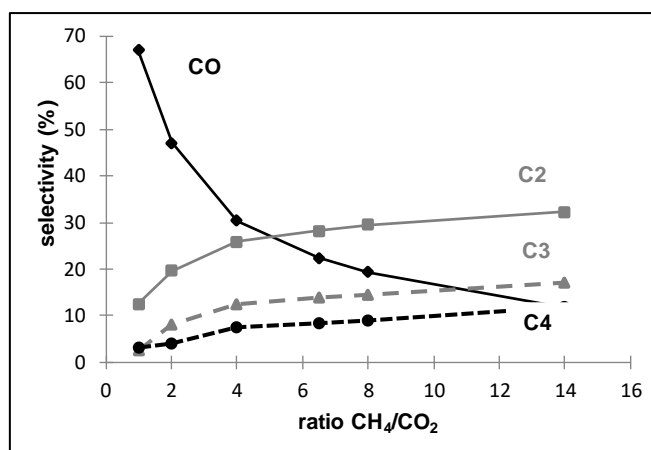


Figure 4: Selectivity to products as a function of the CH<sub>4</sub>/CO<sub>2</sub> molar ratio. Conditions: flow rate: 80 mL min<sup>-1</sup> ; power= 40 W [100]

The hydrocarbons selectivity (from C<sub>2</sub> to C<sub>4</sub>) became important in excess methane. Within C<sub>2</sub> products, ethane selectivity reached 23 % with a ratio equal to 6.5, whereas ethylene and acetylene selectivities were lower than 3 %. The production of hydrocarbons was concomitant with carbon deposition, mainly with a high molar ratio (carbon balance = 75 %). The methane conversion was not strongly modified by the gas ratio, which was close to 20 %.

In a coaxial DBD reactor [101], methane conversion was dependent on the molar ratio, which increased in excess of carbon dioxide. Following the same trend, the hydrogen selectivity increased to nearly 100 % and the carbon monoxide selectivity to 72 %. However, the selectivity of ethane decreased by a factor of 2 while its yield was quite independent of the ratio. It appeared that methane conversion, selectivities and yields of carbon monoxide and hydrogen are favored in excess of carbon monoxide, preventing the recombination of CH<sub>x</sub> species to produce higher hydrocarbons. A similar trend was reported by D. Mei *et al.* [96] who observed

the improvement of methane conversion, carbon monoxide and hydrogen selectivity in excess of carbon dioxide. The selectivity of ethane was notably enhanced at high ratios.

Activation by pulse corona plasma [102] followed the same trend as DBD plasma. The conversion of methane increased in excess of carbon dioxide. The yield of C<sub>2</sub> hydrocarbons decreased with increasing carbon dioxide content in feed reaching, at 40 % carbon dioxide, a maximum yield of 12.7 %. The acetylene concentration was relatively high within the C<sub>2</sub> compounds but decreased with an increase in carbon dioxide content. Ethane and ethylene were also detected and their concentrations increased with the carbon dioxide content.

Recently, the effect of the ratio was studied using parallel electrodes in a gliding plasma configuration [25]. Following the same trend as discussed above, the conversion of methane increased from 48 % to 55 % with the increase of the carbon dioxide content from ~26 % to ~72 %, while the selectivity of acetylene decreased from 40 % to 8 %. Other hydrocarbons were detected with a lower selectivity: ethylene (1.5–2%), butane (0.2–1.7%), benzene (0.2–3.1%) and the selectivity of ethane was not reported.

Table 11: Comparison of product distribution by varying the CH<sub>4</sub>/CO<sub>2</sub> ratios in different types of plasma. \*SEI as a function of the total feed flow; \*\*Approximated values from graph; in italic from text or table.

Plasma	SEI* kJ L <sup>-1</sup>	CH <sub>4</sub> /CO <sub>2</sub> ratio	**CH <sub>4</sub> conversion (%)	**Selectivity (%)					Ref.
				C <sub>2</sub> H <sub>2</sub>	C <sub>2</sub> H <sub>4</sub>	C <sub>2</sub> H <sub>6</sub>	CO	H <sub>2</sub>	
DBD	30	6.5	25	<3	<3	23	13	-	[100]
DBD	36	9	24	-	-	30	8	45	[101]
		3	29	-	-	28	18	48	
		1	41	-	-	22	37	44	
		0.3	51	-	-	20	58	70	
		0.1	62	-	-	14	74	99	
Pulse corona	72	4	20	88.1	6.9	5	27	-	[102]
Parallel electrode Gliding Plasma		2.76	48	40	1.6	-	38	78	[25]
		2.14	50	45	1.9	-	41	70	
		1	52	21	1.7	-	80	75	
		0.5	55	10	1.6	-	90	55	
		0.4	55	8	1.9	-	90	40	
DBD nanosecond pulsed	23.4	4	16	-	-	28	20	28	[96]
		2	18	-	-	22	28	28	
		1	28	-	-	16	39	28	
		0.5	30	-	-	10	58	32	
		0.25	32	-	-	4	70	39	
One inlet- one outlet DBD	36	6	9.7	-	0.15	1.37	1.68	5.7	[99]
		3	11.7	-	0.13	1.31	3.13	6.1	
		1	15	-	0.09	0.97	6.4	6	
		0.33	20	-	0.06	0.44	8.8	5.6	
		0.16	24.5	-	-	0.26	9.06	5.1	

In their study on the effect of the DBD reactor geometry, Uytendhouwen *et al.* [99] also looked at the influence of the CO<sub>2</sub>:CH<sub>4</sub> ratio (from 6:1 to 1:6) and reported a constant decrease in methane conversion as the carbon dioxide content increased. Carbon dioxide conversion went through a maximum at a 3:1 (CO<sub>2</sub>: CH<sub>4</sub>) ratio with 15 %. Increasing the methane content up to 100% methane improved the hydrocarbon content, which reached 72% of C<sub>2</sub>, 17% of C<sub>3</sub>, 2% isobutane, 5% n-butane and 2% 2-methylbutane. However, in terms of energy efficiency and conversions, they reported an optimum energy cost of 1.5 kWh/mol of reactant mixture at a 3:1 and 6:1 (CO<sub>2</sub>: CH<sub>4</sub>) ratios.

### 2.2.3. Effect of the oxidant nature: water and methane

It is established in the literature that the presence of water vapor consumes electrons to form OH radicals but also species such as  $\text{H}_2\text{O}^-$ , reducing the electrons availability for methane activation. Nevertheless, the use of water vapor inhibits carbon deposition efficiently while stabilizing the discharge.

Kado *et al.* [75] studied the conversion of methane using non-equilibrium pulse discharge in the presence of oxygen, carbon dioxide and water steam. The presence of steam decreased methane conversion and  $\text{C}_2$  selectivity as compared with carbon dioxide as oxidant (Figure 5). The formation of carbon monoxide proved also that reforming reaction occurred in addition to coupling reaction.

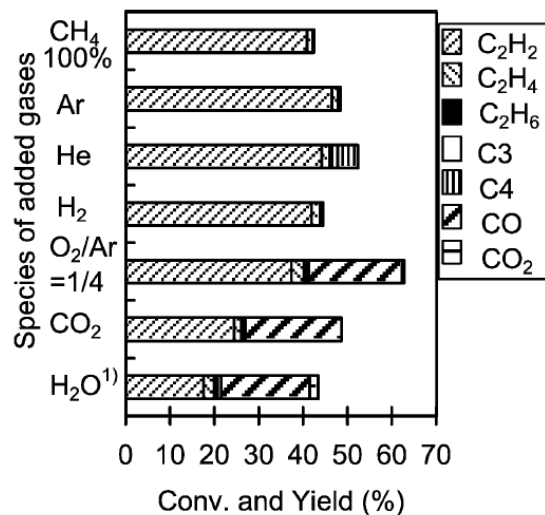


Figure 5: Influence of coexisting gases on products composition, 50 % methane concentration, <sup>1)</sup>150 °C [75]

The conversion of methane in the presence of steam was equally investigated by Zhang *et al.* [59] in a DBD reactor, by changing the power, the gap, the electrode material, the flow rate and steam proportion. A part of the results are presented in Table 12.

Table 12: Effect of flow rate on product selectivities with pure methane and with steam [59].

Flow rate mL min <sup>-1</sup>	Feed	SEI kJ L <sup>-1</sup>	CH <sub>4</sub> conversion %	Selectivity %		
				C <sub>2</sub> H <sub>4</sub>	C <sub>2</sub> H <sub>6</sub>	CO
10	CH <sub>4</sub>	180	38	6.58	38.95	0
20		90	25	6.57	42.75	0
30		60	20	7.60	46.47	0
40		45	15	7.77	46.69	0
10	CH <sub>4</sub> + 19.93 % steam	180	40	3.38	34.26	5.18
20		90	27	3.58	40.83	4.12
30		60	22	3.65	45.16	3.96
40		45	17	4.02	48.20	3.32

The conversion of methane was improved in presence of steam, although the differences were not that significant. The distribution of products, especially ethylene selectivity, was strongly influenced by the presence of the oxidant in the feed. Liu *et al.* [70] studied the steam reforming of methane in a DBD reactor with a controlled external temperature, following the same way as their studies on partial oxidation and dry reforming reaction. They reported the effect of electron induced chemistry and thermo-chemistry (*i.e.* background gas temperature) on the conversions and product selectivities. Water conversion would be dependent on the electron-impact reactions, while methane would be converted by both electron-impact and thermal reactions. Selectivity to ethane was found to be dependent on thermo-chemistry.

### 2.3. Comparison of plasma-alone non-oxidative and oxidative methane coupling

Different input parameters have been studied in order to achieve high CH<sub>4</sub> conversion and olefin yield. As already mentioned, the main products of methane conversion are acetylene, ethane, ethylene, hydrogen and carbon. Data presented in the literature concerning the carbon balance or product yield (mainly hydrogen) is incomplete, since, most of the time, the information is missing. The large number of plasma sources that have been studied for direct methane conversion to added value products makes it difficult to draw an objective comparison between



them when plotting C<sub>2</sub> selectivity versus methane conversion (Figure 6). Nevertheless, pulsed discharges reach the highest C<sub>2</sub> selectivities with methane conversion around 40 %.

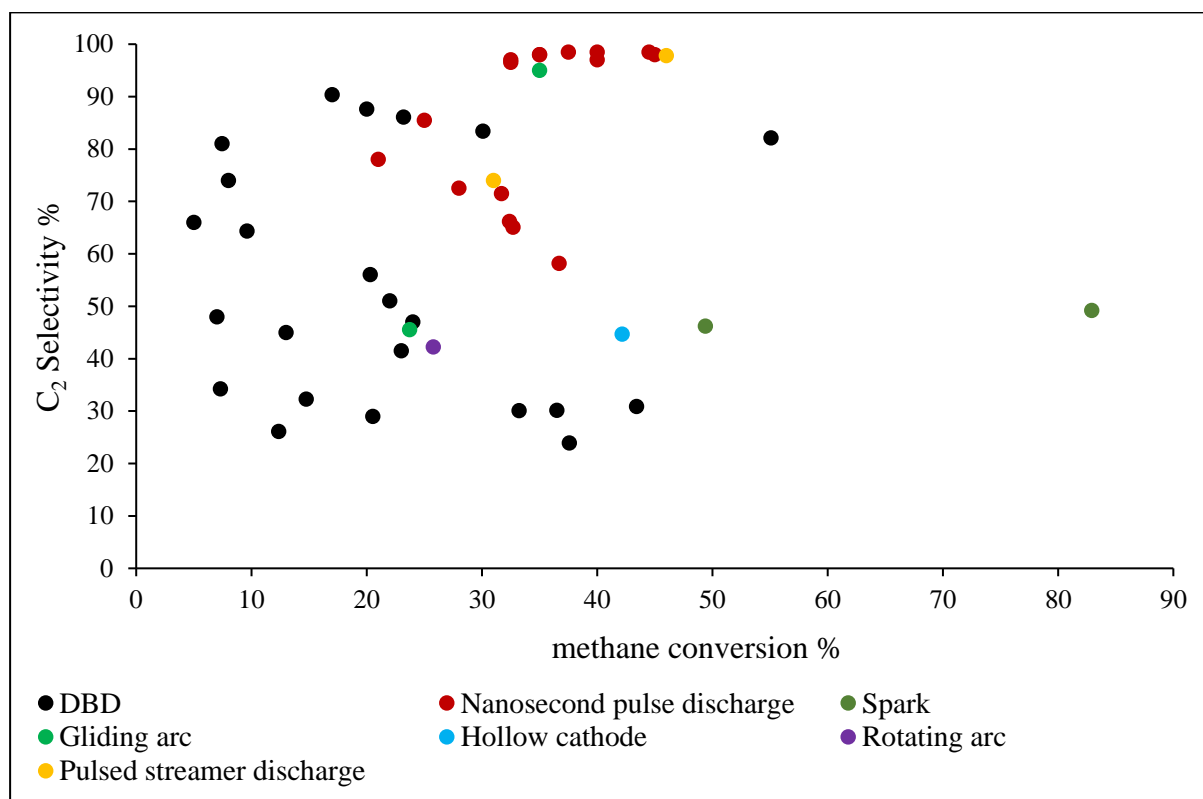


Figure 6: C<sub>2</sub> selectivity as a function of methane conversion in non-oxidative methane coupling with different plasma sources

It was shown from published work that methane conversion is mainly improved by the high electron energy (which depends on the reduced electric field strength) and to thermal effect. Each type of plasma provides a range of electron density and reduced electric strength on which reactivity will depend (Table 13). Due to their simple design and ease of implementation, most of the research to date has been performed with DBDs. To improve the conversion and the product distribution, several approaches have been investigated, including changing the residence time, the applied voltage, the pulse frequency and duration, the gap, the pressure, using different electrode materials and/or mixing with other gases. All those parameters *in fine* altered the SEI. While not present in every publication reported, the specific energy input (SEI) represents a suitable parameter to compare the data.

Specific Energy Input (SEI), is defined as the deposited energy per mole (or liter) of methane and can be estimated as:

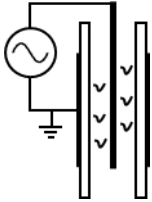
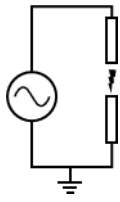
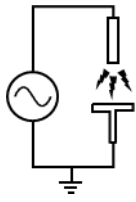
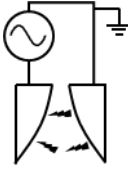
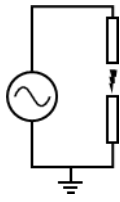
$$SEI (kJ mol^{-1}) = 1345 (s L min^{-1} mol^{-1}) * \frac{Power (W)}{Flow feed (mL min^{-1})}$$

$$SEI (kJ L^{-1}) = 60 (s min^{-1}) * \frac{Power (W)}{Flow feed (mL min^{-1})}$$

With molar volume of 22.4 L mol<sup>-1</sup>

Increasing the SEI not only increases the dissociation reaction rate but also the heat dissipation, which will depend greatly on the plasma source (Figure 7). However, the product selectivities are generally dependent on the SEI. The best conversions were obtained with spark discharges, but pulsed discharges were reported to have the best C<sub>2</sub> selectivities at relatively high conversions (40-50 %) as compared to DBD. It appears that most of the DBD plasma results in methane conversion below 40%, with C<sub>2</sub> selectivity oscillating between 20 % and 60 % for the majority. In fact, DBD favors ethane formation and a little C<sub>3</sub>, C<sub>4</sub> compounds, owing to its low electron density and temperature. When the electron density and energy increases, by increasing the reduced electric field, methane fragmentation shifts from CH<sub>3</sub> radicals to CH<sub>2</sub>, CH radicals and C and favor C<sub>2</sub> products formation. The pulsed nanodischarge approach seems promising as it results in high energy efficiency due to the presence of high energy electrons over a very short pulse duration (usually < 500ns).

Table 13: Properties of plasma in different reactor types. Electron energy and temperature (Temp.), gas temperature values were taken from [42,63,103]; glidarc values from [36]. Schemes were modified from [36]

Reactor type	DBD	Spark	Corona	Gliding arc	Arc
<b>Scheme</b>					
<b>Electron Temp. [eV]</b>	1–10	2–3	1–5	1.4–2.1	~1
<b>Electron density [cm<sup>-3</sup>]</b>	10 <sup>14</sup>	10 <sup>16</sup> –10 <sup>17</sup>	10 <sup>11</sup> –10 <sup>13</sup>	10 <sup>14</sup> –10 <sup>15</sup>	10 <sup>15</sup> –10 <sup>16</sup>
<b>Gas temperature [K]</b>	Near room Temp.	300–500	Near room Temp.	1000–3000	5 × 10 <sup>3</sup> –10 <sup>4</sup>
<b>Reduced field [Td]</b>	1–500	5–15	2–200	0.5–4	10–100

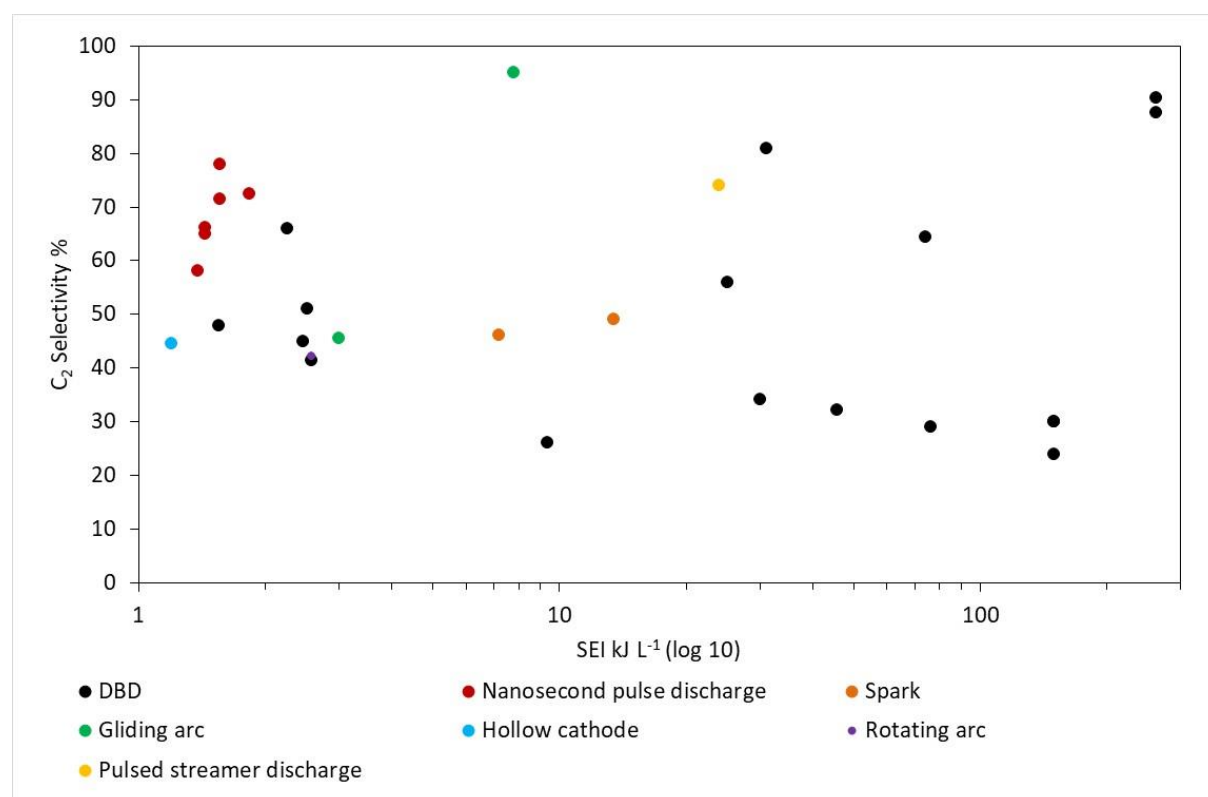


Figure 7: C<sub>2</sub> selectivity in non-oxidative methane coupling in different plasma sources as a function of specific energy input [20,26,32,43,44,47,56,57,60,61,67]

Considering the plasma oxidative coupling of methane, different optimum values for methane conversion and  $C_2$  selectivities have been published. Some publication reported acetylene, ethylene and ethane selectivities separately, but in some cases, only the total  $C_2$  selectivity was given. Figure 8 is an attempt to compare the different sources of plasmas used in the OCM reaction on total  $C_2$  selectivities. The main trend that can be highlighted from Figure 8 is the tendency of  $C_2$  to decrease with the methane conversion for the DBD and corona reactors. It was reported that high methane conversion is linked to high SEI which leads to temperature increase in the discharge channel, shifting the selectivity of  $C_2$  hydrocarbons to  $C_4$ - $C_5$  hydrocarbons, via thermal reactions.

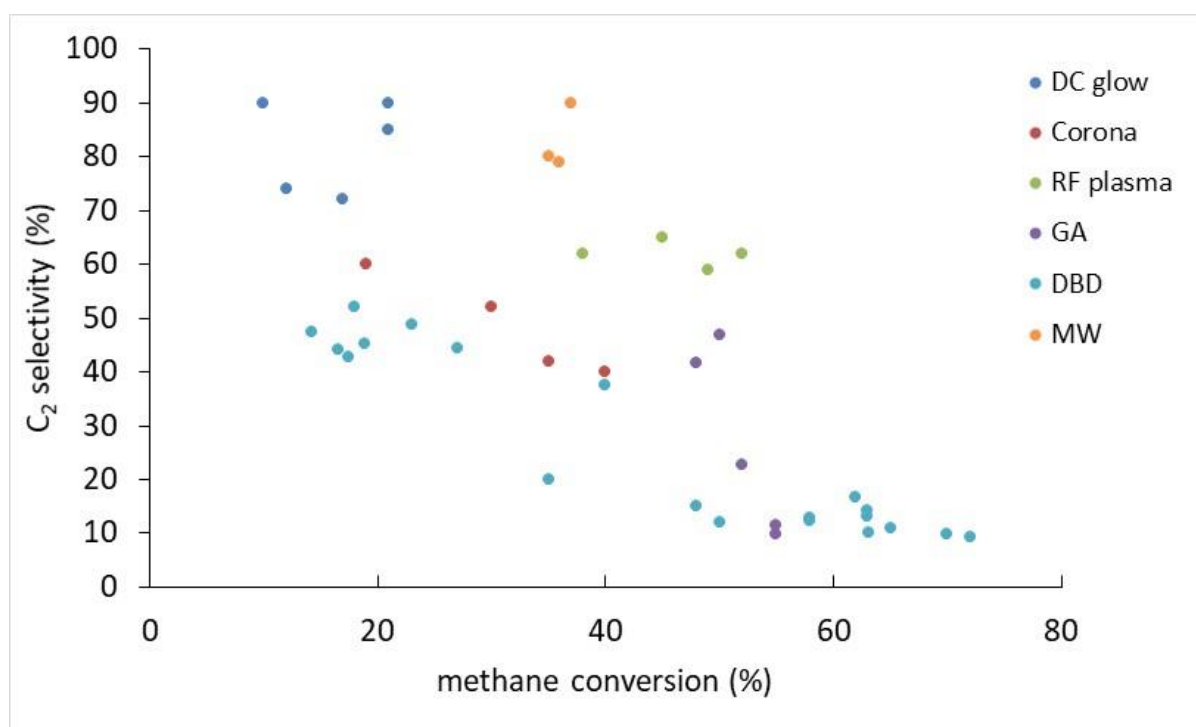


Figure 8:  $C_2$  selectivity as a function of methane conversion for different plasma sources in the OCM reaction. The graph includes the different oxidant gas ratio at various SEI. DC glow consists in a microreactor with SEI:  $2.2 \text{ kJ L}^{-1}$ ; SEI for DBD are above  $100 \text{ kJ L}^{-1}$ ; MW and RF between  $40$ - $60 \text{ kJ L}^{-1}$ ; GA between  $0.4$ - $3 \text{ kJ L}^{-1}$  and Corona SEI was not indicated.

In the case of DBD plasmas, the  $C_2$  selectivity is below 50 %, independently of the type of oxidant or the ratio between the methane and the oxidant. In terms of conversion, however, all of the data shows the same trend, namely conversions superior to 50 % when methane is in

excess in the feed, thanks to the higher collision probability between methane and the plasma active species. The  $C_2$  selectivity in MW and DC glow plasmas is high, with high methane conversion for MW. MW plasma generates a thermodynamic equilibrium at very high temperatures in a very dense plasma in which  $C_2$  species are thermodynamically favored and the most stable.

A comparison between the plasma reaction of methane alone and in presence of an oxidant was performed and the results are presented in Figure 9.

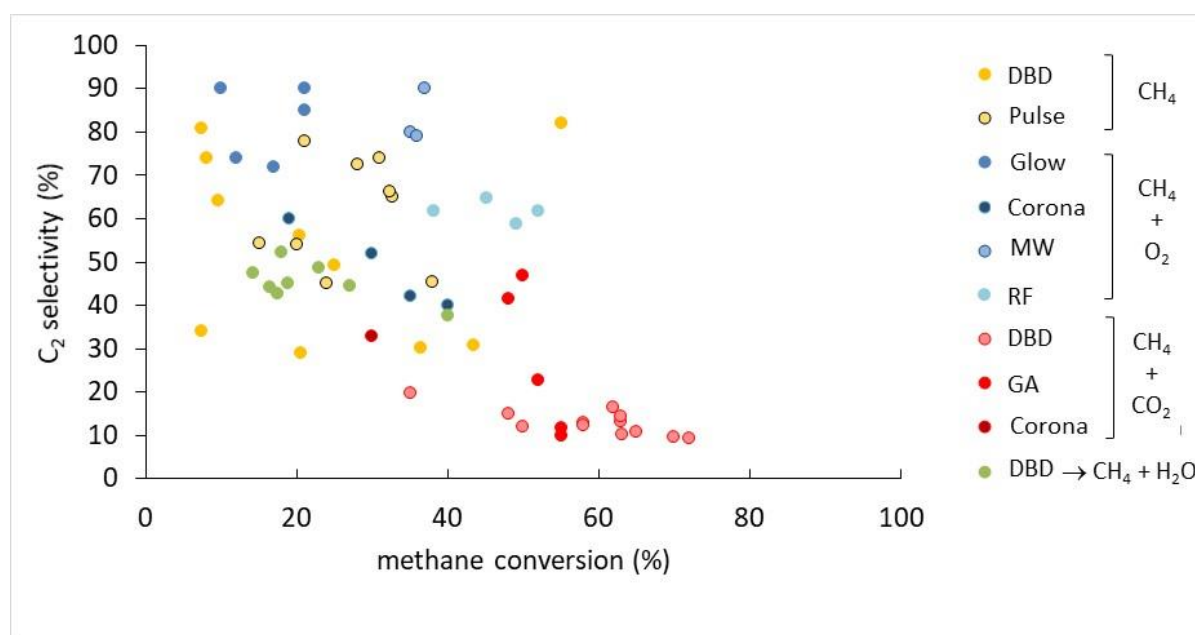


Figure 9: The effect of oxidants on the methane conversion and  $C_2$  selectivity. The yellow dots are for methane alone; in blue dots for oxygen; in red for carbon dioxide and in green for steam. The different color shades highlight the different reactors: glow: micro glow discharge; MW microwave; RF: radiofrequency; GA: glidarc; Pulse: nanosecond pulsed and pulsed spark streamers.

The tendency for  $C_2$  selectivity is similar to the results obtained in absence of oxidant, i.e. the higher the  $C_2$  selectivity, the lower the methane conversion. In OCM reaction,  $C_2$  selectivity is above 50 % for some data, but only for microwave and pulse discharges.  $C_2$  selectivity is also higher for experiments under methane/oxygen when compared to methane /carbon dioxide and is due to differences in the chemical reaction pathways. The oxygen acts as an oxidizer and reacts with methane to form methyl and hydroxyl radicals, reaction (45). Methyl radicals will then subsequently form ethane from recombination (reaction 46) and ethylene from oxidative dehydrogenation of ethane (reaction 49 and 50). On the other hand, when a plasma is generated

in a gas mixture containing methane and carbon dioxide, the main reaction that occurs is the dry reforming of methane to form carbon monoxide and hydrogen as the main compounds and hydrocarbons to a lesser extent.

Pinhão *et al.*[104] linked the plasma reactor to plug flow type reactors where parameters such as particle number, gas volume, concentration of species or volumetric flow rate are altered during the plasma activation. The author proposed two methods to avoid producing approximate results, by integrating either a precise semi-automatic flow measurement with a bubble flow meter or an internal standard (IS) in the process gas. The internal standard method was tested in the case of methane conversion with methane –carbon dioxide mixtures with and without helium but the addition of internal standard interfered with the plasma discharge. The author overcame this problem by inserting the IS at the exhaust of the reactor, upstream from the point of measurement. They found errors up to 20 % on process parameters with volumetric flux changes. They concluded on how process calculations should integrate the changes (*i.e.* gas temperature, volumetric flow rate, presence of condensates) coming from reactions within the reactor.

### **3. Plasma-catalysis for methane coupling**

Many studies looked at the interaction between a plasma and the packing materials inside the discharge region [105–107,31,108] and the results indicated that the discharge characteristics are strongly connected to packing materials that can affect the electric field, the gas breakdown behavior and the electron parameters. A major change concerns the development of the discharge itself. Kim *et al.* [109] published a detailed scheme of the changes induced by the presence of catalyst particles in the discharge volume (Figure 10).

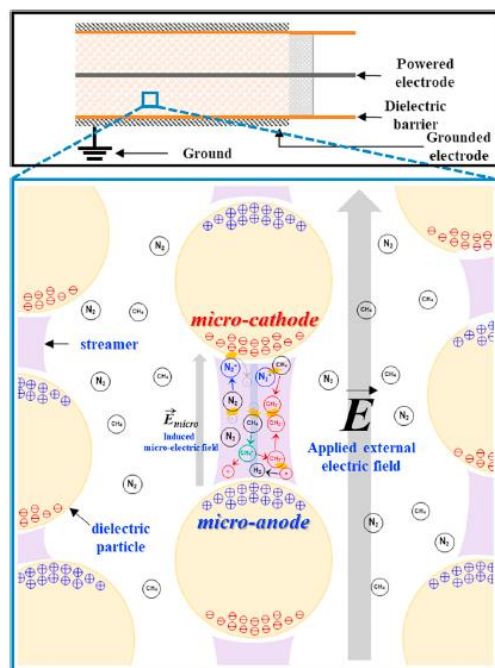


Figure 10: Schematic representation of streamer and reactive intermediates between dielectric particles due to induced micro-electric field. Reprinted with permission from Elsevier [109]

When the high voltage is applied between the electrodes, a micro electric field develops between the catalyst particles, which become micro-anodes and micro-cathodes. Then, micro-discharges are initiated and the electrons between the charged particles collide with methane molecules. In this micro electric field, secondary electrons (generated from the interaction of methane ions with the surface atoms) sustain the plasma discharge.

In a DBD reactor, Tu *et al.* [110] reported, without catalyst, micro-discharges of radii 100-200 $\mu\text{m}$  and 10 ns duration, dispersed in the whole plasma area. The addition of a packed material, filling up the plasma zone, led to a reduction of the plasma volume, interfering with the propagation of micro-discharges. The plasma filaments developed at (and spread over) the surface of the catalyst pellets or beads, resulting in a combination of surface discharge and weak

filamentary micro-discharge. The same authors [111] highlighted that the synergistic effect of plasma-catalysis coupling results from an equilibrium between the modification of the discharge propagation mode and the emerging plasma activity at the catalyst surface. The development of filamentary versus surface discharges would depend on many factors such as particle size, shape and chemical and physical properties, influencing both the propagation and intensity of the discharge.

In practice, it exists a wide range of catalytic materials dedicated to plasma-catalytic coupling and presenting a multitude of pore sizes and dielectric constants. The accessibility of the pore volume is important since the plasma active species might interfere within and modify chemical, physical or structural characteristics. Several computational studies by Bogaerts group, performed in two-dimensional fluid model for atmospheric pressure discharges, have investigated these effects [112–114]. They indicated that the formation of microdischarges is possible when the pores diameter is larger than the Debye length value, between 100 nm to 1 $\mu$ m. This value depends on the electron density and temperature of the plasma streamer. They showed that plasma can diffuse in pores close to 50 nm, corresponding to the upper limit size of mesopores, but to a certain extent and in a very limited time period.

### 3.1. Influence of particle size

Packing catalytic materials in the plasma reactor modifies the discharge electrical properties, such as the electric field strength and electron energy distribution, leading to a modification of the overall performance. Butterworth *et al.* [115] observed both positive and negative effects on the plasma properties by lowering the size of particles in a study on a packed-bed DBD for carbon dioxide conversion. Small particles may limit the formation of the discharge in the reactor volume. Moreover, the decrease in particles size reduces the residence time and increases pressure drop in the reactor at a constant flow rate. Nevertheless, small particle sizes favor the density of contact points initiating discharges, due to an enhanced electric field. It also



increases the interfacial area between the solid and the plasma and enhances the volume fraction of the bed occupied by the plasma. The author highlighted that small particles packed-bed favored surface discharges over filamentary micro-discharges. This conclusion was based on Gallon *et al.* work [111] on methane reforming, which showed that the addition of packed catalyst in a DBD reactor led to a combination of surface discharges on the catalyst and spatially limited micro-discharges in the volume. The absence of catalyst led to strong filamentary micro-discharges. Their conclusions were based on the observation of current signals.

On a MgO/Al<sub>2</sub>O<sub>3</sub> catalyst (specific surface area 184 m<sup>2</sup> g<sup>-1</sup>) in a DBD reactor operating under a CH<sub>4</sub>/Ar flow [116], an increase in CH<sub>4</sub> conversion and C<sub>2</sub> yield was observed with a decrease in the size of particles. It confirmed the dependence of the surface interactions between the plasma active species and the catalyst on the particle sizes. On the other hand, enhancing the contact between the plasma and the catalyst surface favored the formation of solid carbon. The smallest the particle size, the lowest the ethane selectivity and carbon balance.

In a recent publication, Bouchoul *et al.* [117] studied the effect of particle sizes on the C<sub>2</sub> selectivity for the dry reforming of methane reaction using a cylindrical DBD plasma at atmospheric pressure. The important role of particle size (between 900 and 300 μm) on conversions and selectivities was also demonstrated. In particular, the finer the particle size, the better the conversions (of both methane and carbon dioxide) and the lower the selectivity to ethane. They based their conclusion on the development of the plasma in a reactor filled with a catalyst. The plasma discharge would be in two states: 1) plasma in gas phase between the catalyst grains, considered as volume plasma; 2) plasma on the surface of the catalyst (*i.e.* surface plasma). The recorded effect may come from the increase in the total external surface of the smaller catalyst grains, thus favoring the development of the surface plasma and thus catalytic activity. Regarding the secondary reaction products, the larger the grain size, the higher the ethane selectivity, suggesting that the recombination of methyl radicals to form ethane is favored in the gas phase and not at the surface of the catalytic support.

The effect of packed particles was investigated over  $\alpha$ -Al<sub>2</sub>O<sub>3</sub>, sea sand, and KIT-6 and for each material, 3 groups with different sizes were prepared ( $0 < S < 53 \mu\text{m} < M < 100 \mu\text{m} < L < 150 \mu\text{m}$ ) [109]. The data are reported in Table 14. Independently of the nature of the packing material, the maximum methane conversion was achieved in the case of M size particles, as an effect of microelectrodes induced by an external electric field between packed dielectric particles. Acetylene selectivity decreased as the particle size increased. Ethylene selectivity was at its minimum for the M size particles (although the difference was not always significant). The C<sub>2</sub> selectivity was the highest for S particles, most probably due to their high specific surface area. The authors suggested that in the case of small particles (S), CH<sub>2</sub> and CH species had a higher probability of being coupled into unsaturated C<sub>2</sub> hydrocarbons. In contrast, if the size of the particles was large (L) and the space between the particles was also large, the dehydrogenation seemed to occur more frequently than the coupling, which resulted in additional carbon deposition [109]. The increased amount of carbon deposition ensuing from the dehydrogenation reaction seemed to be the result of the increased capacitance of dielectric M particles, leading to a large number of micro-discharges.

This effect was not visible in other studies, like in the case of MgO/Al<sub>2</sub>O<sub>3</sub> particles, since metal-oxide doping affected the micro-discharge efficiency of the system. The addition of MgO caused a difference in the temperature on the surface of the catalyst, resulting in different catalytic activity. In addition, the electric conductivity and surface charge of the catalyst modified the nature of radicals and, in consequence, the product selectivities [116].

Table 14: Results on methane conversion, C<sub>2</sub> selectivities and yields on various catalysts with different mesh sizes

Particles	Mesh size	Feed	SEI (kJ L <sup>-1</sup> )	CH <sub>4</sub> Conv. (%)	Selectivity (%)			Yield (%)			CB (%)	Ref
					C <sub>2</sub> H <sub>2</sub>	C <sub>2</sub> H <sub>4</sub>	C <sub>2</sub> H <sub>6</sub>	C <sub>2</sub> H <sub>2</sub>	C <sub>2</sub> H <sub>4</sub>	C <sub>2</sub> H <sub>6</sub>		
MgO/Al <sub>2</sub> O <sub>3</sub> mesh in mm	0.25	10 % CH <sub>4</sub> in Ar	0.99	23	28	30.3	27.4	6.4	7.0	6.3	71	[116]
	0.5		1.02	16.2	22	25.6	35.5	3.6	4.1	5.8	76	
	1		0.96	9.8	14	23	42.8	1.4	2.3	4.2	80	
	1.75		1.05	9.5	10.0	18.6	48.1	1.0	1.8	4.6	82	
α-Al <sub>2</sub> O <sub>3</sub> mesh in μm	<53	CH <sub>4</sub> :N <sub>2</sub>  1:1, 40 mL min <sup>-1</sup>	66.15	55	46	7	10	25.3	3.9	5.5	98.18	[109]
	53-100		65.25	60	25	6	12	15.0	3.6	7.2	82.70	
	100-150		63.75	45	21	8	23	9.5	3.6	10.4	86.68	
Sea sand mesh in μm	<53		64.5	55	24	5	9	13.2	2.8	5.0	79.97	
	53-100		63	60	19	4	11	11.4	2.4	6.6	75.02	
	100-150		63.45	42	11	5	20	4.6	2.1	8.4	81.10	
KIT-6 mesh in μm	<53		58.5	20	28	14	22	5.6	2.8	4.4	96.84	
	53-100	57.75	52	18	5	11	9.4	2.6	5.7	75.86		
	100-150	54.15	43	17	7	24	7.3	3.0	10.3	85.72		

### 3.2. Influence of the material shape

Jo *et al.* [108] investigated the effects of the surface area and the shape of a packing material to understand how the discharge characteristics are altered in the methane activation reaction. Three different types of  $\text{Al}_2\text{O}_3$  were prepared, as shown in Table 15.

Table 15: Physical characteristics of  $\text{Al}_2\text{O}_3$  beads.  $\gamma\text{-Al}_2\text{O}_3$  grains were prepared from crushing the beads.

Packing material	$\gamma\text{-Al}_2\text{O}_3$ beads	$\gamma\text{-Al}_2\text{O}_3$ crushed beads :16-20 mesh	$\alpha\text{-Al}_2\text{O}_3$ beads
Surface area ( $\text{m}^2 \text{g}^{-1}$ )		151.3	1
Pore volume ( $\text{cm}^3 \text{g}^{-1}$ )		0.44	-
Average pore size (nm)		8.2	no pores on the surface
Diameter (mm)	1	0.85–1.13	1

The discharge was affected by the surface properties of the packed material. A change in the electric field was observed depending on the material placed in the discharge. Both  $\gamma\text{-Al}_2\text{O}_3$  samples showed similar current peaks at a fixed voltage, while  $\alpha\text{-Al}_2\text{O}_3$  beads showed low current peaks. The change in current density modified the electron density and the power.  $\text{CH}_4$  conversion was lower in presence  $\alpha\text{-Al}_2\text{O}_3$  beads. Interestingly, the author reported that methane conversions for  $\gamma\text{-Al}_2\text{O}_3$  beads and crushed beads were identical independently of the applied voltage despite the lower power density when the beads were used. The catalyst shape affected the breakdown voltage (from Lissajous Q-V plots observation), thus changing the local electric field and power (Figure 11).

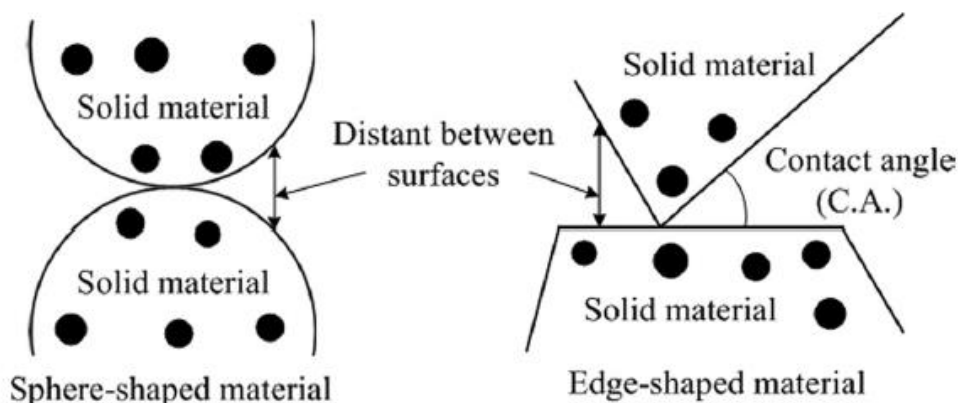


Figure 11: Schematic illustration for characterizing bead- and edge-shaped packing materials [108]

The study proved that, in a DBD reactor, the discharge parameters were strongly affected by the catalyst shape and surface properties.  $\gamma\text{-Al}_2\text{O}_3$  packing proved to be the most efficient in terms of  $\text{CH}_4$  conversion thanks to its lower capacitance compared to  $\alpha\text{-Al}_2\text{O}_3$ , providing both local filamentary discharges in the pores of  $\gamma\text{-Al}_2\text{O}_3$  and surface discharges. However, the authors did not take into account the differences in surface composition and particularly presence of  $\text{-OH}$  groups for  $\gamma\text{-Al}_2\text{O}_3$  [118].

### 3.3. Influence of the dielectric constant

The dielectric constant of the packed material will affect the surface charging, thus the intensity and propagation of the discharge.

Zhang *et al.* [119] reported the importance of surface charging on the plasma propagation inside the catalyst pores with a 2D computational model. They studied the discharge streamer in a cylindrical DBD discharge. They chose characteristic dielectric constants, ranging from 4 to 200, of five metal oxides ( $\text{SiO}_2$ ,  $\text{Al}_2\text{O}_3$ ,  $\text{ZrO}_2$ ,  $\text{TiO}_2$ , and  $\text{CaTiO}_3$ ) with different pore diameters.

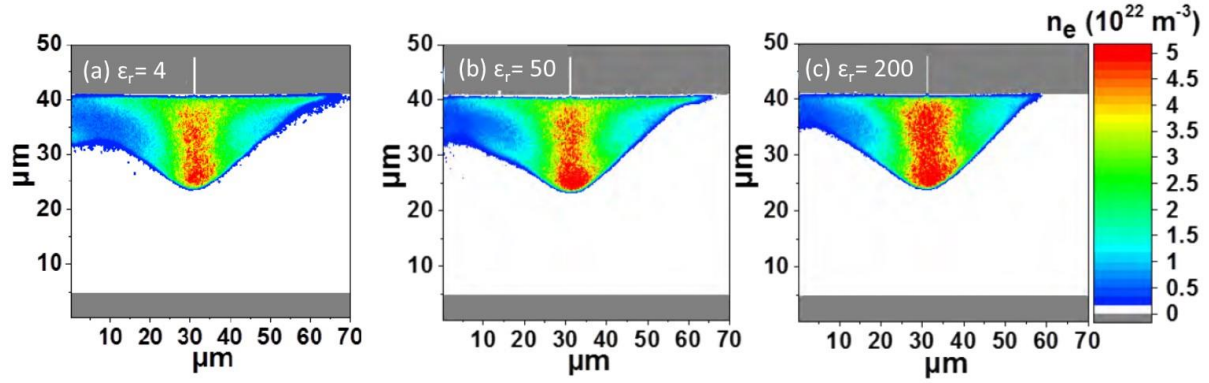


Figure 12: plasma density distribution  $n_e$  ( $\text{m}^{-3}$ ) at 19 ps, for an upper dielectric layer with dielectric constant  $\epsilon_r$  of 4 (a), 50 (b) and 200 (c). The pore diameter is 400 nm [119]

First, they looked at the streamer propagation in the discharge volume. The plasma spreading over the dielectric was reduced as the dielectric constant increased, meaning that the plasma covers a wider area of the dielectric layer at small  $\epsilon_r$  (Figure 12). The direct consequence is a modification of the discharge behavior from a surface discharge to a localized filamentary mode as the dielectric constant increases. Then, they achieved a simulation of the pores and reported the plasma density distribution near and inside the pores, for different pore diameters and dielectric constants. Increasing the dielectric constant led to an increase of the plasma density (maximum at  $\epsilon_r = 50$ ) but to a decrease of the streamer propagation within the pore, due to surface charging. Surface charging occurs when the streamer reaches the pore sidewalls and it depends on the dielectric constant. At  $\epsilon_r < 50$ , surface charging induces surface discharge along the pore sidewalls and favors the streamer propagation in the pores. For  $\epsilon_r > 50$ , dielectric polarization is more pronounced, weakening the surface charging and slowing down the streamer propagation. The discharge is more localized and more electrons will accumulate near the sharp edge of the pore entrance. A moderate  $\epsilon_r$  of 50 showed the highest plasma density with enhanced electric field near the pore entrance, favoring the propagation in the pore.

Taheraslani *et al.* [31] studied methane coupling to  $\text{C}_2$  in a packed bed DBD reactor with materials presenting different porosities and dielectric constants. High dielectric  $\text{BaTiO}_3$

(dielectric constant  $>1000$ ) resulted in a lower conversion of methane (Figure 13) compared to the reactor packed with low dielectric materials  $\delta$ -alumina,  $\alpha$ -alumina (dielectric constant  $\approx 9-10$ ) and silica-SBA-15 (dielectric constant  $\approx 2-5$ ). Silica-SBA-15 catalyst showed a reduced activity compared to  $\alpha$ - and  $\gamma$ -alumina. The authors considered that the high surface area ( $673 \text{ m}^2 \text{ g}^{-1}$ ) and high porosity favored the trapping of charges in the pores of silica-SBA-15, reducing the plasma discharge propagation and electric field. Solid deposits were also observed on SBA-15 which modified the plasma discharge formation and reduced the electric field intensity.

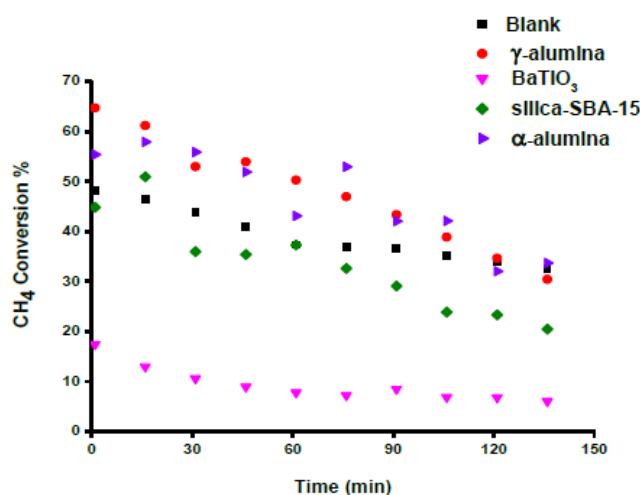


Figure 13: Conversion of methane as a function of time for different packing materials [31]

The author concluded that a high dielectric material with small pores reduces the electric field of the plasma due to the accumulation and mutual polarization of charges inside the pores. Low dielectric materials, despite their very small pores (20 nm for  $\gamma$ -alumina) improved the strength of the electric field, enhancing surface discharge and methane conversion.

Looking at the selectivities on Table 16,  $\text{BaTiO}_3$  exhibited the best selectivity towards  $\text{C}_2\text{H}_2$  and  $\text{C}_2\text{H}_4$  despite its lowest conversion.

Table 16: Selectivity of C<sub>2</sub> products for different packing materials

Particles	CH <sub>4</sub> Conv. (%)	Selectivity (%)		
		C <sub>2</sub> H <sub>2</sub>	C <sub>2</sub> H <sub>4</sub>	C <sub>2</sub> H <sub>6</sub>
Blank	37	7	6	19
BaTiO <sub>3</sub>	9	19	32	18
γ-alumina	35	11	10	13
Silica-SBA-15	25	9	17	15
α-Al <sub>2</sub> O <sub>3</sub>	37	12	8	11

For δ-alumina, α-alumina, and silica-SBA-15, the same trend was followed but to a lower extend. The authors did not comment on the surface chemical properties of materials (e.g. acid base properties), which could explain the results to a certain extent. The correlation of methane conversion in dry reforming process as well as methanol selectivity with a dielectric constant of packed oxides was demonstrated by N. Bouchoul *et al.* [120]. The activity was favored for the catalysts with low dielectric constants, indicating that a low electric field, therefore low density of reactive species, was beneficial for the studied reaction. Debek *et al.* [121] obtained a similar tendency in the carbon dioxide hydrogenation under plasma coupled to catalysis: carbon dioxide conversion decreased with the increasing values of the dielectric constant.

### 3.4. Catalysts in the plasma-assisted oxidative coupling of methane

Most of the catalysts developed for plasma processes are transition metal-based. Oxides of transition metals have been investigated in both thermal catalysis and plasma catalysis, mainly due to their acid-base and redox properties [39]. Efficient catalysts in the catalytic OCM reaction are basic metal oxides. The addition of alkaline metals (lithium, sodium, cesium) to magnesium oxides has led to interesting catalytic performances and C<sub>2</sub> selectivity, but the catalysts were not stable at high temperatures ( $\geq 750$  °C) [122]. The acid-base properties and the oxygen mobility are among the parameters favoring the OCM reaction. The rare earth oxides are relatively more active than other alkaline oxides and allow the production of C<sub>2+</sub>



hydrocarbons at lower temperatures. Sheng *et al.* [123] showed that the non-oxidative methane coupling at 650°C over Mo<sub>2</sub>C/[B]ZSM-5 catalyst produces ethylene with very high selectivity (> 90 %). Nevertheless, the conversion of methane was limited at 1 %. In order to enhance catalytic activity in long-running processes, they must be stable and resistant to abrasion and attrition loss. Addition of a porous support, thermally stable and inert will avoid pressure drop and catalyst fouling [9]. The catalytic activity (selectivity or yield) can be strongly influenced by the chemical interactions between the active catalyst component and the support, which depend on their chemical nature [124].

Porous support materials offer potential advantages such as high surface area, facile mass transport and homogeneous dispersion of active sites. Different silicon dioxide materials [125], silicon carbide [126], alumina [127] are common supports in the catalytic oxidative coupling of methane.

In the plasma-assisted OCM, the supports are no different than those used in the conventional catalytic process. Many studies have been reported on the utilization of alumina either alone, as support for metal oxides or in the presence of a metal (mainly nickel). It is worth mentioning that nickel on alumina catalysts have been generally employed for syngas production (in the presence of methane and carbon dioxide feed but not at an optimal ratio to produce hydrocarbons). However, some studies have reported relatively high C<sub>2</sub> selectivities and are included in the upcoming section.

### 3.4.1. Effect of alumina-based catalysts

#### 3.4.1.1. *Effect of alumina catalysts*

Li *et al.* [61] studied the effect of alumina pellets in different types of plasma discharges on pure methane. For all the discharge processes, the insertion of the  $\gamma$ -alumina pellets increased methane conversion and C<sub>2</sub> yield (Table 17). They highlighted that in the case of pulsed streamer discharge plasma, introducing  $\gamma$ -alumina can decrease deposited carbon (estimated at 3 % with catalyst against 14 % without catalyst) and improve C<sub>2</sub> selectivity. Although the

highest CH<sub>4</sub> conversion (35 %) and C<sub>2</sub> (25 %) yield were registered for the pulsed streamer discharge, the predominant product among C<sub>2</sub> hydrocarbons was acetylene. Positive effects on alumina catalysts on the conversion of methane were also shown by Kasinathan *et al.* [116] who studied the non-oxidative methane activation using 10 % methane in argon in a DBD reactor. The conversion of methane over alumina reached 10.4 % at 6 kV, as compared to 7.2 % obtained with the plasma alone. The acetylene and ethylene selectivities increased by ~20 % when an alumina catalyst was placed in the reactor, while the selectivity of ethane dropped by approximately 20 %. The same effect on the C<sub>2</sub> hydrocarbons selectivities was observed by Gallon *et al.* [111]. When alumina catalyst was introduced into the reactor, it caused a slight decrease in ethane selectivity and a slight increase in acetylene and ethylene selectivities.

The  $\alpha$ - and  $\gamma$ -alumina grains of 355-650  $\mu\text{m}$  were compared in methane coupling using carbon dioxide in a DBD reactor [120]. The conversion of methane was greater for  $\gamma$ -alumina (30%) than for  $\alpha$ -alumina (22 %) owing to a higher degree of hydroxylation. As it was suggested by Liu *et al.* [23], the materials with strong dipole character and a great concentration of surface hydroxyls are easily charged. Once the degree of polarization is excessive, dehydration may occur; leaving oxygen vacancies, which may react to form active sites for methyl radical generation. Considering the formation of hydrocarbons and oxygenates, the catalysts showed selectivity mainly towards ethane: 8.8% and 11% for  $\gamma\text{-Al}_2\text{O}_3$  and  $\alpha\text{-Al}_2\text{O}_3$ , respectively. In lesser amount the catalysts exhibited the selectivity to ethylene, 0.3% and 1.0%; propane, 1.2% and 0.7%; methanol, 0.4% and 0.5%; formaldehyde, 0.9% and 1.4%; acetaldehyde, 0.2% and 0.3% for  $\gamma\text{-Al}_2\text{O}_3$  and  $\alpha\text{-Al}_2\text{O}_3$ , respectively, and C<sub>3</sub>H<sub>6</sub>O, 0.6% for both.

However, in some publications, the introduction of alumina particles in the plasma volume of a methane and carbon dioxide mixture can also have a negative effect on the methane conversion [105]. Recently, Andersen *et al.* [128] observed a drop in methane conversion, ethylene and acetylene total selectivity with the introduction of  $\gamma$ -alumina beads (diameter 3.5-

4.4 mm) compared to plasma alone in the reaction of dry reforming of methane. The methane conversion and total ethylene and acetylene selectivity were 32.5% and 0.724% for plasma only, and 27.5% and 0.322% with alumina beads. While the selectivity to ethane were not substantially different: 11.6% and 11.8% for plasma only and with  $\gamma$ -alumina, respectively. The authors attributed the decrease in methane conversion to the shorter residence time of the feed due to the introduction of packing material. Despite the enhanced electric field at the contact points of the catalyst, and thus increased electron temperature and electron impact dissociation, it did not compensate for the effect of a shorter residence time at the same power.

The variability of the results obtained for the alumina catalysts confirms once again the importance of the catalyst morphology, and most probably the nature of surface chemical species like the presence of hydroxyl groups at the surface of  $\gamma$ -alumina. These results were explained in the early works of Liu *et al.* [23], who suggested that the methane conversion to higher hydrocarbons is promoted by the concentration of polarized OH groups. Gadzhieva *et al.* [129] used IR spectroscopy to show that methane adsorption sites are formed on  $\gamma$ -alumina by molecular and dissociative mechanisms under plasma discharge leading to surface hydroxyl groups.

Table 17: Comparison between an empty plasma reactor and reactor filled with alumina catalyst for oxidative methane coupling and non-oxidative methane coupling. C<sub>2</sub> selectivities are reported either in term of total C<sub>2</sub>, or acetylene + ethylene. \*Approximated data from the plot figure

Discharge	Catalyst	Feed	SEI kJ L <sup>-1</sup>	CH <sub>4</sub> Conv %	C <sub>2</sub> Selectivity %			C <sub>2</sub> Yield %			Comments	Ref
					C <sub>2</sub> H <sub>2</sub>	C <sub>2</sub> H <sub>4</sub>	C <sub>2</sub> H <sub>6</sub>	C <sub>2</sub> H <sub>2</sub>	C <sub>2</sub> H <sub>4</sub>	C <sub>2</sub> H <sub>6</sub>		
DC DBD	Blank	CH <sub>4</sub>	20.8	*7.5	66.6			*5			-	[61]
	γ-Al <sub>2</sub> O <sub>3</sub>			*11	54.5			*6			Pellets 1-1.5 mm diameter	
Pulsed streamer	Blank		22.8	*30	73.3			*22			-	
	γ-Al <sub>2</sub> O <sub>3</sub>		*35	77			*27			Pellets 1-1.5 mm diameter		
AC DBD	Blank		33.7	*7	43			*3			-	
	γ-Al <sub>2</sub> O <sub>3</sub>			*11	54			*6			Pellets 1-1.5 mm diameter	
DBD	Blank	Ar-CH <sub>4</sub> -CO <sub>2</sub>	-	56.8	0.5		10	0.28		5.6	-	[105]
	Al <sub>2</sub> O <sub>3</sub>		-	52.2	0.6		10.2	0.31		5.3	S <sub>BET</sub> =2.3 m <sup>2</sup> g <sup>-1</sup> , 240 °C	
DBD	Blank	Ar-CH <sub>4</sub>	-	7	*12	*16	*50	0.8	1.12	3.5	-	[116]
	Al <sub>2</sub> O <sub>3</sub>		1.25	11	*29	*30	*33	3.2	3.3	3.6	S <sub>BET</sub> =201 m <sup>2</sup> g <sup>-1</sup>	
DBD	Blank	CH <sub>4</sub> -CO <sub>2</sub>	42	*25	*2		*10	0.5		2.5	-	[111]
	γ-Al <sub>2</sub> O <sub>3</sub>			*23	*3		*9	0.69		2	Pellets 500-800 μm	
DBD	Blank	CH <sub>4</sub> :CO <sub>2</sub> 1:1	0.054	32.5	0.187	0.537	11.6	0.06	0.174	3.77	Catalyst Ø: 3.5-4.4 mm; ambient T°C and pressure gas flow : 50 Nml/min	[128]
	γ-Al <sub>2</sub> O <sub>3</sub>			27.5	0.088	0.234	11.8	0.02	0.06	3.25		
DBD	γ-Al <sub>2</sub> O <sub>3</sub>	CH <sub>4</sub> :CO <sub>2</sub> 1:2	12	30	-	0.3	8.8	-	0.1	2.6	Pellets 355-640 μm;	[120]
	α-Al <sub>2</sub> O <sub>3</sub>			22	-	1.0	11	-	0.2	2.4		

												Helium: 75%;	CB : 85%  Other products: C <sub>3</sub> H <sub>8</sub> , MeOH, C <sub>3</sub> H <sub>6</sub> O, CH <sub>2</sub> O, C <sub>2</sub> H <sub>4</sub> O, CO, H <sub>2</sub>	
--	--	--	--	--	--	--	--	--	--	--	--	-----------------	---	--

### 3.4.1.2. *Effect of the metal over alumina*

The interaction of plasma with various noble (Pd, Pt) and non-noble metals (Ni, Cu...) supported on Al<sub>2</sub>O<sub>3</sub> was investigated by different authors. In order to highlight the effect of the metal, it is important to compare the results obtained in the plasma - “metal over alumina” reaction to those obtained in the plasma - “alumina alone” reaction. This comparison is not always possible, since many authors studied the reaction directly in the presence of the metal supported on alumina, failing to report the results without the metal. In the following section, the data with plasma-alone are provided for comparison whenever the data with plasma-alumina alone is not indicated. As previously mentioned, the metal over alumina catalysts are mainly used in the reforming reaction and are not optimized for high yields of C<sub>2</sub> hydrocarbons.

#### 3.4.1.2.1 Effect of nickel over alumina

The results reported with Ni/Al<sub>2</sub>O<sub>3</sub> are summarized in Table 18. It was reported that adding nickel on alumina enhances the conversion of methane and shows a synergistic effect for methane conversion under plasma [101]. On the other hand, the presence of nickel has a negative effect on C<sub>2</sub> selectivity. However, the reduction of nickel-alumina catalyst by methane in a DBD coaxial reactor was reported to have a negative effect on methane conversion [110,130]. Although the data without the catalyst were not reported, the authors stated that the presence of nickel on alumina led to a decrease in conversions of methane and carbon dioxide. These results were explained by the discharge modifications inherent to the catalyst packing in the plasma reactor [110]. Nickel contributed to the expansion of the discharge and enhancement of charge transfer (Figure 14). Antagonist effects were identified as: 1- filamentary micro-discharges fading in detriment to weak filamentary and surface discharge, reducing the plasma reactivity; 2- the presence of nickel on alumina favored the intensity and spreading of surface discharges, thus reactivity, but without counteracting totally the loss induced by the discharge alteration.

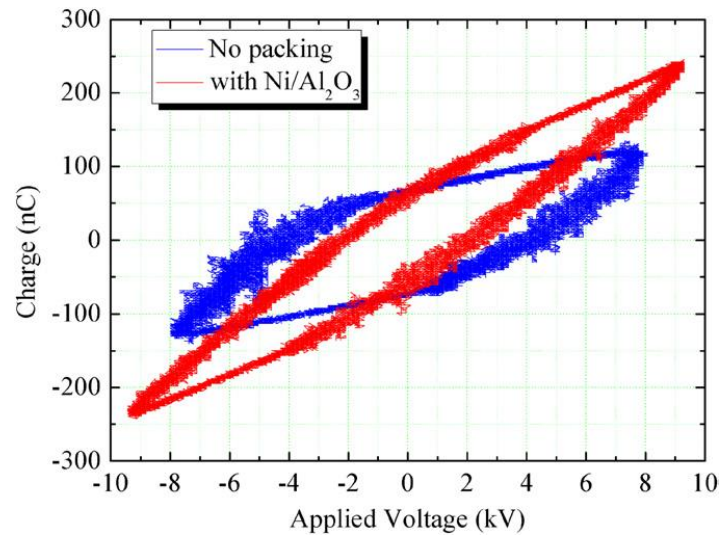


Figure 14: Lissajous figures of the  $\text{CH}_4/\text{CO}_2$  DBD with and without reduced  $\text{Ni}/\text{Al}_2\text{O}_3$  catalyst at a constant discharge power of 50 W [110]

Table 18: Comparison of different Ni/Al<sub>2</sub>O<sub>3</sub> catalysts efficiency for OCM reaction with carbon dioxide in terms of methane conversion and C<sub>2</sub> selectivities and yields. \*Approximative value taken from plot figure

Discharge	Catalyst	Feed	SEI kJ L <sup>-1</sup>	CH <sub>4</sub> Conv %	C <sub>2</sub> Selectivity %			C <sub>2</sub> Yield %			Comments	Ref
					C <sub>2</sub> H <sub>2</sub>	C <sub>2</sub> H <sub>4</sub>	C <sub>2</sub> H <sub>6</sub>	C <sub>2</sub> H <sub>2</sub>	C <sub>2</sub> H <sub>4</sub>	C <sub>2</sub> H <sub>6</sub>		
DBD	Plasma only	CH <sub>4</sub> -CO <sub>2</sub> 1:1	9	14*			30			4.2	-	[101]
	10 wt% Ni/Al <sub>2</sub> O <sub>3</sub> 400-841 μm			19.5*	-	-	21.5	-	-	4.2		
DBD	Plasma only	CH <sub>4</sub> : CO <sub>2</sub> 1:1	260	57.6	9.7			5.6			C <sub>B</sub> = 67.4 %	[130]
	γ-Al <sub>2</sub> O <sub>3</sub>			50.3	12.0			6.0			*C <sub>B</sub> = 68.9 %	
	5 wt% Ni/Al <sub>2</sub> O <sub>3</sub> 10-20 mesh			55.7	10.1			5.9			C <sub>B</sub> = 80 %	
DBD	No data provided for Al <sub>2</sub> O <sub>3</sub> alone or plasma reactor only											[110]
	26 wt % Ni- Al <sub>2</sub> O <sub>3</sub>	CH <sub>4</sub> -CO <sub>2</sub>	116.4	18	< 5	< 5	< 5				18.6 g 0.85-5 mm pellets	



#### 3.4.1.2.2 Effect of noble metals over alumina catalysts

The influence of palladium on alumina was studied in a pulse corona plasma operating under a methane and carbon dioxide feed [102], as detailed in Table 19. A methane conversion of 43.3 % and C<sub>2</sub> selectivity of 30.6 %, in which acetylene was in proportion of 74 % with only  $\gamma$ -alumina. In contrast, the Pd/ $\delta$ -Al<sub>2</sub>O<sub>3</sub> catalyst had a high ethylene content (> 65 %) with C<sub>2</sub> selectivity of ~ 40 %. The Pd-La<sub>2</sub>O<sub>3</sub>/ $\delta$ -Al<sub>2</sub>O<sub>3</sub> catalyst ended with the highest C<sub>2</sub> selectivity (70 %) and high ethylene content (~ 65 %), making the Pd-La<sub>2</sub>O<sub>3</sub>/ $\delta$ -Al<sub>2</sub>O<sub>3</sub> catalyst a promising candidate in acetylene hydrogenation. A possible explanation of this effect comes from the potential interactions between lanthanum oxide and alumina, which generates new active sites for the catalytic conversion of methane.

The combination of a gliding discharge with a mobile bed of catalyst was studied by Mlotek *et al.* [131] using platinum and palladium supported on alumina ceramic (size 0.16-0.315 mm) under a mixture of methane and hydrogen (40 vol% CH<sub>4</sub>). The results showed that the presence of the noble metal did not change the global methane conversion into C<sub>2</sub> hydrocarbons, as compared to the bare support, but it strongly modified the distribution of C<sub>2</sub> hydrocarbons: acetylene was only produced over  $\alpha$ -alumina while ethylene and ethane became the main gaseous products over platinum and palladium. The highest yield in ethane was obtained using Pd/ $\alpha$ -Al<sub>2</sub>O<sub>3</sub>, which is consistent with the literature as both platinum and palladium are known to be active in hydrocarbon hydrogenation reaction [132]. Carbon deposition was observed with high selectivity (27 %) on bare  $\alpha$ -alumina but decreased to 25 % in the presence of palladium and to 16 % in the presence of platinum, due to the enhanced reaction of solid carbon with hydrogen in presence of noble metal, producing hydrocarbons. The influence of palladium on the alumina was studied in a pulse corona plasma operating under a methane and carbon dioxide feed [102], as detailed in Table 19.

Table 19: Influence of noble metals on Al<sub>2</sub>O<sub>3</sub> catalyst for oxidative and non-oxidative methane coupling: SEI, methane conversion, C<sub>2</sub> selectivities and yields

Discharge	Catalyst	Feed	SEI kJ L <sup>-1</sup>	CH <sub>4</sub> Conv %	C <sub>2</sub> Selectivity %			C <sub>2</sub> Yield %			Comments	Ref		
					C <sub>2</sub> H <sub>2</sub>	C <sub>2</sub> H <sub>4</sub>	C <sub>2</sub> H <sub>6</sub>	C <sub>2</sub> H <sub>2</sub>	C <sub>2</sub> H <sub>4</sub>	C <sub>2</sub> H <sub>6</sub>				
Pulse corona	$\gamma$ -Al <sub>2</sub> O <sub>3</sub>	CH <sub>4</sub> :CO <sub>2</sub> =2	-	43.4	30.6			13.4			Powder, 400-841 $\mu$ m	[102]		
	0.01%Pd/ $\delta$ -Al <sub>2</sub> O <sub>3</sub>			38.5	34.5			13.3						
	0.01%Pd-5% La <sub>2</sub> O <sub>3</sub> / $\delta$ -Al <sub>2</sub> O <sub>3</sub>			23.8	70.4			16.7						
Gliding discharge	$\alpha$ -Al <sub>2</sub> O <sub>3</sub>			11	73	0	0	8.0	0	0	T: 170 °C, C: 27 %	[131]		
	~3 wt% Pt/ $\alpha$ -Al <sub>2</sub> O <sub>3</sub>	CH <sub>4</sub> :H <sub>2</sub> =0.4:0.6	2.4	12	42	25	17	5.0	3.0	2.0	T: 230 °C, C: 16 %			
	~3 wt% Pd/ $\alpha$ -Al <sub>2</sub> O <sub>3</sub>			12	0	25	50	0	3.0	6.0	T: 200 °C, C: 25 %			
DBD	$\gamma$ -Al <sub>2</sub> O <sub>3</sub>	CH <sub>4</sub> :Ar=0.1:0.9	1.8	13.5*	10*	10	33	1.4	1.4	4.5	Beads of 1 mm	[133]		
	8wt%Pt/ $\gamma$ -Al <sub>2</sub> O <sub>3</sub>			12*	6	11	45	0.7	1.3	5.4				
DBD	$\gamma$ -Al <sub>2</sub> O <sub>3</sub>	CH <sub>4</sub> :Ar=0.05:0.95	10-12	62	4.2	4.1	10.0	2.6	2.5	6.2	powder	[134]		
	5wt%Pd/ $\gamma$ -Al <sub>2</sub> O <sub>3</sub>			52	0	2.1	57	0	1.1	29.6				
DBD	Blank	CH <sub>4</sub> :Ar=0.06:0.94	2	40	4	3	15	1.6	1.2	6.0	-	[30]		
	14wt%Pd/ $\gamma$ -Al <sub>2</sub> O <sub>3</sub>			32.5	3	6	23	1.0	2.0	7.5	Catalytic film: 1.7 mg			
				32.5	0	2.5	42	0.0	0.8	13.7	Catalytic film: 5.9 mg			
				38	0	1.5	32.5	0.0	0.6	12.4	Powder at the end of plasma zone (2 mm)			
DBD	Catalyst	CH <sub>4</sub> -CO <sub>2</sub> 1:1	0.054	CH <sub>4</sub> Conv %	C <sub>2+</sub> Selectivity %							Diameter of catalyst: 3.5-4.4 mm; ambient temperature and pressure (1.16 atm); gas flow: 50 Nml/min	[128]	
	$\gamma$ -Al <sub>2</sub> O <sub>3</sub>				C <sub>2</sub> H <sub>2</sub>	C <sub>2</sub> H <sub>4</sub>	C <sub>2</sub> H <sub>6</sub>	C <sub>2</sub> H <sub>6</sub> O DME	C <sub>2</sub> H <sub>6</sub> O ethanol	C <sub>3</sub> H <sub>8</sub>	i- C <sub>4</sub> H <sub>10</sub>			n- C <sub>4</sub> H <sub>10</sub>
	10wt% Ag/ $\gamma$ -Al <sub>2</sub> O <sub>3</sub>				0.088	0.234	11.8	0.052	0.259	3.69	0.387			0.505
	1wt%Pt/ $\gamma$ -Al <sub>2</sub> O <sub>3</sub>				0.093	0.240	11.8	0.052	0.249	3.80	0.412			0.559
				32.0	0.042	0.207	10.8	0.052	0.275	3.86	0.382	0.534		

Using a DBD reactor, Jo *et al.* [133] confirmed that the presence of platinum modifies the selectivity towards C<sub>2</sub> hydrocarbons and favors the production of ethane. However, methane conversion decreased to 12 % with platinum compared to 13.5 % with the bare support with beads of 1 mm diameter due to the decrease in the electric field intensity in presence of the noble metal.

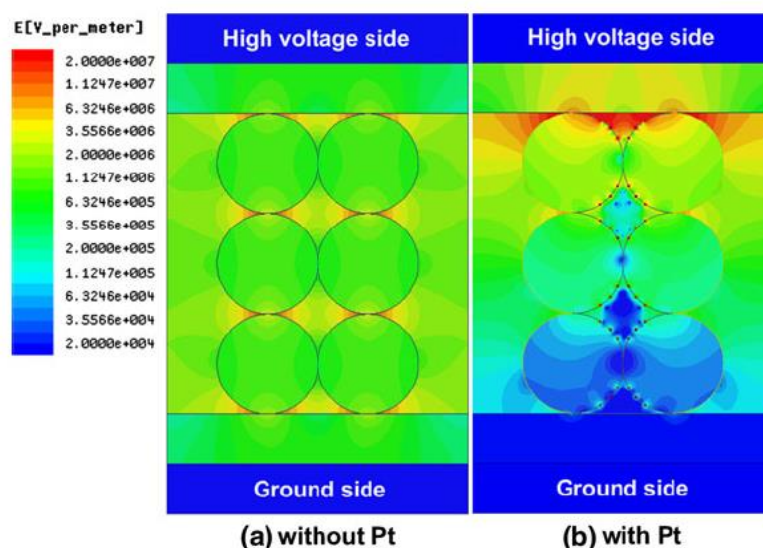


Figure 15: Evolution of the calculated electric field in the DBD reactor packed with Al<sub>2</sub>O<sub>3</sub> beads (a) without and (b) with Pt. Applied voltage: 5kV. Only the electric field generated by external sources (i.e. applied voltage) is calculated. Internal sources (induced by local differences in the distributions of ions and electrons within the reactor) is too difficult to compute. The author considered that densities of the ions and electrons that generate such fields are proportional to the external applied voltage [133].

The author used a Maxwell program and a simplified model consisting of spherical alumina beads and platinum particles to calculate the electric field. A strong and homogeneous electric field developed at the contact surfaces of the alumina beads and in the space in close proximity (Figure 15). When the metallic particles were added, the electric field became highly distorted, being the strongest at the high voltage electrode and the weakest at the ground. It resulted in a reduced propagation of the electric field, thus hindering electron acceleration and temperature rise, which are essential for methane activation.

Taheraslani *et al.* [134] confirmed that the presence of palladium on  $\gamma$ -alumina led to a decrease in methane conversion compared to the bare support. However, the authors showed that

palladium particles favored the production of unsaturated hydrocarbons (mainly ethane) and limited the formation of carbon deposits. The group of Lefferts [30] explained this effect by a fast hydrogenation rate of  $\text{CH}_x$  and  $\text{C}_2\text{H}_y$  on the catalyst surface due to the presence of Pd, minimizing carbon deposition. A positive effect on product selectivities was also observed in the presence of hydrogen. They investigated the effect of the catalytic layer thickness on the walls of a structured reactor. The catalyst thickness did not influence the methane conversion, which is only affected by the plasma properties, but it did influence the product distribution. Increasing the thickness, *i.e.* the catalyst loading from 1.7 to 5.9 mg, decreased the acetylene formation and carbon deposition, while increasing ethylene and ethane selectivities along with the other saturated hydrocarbon. The same study reported improved performance of structured catalyst (thin film on the reactor wall) compared to packed material in a fixed-bed reactor. The authors suggested that the contact between plasma and the external surface of the catalyst in catalytic wall reactor is maximized compared to packed material.

In the study of Andersen *et al.* [128], the presence of 1 wt% Pt over  $\gamma$ -alumina enhanced the conversion of methane in the dry reforming process using a DBD system compared to bare and with 10 wt% silver impregnated supports. An opposite trend was observed when comparing the selectivity to  $\text{C}_2$ . In the defined conditions, the main  $\text{C}_2$  product in the gas phase was ethane, with more than 10% selectivity for all the catalysts. The authors also reported the formation of higher hydrocarbons such as propane and isomers of butane and multiple liquid phase products such as methanol, ethanol, dimethyl ether and formic acid, with similar selectivity for the different catalysts. They suggested that the high-energy plasma facilitates the reforming reaction and promotes interactions between the electrode surface and adsorbed species, leading to methane decomposition and carbon deposition. The latter would block the sites for further reactions, explaining the similarities in selectivity between these catalysts.

As previous authors suggested, the modification of the discharge characteristics in the presence of a catalyst which in parallel enhances the activity, affects both conversions and selectivities according to defined plasma or chemical conditions.

#### 3.4.1.2.3 Effect of other metals over alumina catalysts

The interaction of plasma with various other metals supported on alumina was investigated as summarized in Table 20. When compared to the empty reactor or filled with alumina, the presence of iron had negative effects on the conversion of methane and product selectivities. In the case of the other metals, no significant effects were recorded as compared to alumina alone or the empty reactor. Overall, in the presence of carbon dioxide, the catalysts supported on alumina do not provide satisfactory results. Even though in some cases the textural properties of the catalysts supported on alumina were very similar (specific surface area in the range of 144.5-151.4 m<sup>2</sup> g<sup>-1</sup>, and average pore diameter 5.01-5.05 Å), the results indicated that the effect of the catalysts did not depend on the textural properties of the supported metal catalysts [101]. In contrast, 10 wt% copper on  $\gamma$ -alumina showed improved methane conversion in dry reforming process compared to alumina alone, but quite comparable to results without packing material. The selectivity to C<sub>2</sub> products was similar to alumina alone due to the presence of carbon residues blocking the active site as already mentioned. In addition, copper-supported alumina showed significant enhancement of methanol selectivity (not shown in Table 20) compared to alumina alone and other deposited metals (3.16% compared to 1.17-1.40%). The highest methanol selectivity was ascribed to a two-way mechanism: one is by the gas phase reaction between methyl and hydroxyl radicals, and another, surface-catalyzed carbon dioxide activation leading to formate, a peculiarity known for Cu/Al<sub>2</sub>O<sub>3</sub> from thermal catalysis. The combination of copper with ZnO/Al<sub>2</sub>O<sub>3</sub> catalyst registered the best results in terms of conversion and selectivity under a mixture consisting of 50 % methane, 12.5 % hydrogen and 37.5 % argon [107]. With neutral quartz glass packing, the overall products selectivity was

slightly higher as compared to an empty reactor. When the catalyst bed was present in the reactor, the methane conversion was closer to that obtained for an empty reactor than the reactor containing quartz glass. However, the presence of the catalyst directly in the discharge zone resulted in approximately 20 % increase of C<sub>2</sub> selectivity, improving the yield as compared to the empty reactor and the reactor filled with quartz glass. For comparison, it would have been interesting to see the results with alumina alone.

Table 20: Influence of different metals supported on alumina on the oxidative and non-oxidative coupling of methane reaction in terms of SEI, methane conversion, C<sub>2</sub>, C<sub>3</sub>, C<sub>4</sub>, methanol and ethanol selectivity

Discharge type	Catalyst	Feed	SEI kJ L <sup>-1</sup>	CH <sub>4</sub> Conv %	C <sub>2+</sub> Selectivity %							Comments		Ref		
					C <sub>2</sub> H <sub>2</sub>	C <sub>2</sub> H <sub>4</sub>	C <sub>2</sub> H <sub>6</sub>	CH <sub>2</sub> OH	C <sub>2</sub> H <sub>6</sub> O	C <sub>3</sub> H <sub>8</sub>	i-C <sub>4</sub> H <sub>10</sub>	n-C <sub>4</sub> H <sub>10</sub>				
DBD	Blank	Ar-	-	56.8	0.5	10	-	-	-	-	-	-	-	[105]		
	Al <sub>2</sub> O <sub>3</sub>	CH <sub>4</sub> -		52.2	0.6	10.2	-	-	-	-	-	-			S <sub>BET</sub> =3.3 m <sup>2</sup> g <sup>-1</sup> , 240 °C	
	Fe/Al <sub>2</sub> O <sub>3</sub>	CO <sub>2</sub>		45.9	1.3	9.1	-	-	-	-	-	-				
DBD	Blank	CH <sub>4</sub> - CO <sub>2</sub> 1:1	9	14	-	-	30	-	-	-	-	-	-	[101]		
	Co/Al <sub>2</sub> O <sub>3</sub>			15	-	-	29.4	-	-	-	-	-	-		C <sub>B</sub> =95 %	10wt% M, pellets, 400-841 μm, S <sub>BET</sub> =144.5-151.4 m <sup>2</sup> g <sup>-1</sup> , average pore diameter =5.01-5.05A
	Cu/Al <sub>2</sub> O <sub>3</sub>			14	-	-	29	-	-	-	-	-	-		C <sub>B</sub> =96 %	
	Mn/Al <sub>2</sub> O <sub>3</sub>			18	-	-	23	-	-	-	-	-	-		C <sub>B</sub> =93 %	
DBD	Blank	CH <sub>4</sub> - H <sub>2</sub> -Ar	-	21.4	48.2		-	-	-	-	-	-	-	[107]		
	Quartz glass			22.7	51.2		-	-	-	-	-	-	-			
	Cu/ZnO/Al <sub>2</sub> O <sub>3</sub>			21.7	67		-	-	-	-	-	-	-		32 m <sup>2</sup> g <sup>-1</sup>	
DBD	Blank	CH <sub>4</sub> - CO <sub>2</sub> 1:1	0.054	32.5	0.187	0.537	11.6	0.666	0.264	3.92	0.428	0.583	Diameter of catalyst: 3.5-4.4 mm; ambient temperature and pressure (1.16 atm); gas flow: 50 Nml/min	[128]		
	γ-Al <sub>2</sub> O <sub>3</sub>			27.5	0.088	0.234	11.8	1.41	0.259	3.69	0.387	0.505				
	10wt% Cu/γ-Al <sub>2</sub> O <sub>3</sub>			32.0	0.010	0.277	11.0	3.16	0.440	3.45	0.311	0.555				

Table 21: Influence of different oxides supported on alumina for the oxidative and non-oxidative coupling of methane in terms of SEI, methane conversion, C<sub>2</sub> selectivity and yields

Discharge	Catalyst	Feed	SEI kJ L <sup>-1</sup>	CH <sub>4</sub> Conv %	C <sub>2</sub> Selectivity %			C <sub>2</sub> Yield %			Comments		Ref
					C <sub>2</sub> H <sub>2</sub>	C <sub>2</sub> H <sub>4</sub>	C <sub>2</sub> H <sub>6</sub>	C <sub>2</sub> H <sub>2</sub>	C <sub>2</sub> H <sub>4</sub>	C <sub>2</sub> H <sub>6</sub>			
DBD	MgO/Al <sub>2</sub> O <sub>3</sub>	Ar-CH <sub>4</sub>	1.08	16	22	22	36.5	11	12.8	18.2	S <sub>BET</sub> =184 m <sup>2</sup> g <sup>-1</sup> S <sub>BET</sub> =212 m <sup>2</sup> g <sup>-1</sup>	0.5 mm alumina	[116]
	TiO <sub>2</sub> /Al <sub>2</sub> O <sub>3</sub>		1.008	14	20	25	40	8	10	16			
DBD	40%La <sub>2</sub> O <sub>3</sub> /γ-Al <sub>2</sub> O <sub>3</sub>	He-CH <sub>4</sub> - CO <sub>2</sub> :65-14-1 mL min <sup>-1</sup>	33.75	19.5	42.9			8.3			C <sub>B</sub> =72 %, Room temp C <sub>B</sub> =74 %, 200 °C C <sub>B</sub> =81 %, 400 °C	Alumina balls 2 mm	[100]
			39	20.9	41.2			8.6					
			39.75	21.4	39.5			8.4					
Pulse corona	5%La <sub>2</sub> O <sub>3</sub> /δ-Al <sub>2</sub> O <sub>3</sub>	CH <sub>4</sub> :CO <sub>2</sub> =2, 25 mL min <sup>-1</sup>	-	24.5	70.6			17.3			Powder, 400-841 μm	[102]	
	7%La <sub>2</sub> O <sub>3</sub> /δ-Al <sub>2</sub> O <sub>3</sub>		-	24.9	72.8			18.1					
	10%La <sub>2</sub> O <sub>3</sub> /δ-Al <sub>2</sub> O <sub>3</sub>		-	24.3	68.2			16.6					
	12%La <sub>2</sub> O <sub>3</sub> /δ-Al <sub>2</sub> O <sub>3</sub>		-	24.1	64.4			15.2					



#### 3.4.1.3. *The influence of oxides over alumina support*

The different oxide catalysts supported on alumina are summarized in Table 21. Lanthanum oxide is considered one of the most efficient oxide catalysts for oxidative methane coupling and has been investigated by several groups. They have either examined the influence of lanthanum oxide weight percent, or the effect of temperature. Zhang *et al.* [102] reported that all weight percent (5-12 wt%) catalysts provided a C<sub>2</sub> hydrocarbon selectivity greater than 60 %, but with a declining trend with increasing lanthanum oxide weight percent, while the methane conversion level was maintained at roughly 24 %. No change was observed in the distribution of C<sub>2</sub> products, with acetylene being the major product independently of the catalyst weight percent. It would have been interesting to see if and how the plasma power was influenced by the weight percent of the catalyst, but unfortunately the authors did not provide this information. Pham *et al.* [100] used a high loading of lanthanum oxide (40 wt%), which was tested at different temperatures. The catalyst was supported on alumina balls to avoid the use of a catalytic bed that would favor a homogeneous phase reaction. First, the authors showed that at room temperature the presence of lanthanum oxide does not significantly modify the methane and carbon dioxide conversions, or the hydrocarbon selectivity, the results being approximately the same as those obtained with pure alumina balls. The methane conversion increased slightly with the increase in temperature. Titanium oxide and magnesium oxide had the best catalytic activity among the oxides supported on alumina, with ethane yields superior to the total yield of C<sub>2</sub> products obtained in the case of lanthanum oxide.

#### 3.4.2. Effect of zeolite catalysts

The interest in zeolite as materials in plasma catalysis comes from their physico-chemical characteristics (permittivity, acidity-basicity, specific surface). Their capacity to generate a plasma with a strong electric field near the pores of their micro- and nano-featured structures allows reactions that thermal catalysis cannot provide [39].

### 3.4.2.1. Effect of coupling zeolites with plasma

Modifications of the zeolite support or of the supported metal properties have been the two pathways investigated for low-temperature methane conversion over zeolites. The electrical charging of a Y zeolite by a corona discharge modified its catalytic properties in terms of electrostatic potential and work function at the surface [23].

A comparative investigation of plasma catalytic methane conversion to C<sub>2</sub> hydrocarbons over different kinds of zeolite is presented in Table 22. Zeolite X and Y are aluminosilicate molecular sieves with a faujasite-type structure (FAU). The Si/Al atomic ratio determines the zeolite designation as X for ratios in the 1 to 1.5 range and higher for Y-type zeolite, with a high ratio being thermally stable [135,136].

The NaX zeolite slightly improved the selectivity of C<sub>2</sub> products as compared to the empty reactor. The NaY zeolite had negative effects compared to plasma alone and a decrease in methane conversion and C<sub>2</sub> selectivity was observed. When comparing the two zeolites in the same conditions, the NaX zeolite performed better than the NaY, with a C<sub>2</sub> yield of 16.2 %, as compared to 12.1 % for the NaY zeolite.

A rather complex catalyst based on modified zeolite Y revealed a high conversion of methane into ethylene [137]. The material consisted of oxalate ligand-functionalized copper modified zeolite Y (prepared *via* the surface organometallic chemistry approach) resulting in 5 wt% Cu incorporated into zeolite Y. Then the latter was modified using in high frequency ultrasonic technique with Pt partially encapsulated onto CeO<sub>2</sub> powder (prepared by flame spray pyrolysis of Pt acetylacetonate with CeO<sub>2</sub>). The author suggested that the high methane conversion (74%) and selectivity to ethylene (~32 %) are governed by a strong-metal-support interaction, which shifted downward the d-band center of Pt with respect to Fermi level. The consequence was a weak adsorption of the C<sub>2</sub>H<sub>4</sub>  $\pi$ -bond at the Pt site, preventing its hydrogenation into ethane.

Table 22: Effect of zeolites used in the plasma-catalytic oxidative coupling of methane reaction. \* case study on the non-oxidative coupling of methane

Discharge	Zeolite	Feed	SEI kJ L <sup>-1</sup>	CH <sub>4</sub> Conv %	C <sub>2</sub> Selectivity %			C <sub>2</sub> Yield %			Comments	Ref
					C <sub>2</sub> H <sub>2</sub>	C <sub>2</sub> H <sub>4</sub>	C <sub>2</sub> H <sub>6</sub>	C <sub>2</sub> H <sub>2</sub>	C <sub>2</sub> H <sub>4</sub>	C <sub>2</sub> H <sub>6</sub>		
Corona	NaX	CH <sub>4</sub> : CO <sub>2</sub> 4:1	20.16	48.1	33.7			16.2			0.1 g powder	[138]
DBD	NaX	CH <sub>4</sub> : CO <sub>2</sub> 2:1	200	51.6	2	2	11.1	1.03	1.03	5.7	9 g, 150 °C	[139]
	Blank		200	64.3	1.2	1.2	8.5	0.7	0.7	5.4		
DBD	NaY	CH <sub>4</sub> : CO <sub>2</sub> : Ar	-	48.7	0.8	5.7		0.3		2.7	S <sub>BET</sub> = 574 m <sup>2</sup> g <sup>-1</sup> 240 °C	[105]
	Blank			56.8	0.5	10		0.28		5.6		
Corona	NaY	CH <sub>4</sub> : CO <sub>2</sub> 4:1	20.16	49	24.8			12.1			0.1 g powder	[138]
Corona	NaOH treated Y	CH <sub>4</sub> : CO <sub>2</sub> 1:0.5	20.16	45	31.2			14.08			200 °C	[138]
		CH <sub>4</sub> : H <sub>2</sub> :O <sub>2</sub> 10:15:1	7.8	23.9	60.3			14.4			100 °C	
		CH <sub>4</sub> : H <sub>2</sub> O 1.27:1	8.4	25.3	55.9			16.1			100 °C	
DBD*	PtCe/CuX- ZY	CH <sub>4</sub>	1.8	74	-			-	24	2	50 ml/min; catalyst loading 0.1g	[137]

Zeolite structural modifications by sodium hydroxide treatment aim at dissolving part of the silicon to increase the catalyst's polarizability and basicity. The advantage of a high degree of polarization would be the formation of oxygen vacancies on the surface, due to possible dehydration, which would form an active site for  $\text{CH}_3$  radical formation, as seen in previous section [23]. The sodium hydroxide-treated Y zeolite registered superior results in terms of  $\text{C}_2$  selectivity and yield, as compared to the NaY zeolite. The results are even comparable to those obtained using the NaX zeolite, since sodium-hydroxide treated Y has the highest density of basic sites and NaX has the strongest basic sites. If hydrogen radicals were meant to promote higher hydrocarbons, they also led to polymerization, catalyst deactivation and low yields of higher hydrocarbon. This effect was limited by the addition of oxygen, which generated active species like  $\text{O}^\bullet$ ,  $\text{O}^-$  and OH radicals, maintaining the discharge and avoiding polymerization within the sodium hydroxide-treated Y zeolite.

#### *3.4.2.2 Effect of coupling metal/zeolite with plasma*

A comparative study on plasma catalytic methane conversion to  $\text{C}_2$  hydrocarbons over different metals supported on ZSM-5 zeolite in the presence of oxygen or carbon dioxide [34] is summarized in Table 23. Oxygen in the feed provides active oxygenated species that enhance methane activation. Adding iron enhanced  $\text{C}_2$  selectivities compared to the sole zeolite, mainly acetylene and ethylene due to the presence of carbon monoxide and carbon dioxide which affected the recombination of methyl and/or ethyl radicals from methane conversion [34]. Nickel led to the smallest  $\text{C}_2$  selectivities (ethylene or acetylene) compared to the other Fe-ZSM-5 catalysts, due to the loss of activity by oxidation of its surface. However, the authors highlighted that despite a low conversion, the property of nickel to generate  $\text{C}_2$  radicals from methane leads to intermediate species, which are important in gas phase reactivity. The highest methane conversion was obtained with Co-ZSM-5. According to the authors, co-polymerization and coking enhanced the generation of  $\text{C}_2$  radicals in hydrogen abstraction from

methane. In the presence of Co-ZSM-5, C<sub>2</sub> selectivity was found to be higher in microwave (MW) plasma (~90 %) compared to radiofrequency (RF) plasma (62 %) despite a higher methane conversion in RF plasma (RF = 78.4% against MW= 54.9 %). The formation of CO<sub>x</sub> inhibiting C<sub>2</sub> products was pointed out as responsible for this activity loss.

Comparing modified catalysts (NaX and NaOH treated Y), Na-ZSM-5 was the most acidic, which led to a poor plasma-catalytic activity [138]. Na-ZSM-5 catalyst was rapidly deactivated due to the carbon contamination produced during the plasma reaction, shifting the discharge propagation mode towards an arc. The overall activity was reduced in this case, which was not observed in the other zeolites. Krawczyk *et al.* [105] observed similar carbon contamination and suggested that soot and other organic compounds (arising from higher hydrocarbons) blocked the zeolite active centers (Figure 16).



*Figure 16: The surface of Na-ZSM-5 catalyst (A) before and (B) after the measurement of activity [105]*

Table 23: Plasma catalytic methane conversion to C<sub>2</sub> hydrocarbons over different metals supported on ZSM-5 zeolite

Discharge	Catalyst	Feed	SEI kJ L <sup>-1</sup>	CH <sub>4</sub> Conv %	C <sub>2</sub> Selectivity %			C <sub>2</sub> Yield %			Comments	Ref	
					C <sub>2</sub> H <sub>2</sub>	C <sub>2</sub> H <sub>4</sub>	C <sub>2</sub> H <sub>6</sub>	C <sub>2</sub> H <sub>2</sub>	C <sub>2</sub> H <sub>4</sub>	C <sub>2</sub> H <sub>6</sub>			
Microwave	H-ZSM5	CH <sub>4</sub> : O <sub>2</sub> 4:1	48	39.3	33.4	25	20	13.1	9.8	7.8	S <sub>BET</sub> = 425 m <sup>2</sup> g <sup>-1</sup>	Powder form 1 g	[34]
	Fe-ZSM5		48	52.6	52.2	27.2	9.3	27.5	14.2	4.9	S <sub>BET</sub> = 354 m <sup>2</sup> g <sup>-1</sup>		
	Ni-ZSM5		57.6	38.9	46	32.7	12.2	17.9	12.7	4.7	S <sub>BET</sub> = 231 m <sup>2</sup> g <sup>-1</sup>		
	Cu-ZSM5		57.6	53	32	46.6	13.2	16.9	24.7	7	S <sub>BET</sub> = 335 m <sup>2</sup> g <sup>-1</sup>		
	Co-ZSM5		57.6	54.9	49.9	29.8	10	27.4	16.3	5.5	S <sub>BET</sub> = 349 m <sup>2</sup> g <sup>-1</sup>		
RF	Co-ZSM5		384	78.1	43.3	10.6	13.9	33.8	8.3	10.9			
DBD	Na-ZSM5	CH <sub>4</sub> : CO <sub>2</sub> : Ar	-	65.1	0.1		6.7	0.06		4.4	S <sub>BET</sub> = 326 m <sup>2</sup> g <sup>-1</sup> 240 °C		[105]
Corona	Na-ZSM5	CH <sub>4</sub> : CO <sub>2</sub> 4:1	13.56	44.6	31.2			13.9			0.1 g powder		[138]

### 3.4.3. Effect of SBA-15 catalysts

In heterogeneous catalysis, mesoporous silica (SBA-15) gained distinct attention as a promising catalyst and support due to its large surface area, large pore size and high stability.

The group of Subrahmanyam [140] tested SBA-15 in methane OCM in a DBD reactor, alone and with Pd-supported nanoparticles reduced by conventional thermal treatment and by in-situ plasma treatment (Table 24). The authors reported the formation of hydrogen, carbon monoxide, carbon dioxide and ethane, with the largest selectivity to ethane (17%) for SBA-15 sample alone and a methane conversion of 7 %. Pd-decorated samples showed improved conversion of methane (10 %) though lower selectivity towards ethane (12%), emphasizing the presence of secondary reactions, namely coupling, cleavage, H-transfer and CO/CO<sub>2</sub> hydrogenation, leading to the improvement of product selectivity in the liquid phase (methanol, formic acid, formaldehyde, ethanol and acetone). A total liquid selectivity for in-plasma reduced Pt-SBA-15 was 70% (comparable to classical reduction of Pd), in contrast to 58% for SBA-15 alone. The adsorption-desorption process on palladium, being an active site with basic properties, was responsible for this enhanced activity. In addition, the authors emphasized the formation of oxygenates thanks to the mesopores of SBA-15. The decomposition of adsorbed CH<sub>x</sub>O species to carbon monoxide is avoided since the generation of plasma streamers is suppressed within small pores.

Table 24: Plasma catalytic methane conversion to C<sub>2</sub> hydrocarbons over SBA-15 and Pd-SBA-15

Discharge	Catalyst	Feed	SEI kJ L <sup>-1</sup>	CH <sub>4</sub> Conv %	C <sub>2</sub> Selectivity %			C <sub>2</sub> Yield %			Comments	Ref	
					C <sub>2</sub> H <sub>2</sub>	C <sub>2</sub> H <sub>4</sub>	C <sub>2</sub> H <sub>6</sub>	C <sub>2</sub> H <sub>2</sub>	C <sub>2</sub> H <sub>4</sub>	C <sub>2</sub> H <sub>6</sub>			
DBD	SBA-15	CH <sub>4</sub> : O <sub>2</sub> = 5:1	3.4	7	-	-	17	-	-	1.19	Total flow 30 ml min <sup>-1</sup> .  Gap: 5.5 mm, discharge length: 9 cm.  2 g of catalyst	S <sub>BET</sub> =917 m <sup>2</sup> g <sup>-1</sup> ; Selectivity 58% liquid products	[140]
	Pd- SBA-15 (in-situ)			10	-	-	12	-	-	1.2		S <sub>BET</sub> =794 m <sup>2</sup> g <sup>-1</sup> ; Selectivity 70 % liquid products :	
	Pd- SBA-15 (H <sub>2</sub> )			9	-	-	12	-	-	1.1		S <sub>BET</sub> =726 m <sup>2</sup> g <sup>-1</sup> ; Selectivity 65 % liquid products	



#### 3.4.4 Effect of other metal oxides

The activity of different oxides such as BaO, La<sub>2</sub>O<sub>3</sub>, ZnO, CaO, MgO, TiO<sub>2</sub> and CeO<sub>2</sub> was followed in the oxidative coupling of methane using carbon dioxide in a DBD reactor at a fixed power of 8 W, with 75 % helium [120]. The data are summarized in Table 25. The lowest reported activity was with TiO<sub>2</sub>, reaching only 5.6 % of methane conversion. The conversion of methane over ZnO, BaO and CeO<sub>2</sub> were improved compared to TiO<sub>2</sub>, resulting in 14.9, 21.3 and 20.5 %, respectively. However, a poor carbon balance suggested a significant amount of carbon deposition. The best results were obtained with CaO, La<sub>2</sub>O<sub>3</sub> and MgO with 25, 22 and 26 % methane conversion, and 97, 93 and 89 % carbon balance, respectively. Regarding the hydrocarbons and oxygenates products, the catalysts showed mainly selectivity to ethane (8.8-13 %). To a minor extent, the catalysts showed selectivity to ethylene (0-0.5 %), propane (0-1.4 %), methanol (0-1.0 %), formaldehyde (0-1.7 %), acetaldehyde (0-0.3 %) and C<sub>3</sub>H<sub>6</sub>O (0-0.7 %). The different activities in methane conversion were linked to the permittivity of the materials. The greater the permittivity, the lower the conversion of carbon dioxide and methane, as seen previously.

The effect of cerium oxide in a Ni/C catalyst was examined for the dry reforming of methane in a DBD plasma reactor [141]. The presence of cerium oxide showed a strong interaction with nickel nanoparticles, preventing their growth and improving the dispersion. Therefore, small and homogeneously distributed nickel nanoparticles lowered the activation energy of methane, improving its conversion. The increase in the cerium oxide molar ratio from 0 to 5 % mol. in Ni/C led to a methane conversion increase from 50.5 to 58.3 %. On the other hand, the carbon dioxide conversion increased with the increase of cerium oxide from 0 to 1 % mol. and decreased at higher loadings. The increase in carbon dioxide conversion was explained by the positive effect of strong basic sites inherent to cerium oxide, thus a good affinity to adsorb and activate carbon dioxide. As for the drop of carbon dioxide conversion, it was due to the shrinkage of specific surface area of the catalyst due to cerium oxide size growth at higher

loading. It resulted in a decrease of active sites for carbon dioxide adsorption. Among the hydrocarbons, alkanes were present as the main products with an increase in ethane selectivity from 16.7 to 17.8 % with higher cerium oxide content. The selectivity of propane was as high as 4.5-5.7 %, followed by unsaturated hydrocarbons: ethylene (~1 %), acetylene (~1 %) and propene (<0.5 %).

Hu *et al.* [142] investigated the effect of cerium oxide prepared by the hydrothermal method and 0.5wt% Pd/ CeO<sub>2</sub> on methane conversion at different external temperatures and in a nanosecond pulsed DBD. The conversion of methane was greater in the plasma-catalytic system at 980°C compared to catalytic system alone for both cerium oxide and Pd/CeO<sub>2</sub>. Methane conversion of 5% and 11.5% for cerium oxide, 12.9% and 23.6% for Pd/CeO<sub>2</sub> was obtained without and with plasma, respectively. Both CeO<sub>2</sub> and Pd/CeO<sub>2</sub> catalysts, with or without plasma, led to ethylene as the major C<sub>2</sub> product (~ 10%), followed by acetylene (~ 4%) and ethane (<1%). This indicates that plasma and the presence of palladium activate methane and influence the formation of methyl radicals, but do not influence subsequent reactions. Nevertheless, the selectivity was strongly influenced by the external temperature. The conversion of methane increased with the temperature rise from 800°C to 900°C, compromising the selectivity to hydrocarbons and increasing the selectivity to hydrogen, indicating carbon deposition at higher temperatures. Nevertheless, compared to conventional catalysis, the addition of plasma increased the catalyst's coke-resistance.

Another CeO<sub>2</sub>-based system was studied by the group of S. Kawi [29] on non-oxidative coupling of methane at low temperature, using a mixture of CH<sub>4</sub>/He in 1/1 ratio (total flux 20 ml/min). The authors compared the activity of atomically dispersed single atoms (Pt/CeO<sub>2</sub>-SAC) prepared by atom-trapping method and nanoparticles of Pt species (Pt/CeO<sub>2</sub>-NP). The conversion of methane and yield to C<sub>2</sub> products at 72 W applied power in a mixture of CH<sub>4</sub>/He over a Pt-single atom were greater (43% and 20%) compared to plasma alone (35% and 6%), CeO<sub>2</sub> (35% and 8%) and nanoparticulate Pt over CeO<sub>2</sub> (40% and 14%). The authors suggested

that the presence of uncoordinated Pt species can convert vibrationally excited methane, that usually does not contribute significantly to the methyl radical formation (<1%) compared to electronically excited methane, but consumes more than 50% of total energy provided to the system. As a result, vibrationally excited methane can be dissociated over single atoms of Pt and  $\text{CH}_3^*$ -,  $\text{CH}_2^*$ - and  $\text{CH}^*$ - moieties are involved in the coupling process over two neighboring Pt sites, avoiding the formation of coke and oligomerization. After 2 hours of reaction at 54 W, the spent catalyst revealed the presence of Pt nanoclusters instead of uncoordinated Pt species, which explains why  $\text{C}_2$  selectivity has decreased since unselective coke formation over Pt nanoparticles favors deep dehydrogenation. Table 26 provides a summary of the findings.

Table 25: Plasma catalytic methane conversion to C<sub>2</sub> hydrocarbons over different metal oxides

Discharge	Catalyst	Feed	SEI kJ L <sup>-1</sup>	CH <sub>4</sub> Conv %	C <sub>2</sub> Selectivity %		C <sub>2</sub> Yield %		Carbon balance (%)	Comments	Ref	
					C <sub>2</sub> H <sub>4</sub>	C <sub>2</sub> H <sub>6</sub>	C <sub>2</sub> H <sub>4</sub>	C <sub>2</sub> H <sub>6</sub>				
DBD	CaO	CH <sub>4</sub> :CO <sub>2</sub> 1:2	12	25.0	0.2	11	0.1	2.8	97	Pellets 355-640 μm; Total flow: 40 mL min <sup>-1</sup> ; Helium: 75%; Other products: C <sub>3</sub> H <sub>8</sub> , MeOH, C <sub>3</sub> H <sub>6</sub> O, CH <sub>2</sub> O, C <sub>2</sub> H <sub>4</sub> O, CO, H <sub>2</sub>	S <sub>BET</sub> =4.5 m <sup>2</sup> g <sup>-1</sup>	[120]
	La <sub>2</sub> O <sub>3</sub>			22.0	0.4	12	0.1	2.6	93		S <sub>BET</sub> <1 m <sup>2</sup> g <sup>-1</sup>	
	MgO			26.0	0.3	11	0.1	2.9	89		S <sub>BET</sub> =9.5 m <sup>2</sup> g <sup>-1</sup>	
	TiO <sub>2</sub>			5.6	0	11	0.0	0.6	77		S <sub>BET</sub> =77 m <sup>2</sup> g <sup>-1</sup>	
	CeO <sub>2</sub>			20.5	0	8.8	0.0	1.8	73		S <sub>BET</sub> =79 m <sup>2</sup> g <sup>-1</sup>	
	BaO			21.3	0.5	10	0.1	2.1	78		S <sub>BET</sub> <1 m <sup>2</sup> g <sup>-1</sup>	
	ZnO			14.9	0	13	0.0	1.9	75		S <sub>BET</sub> <1.4 m <sup>2</sup> g <sup>-1</sup>	
DBD	8%mol Ni/C	CH <sub>4</sub> : CO <sub>2</sub> 1:1	48	51	1.2	16.7	<1	8.6	87.6	Total flow 50 ml min <sup>-1</sup> . Ground electrode length: 5 cm. 250 mg of catalyst	S <sub>BET</sub> =517 m <sup>2</sup> g <sup>-1</sup> ;	[141]
	8%mol Ni /1%molCeO <sub>2</sub> /C			56	1.3	17.0	<1	9.0	88		S <sub>BET</sub> =398 m <sup>2</sup> g <sup>-1</sup>	
	8%mol Ni /5%molCeO <sub>2</sub> /C			58	1.4	17.8	<1	9.7	82		S <sub>BET</sub> =250 m <sup>2</sup> g <sup>-1</sup>	

Table 26: Plasma catalytic methane conversion to C<sub>2</sub> hydrocarbons over Pt and Pd supported on CeO<sub>2</sub>

Discharge	Catalyst	Feed	SEI kJ L <sup>-1</sup>	CH <sub>4</sub> Conv %	Total C <sub>2</sub> selectivity (%)					Comments	Ref	
DBD (nanosecond)	Blank	CH <sub>4</sub>	-	5	18	2	1	<1	98	3 kHz, 980°C, discharge gap 2 mm, discharge length 130 mm	-	[142]
	CeO <sub>2</sub>			13	10	<1	1.5	<1	91	3 kHz, 980°C, discharge gap 2 mm, discharge length 130 mm; 0.5 g of catalyst (20- 40 mesh	S <sub>BET</sub> =77 m <sup>2</sup> g <sup>-1</sup>	
	0.5wt%Pd/CeO <sub>2</sub>			24	10	<1	1.8	<1	80		S <sub>BET</sub> =0.19 m <sup>2</sup> g <sup>-1</sup>	
DBD	Blank	CH <sub>4</sub> :He 1:1	216	35	17					Total flow 20 ml/min; particle size <50µm; 100 mg catalyst	[29]	
	CeO <sub>2</sub>			35	21							
	Pt/CeO <sub>2</sub> -SAC			40	35							
	Pt/CeO <sub>2</sub> -NP			43	47							

### 3.5. Post-plasma catalysts for the oxidative coupling of methane

Post-plasma palladium catalysts were also tested for the production of C<sub>2</sub> hydrocarbons from methane. Delikonstantis *et al.* [143] reported an optimized nanosecond pulsed discharge reactor with a post plasma catalyst in terms of energy cost and selectivity to acetylene by varying flow rate, flow and catalyst composition and inter-electrode gap. Based on their findings and the data reported in the literature, a comparison was drawn between the different 2-stage setups (plasma followed by catalyst) and displayed in Table 27.

Table 27: Comparison of hybrid plasma catalytic reactor with other plasma and catalytic reactor systems

Setup	Plasma	Catalyst	C <sub>2</sub> H <sub>4</sub> yield %	Energy cost kJ mol <sup>-1</sup> C <sub>2</sub> H <sub>4</sub>	Ref
Hybrid reactor	Nanosecond pulsed	0.5 g Commercial Pd based (Johnson Matthey)	25.7	1642	[143]
Recycle AC Plasma + Catalytic reactor	Nanosecond pulsed Spark discharge	0.5g of 0.3 wt% Pd-0.6 wt% Ag/MgAl <sub>2</sub> O <sub>4</sub> in 5g α-Al <sub>2</sub> O <sub>3</sub>	52.1	3266 + Hydrogenation at 150 °C	[144]
		0.5g of 2.5 wt% Ni-7.5 wt% Zn/MgAl <sub>2</sub> O <sub>4</sub> in 5g α-Al <sub>2</sub> O <sub>3</sub>	35	4337 + Hydrogenation at 175°C	
AC Plasma + Catalytic reactor	Spark discharge	0.15g of 0.3wt% Pd- 0.6 wt% Ag/SiO <sub>2</sub> in 0.3g quartz	52.1	3302 + Hydrogenation at 120 °C	[145]
DC pulsed plasma + catalyst reactor	Pulsed spark discharge	0.02 wt% Ag- 0.02wt% Pd/SiO <sub>2</sub>	57	not available	[51]
DC plasma reactor	Spark discharge	Lindlar catalyst (N.E. Chemcat Corporation) PbO-PdO/CaCO <sub>3</sub>	47	not available	[146]
DC plasma reactor + heating/cooling system	Corona discharge	0.025 wt.% Ag– 0.025 wt.% Pd-Y-zeolite	19.3	8442 + Hydrogenation	[147]

The hybrid reactor [143] showed the best ethylene performance in terms of energy cost as compared with the other systems despite its lower yield. Though the advantage of gas recirculation in the AC plasma catalytic reactor [144] should be taken into account. In fact, the improved collision probability of methane molecules with the plasma led to higher conversion (66 to 74 % for recycle ratios from 0 to 4), lowering the energy cost from 10.6 eV/molecule to 9.3 eV/molecule in this specific case. The yield of ethylene in the recycle plasma reactor reached 55 % with a Pd based catalyst. The author also reported good selectivity for ethylene (35 %) and other C<sub>3</sub>–C<sub>5</sub> light olefins (23 %) on a cheaper catalyst based on nickel-zinc in the hydrogenation of acetylene.

Palladium supported catalyst is commonly used for the selective hydrogenation of small amounts of acetylene in the purification of ethylene. The silver-palladium catalysts following a spark discharge can give ethylene yields up to 50-60 % [51,144,145]. The addition of palladium to the NaOH-treated Y-zeolite allowed the selective hydrogenation of acetylene to ethylene but at a low yield (19.3 %) and high energy cost as compared with the other processes [147]. The addition of a catalyst in post discharge presents undeniable advantages for ethylene production since single plasma favors acetylene selectivity. Combining gas recirculation with an optimized hybrid reactor would be a good solution to improve both ethylene yield and lower energy costs.

#### **4. Compiling plasma alone and plasma-catalysis results**

Numerous plasma-assisted processes have been investigated and proposed for the coupling of methane to C<sub>2</sub> added value products. Hybridization of plasma and catalyst into one system does provide a synergistic result for activation at low temperatures. It has the potential to enhance the conversion of methane and to improve the selectivity toward the desirable C<sub>2</sub> products, but it is not all that elementary. The reviewed studies have shown a positive effect of plasma–catalysis combination processes on the methane coupling reaction. However, the combined data plotted in Figure 17 shows a large array of scattered results from the plasma-alone and the

plasma-catalytic processes. It reveals how strongly interconnected all the parameters described in this review are.

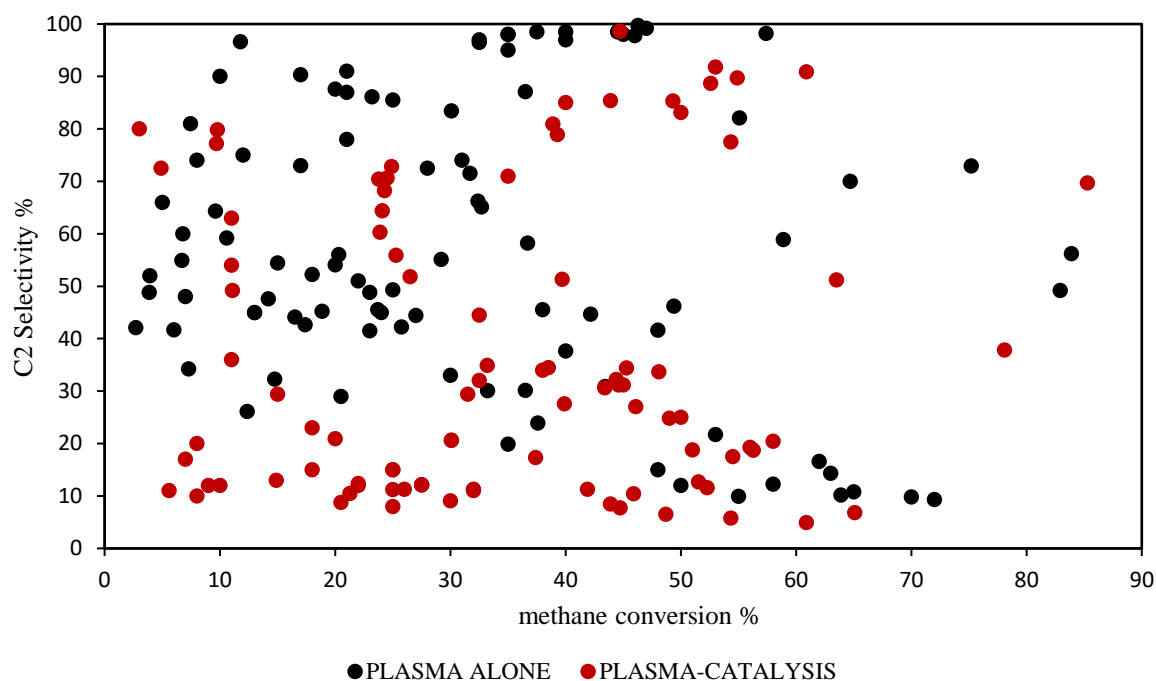


Figure 17: methane conversion and C<sub>2</sub> selectivity in plasma reaction and plasma-catalytic reaction

In any plasma-catalytic process, the complexity of the catalyst surface and gas-phase chemistry are strongly correlated to the physical properties of the individual plasma and catalyst. First of all, the comparison of different plasma sources is challenging since the reactors, the generators and discharge characteristics (specific energy, electron energy distribution and electron density) differ strongly from one study to another. Second of all, the target products and the chosen methodologies to determine their presence and concentration differ as well. Some literature reports are either incomplete or inaccurate and may lead to early conclusions. The specific energy input represents a suitable parameter for the comparison of the data (Figure 18), even though this parameter is not present in every publication reported. The plasma alone and the plasma-catalytic processes, for which SEI has been provided or determined, have values varying from 1 to 512 kJ L<sup>-1</sup> of methane feed. The methane conversion for plasma alone is usually below 50 % for SEI values up to ~64 kJ L<sup>-1</sup> and the selectivities for C<sub>2</sub> products are



over 40 %. However, for SEI values varying from 64 to 512 kJ L<sup>-1</sup>, higher conversions of methane (>50 %) were achieved, but the selectivities of C<sub>2</sub> products dropped, in some cases, to under 50 %.

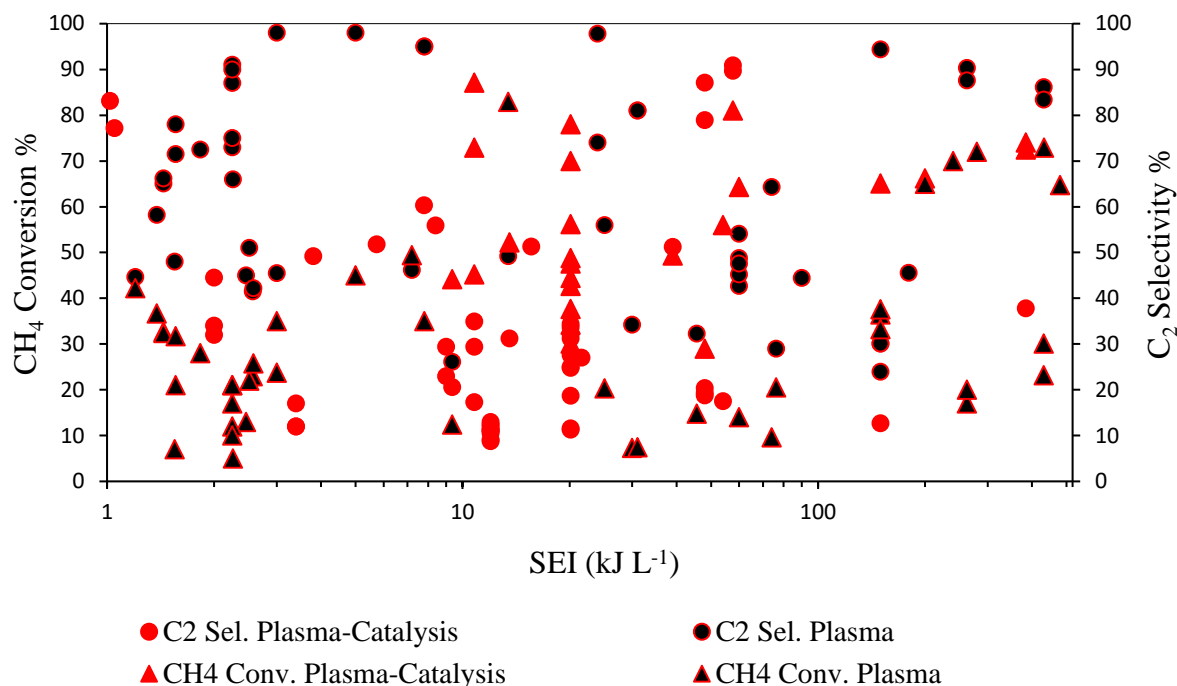


Figure 18: methane conversion and C<sub>2</sub> selectivity as a function of SEI in plasma alone and plasma-catalytic processes. The X axis is presented on a logarithmic scale

Most of the data in the plasma-catalytic processes is comprised between 4 and 64 kJ L<sup>-1</sup>, but with conversion and selectivity below 50 %. The SEI range has an effect on methane conversion and C<sub>2</sub> selectivity, both in plasma alone and in plasma-catalytic systems: low SEI will favor high selectivities but low conversions, while high SEI will increase the conversion but lower the selectivity. C<sub>2</sub> yield as a function of SEI (Figure 19) highlights that both plasma and plasma-catalysis processes are efficient to produce light hydrocarbons and some publications have shown enhanced C<sub>2</sub> yield at moderate energy input.

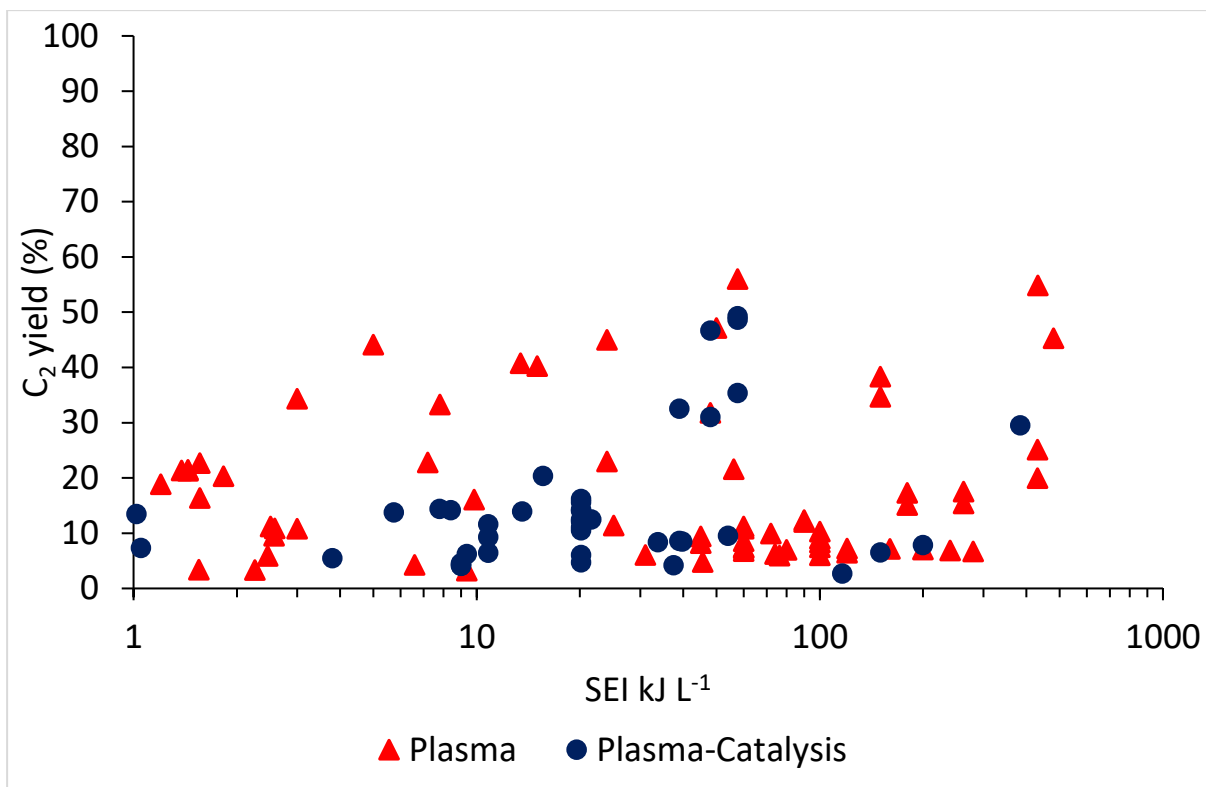


Figure 19: C<sub>2</sub> yield as a function of SEI in plasma alone and plasma-catalytic processes. The X axis is presented on a logarithmic scale

Delikonstantis *et al.* [53] reported a 44% yield in C<sub>2</sub> with 5 kJ L<sup>-1</sup> in a nanosecond pulsed discharge in presence of hydrogen that comforted the studies of Kado *et al.* [62] who reported 40.2 % C<sub>2</sub> yield (15 kJ L<sup>-1</sup>) in a DC pulsed discharge in pure methane, both in a plasma alone configuration. Li *et al.* [61] showed that adding alumina pellets reduced carbon deposition from 28 % to 8.5 % in pure methane with improved methane conversion (30 to 35 %) and C<sub>2</sub> yield (22 to 27 %) using a pulsed streamer discharge (22.8 kJ L<sup>-1</sup>). Methane conversion of 54.9 % and 49.2 % C<sub>2</sub> selectivity were obtained with Co-ZSM-5 zeolite in a microwave plasma with a mixture of methane with oxygen at 57.6 kJ L<sup>-1</sup> [34]. These data illustrate the usefulness of the catalyst addition in the plasma discharge and the importance to develop well-defined catalysts.

To be more accurate, energetic consideration should be standardized and expressed in terms of energy efficiency that relies on specific energy and enthalpy of reaction, as highlighted in Scapinello review [21].

The energy requirement (ER) is the energy necessary to produce one mole of one C<sub>2</sub> product and considers the specific energy input:

$$ER (kJ mol^{-1}) = 2 \times \frac{SEI}{CH_4 \text{ conversion} \times C_2 \text{ product selectivity}}$$

The factor 2 being related to the presence of 2 carbons in C<sub>2</sub> products

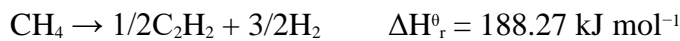
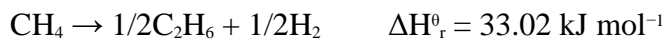
The specific energy requirement (SER) is the energy required for full conversion of one CH<sub>4</sub> mole is expressed as:

$$SER (kJ mol^{-1}) = \frac{SEI}{CH_4 \text{ conversion}}$$

The enthalpy of the global CH<sub>4</sub> coupling reaction depends on the acetylene, ethylene and ethane coefficients and can be expressed as following:

$$\Delta H_r^{\circ} (kJ mol^{-1}) = 2(33.02 \alpha + 101.12 \beta + 188.27 \gamma) + 74.87 (1 - 2\alpha - 2\beta - 2\gamma)$$

where  $\alpha$ ,  $\beta$  and  $\gamma$  are the reaction coefficients calculated by the product stream analysis calculated by the acetylene, ethylene and ethane stream analysis. The energetic thresholds for each reaction being:




Finally, the efficiency, is expressed as:

$$\eta(\%) = 100 * \frac{\Delta H_r^{\circ}}{SER}$$

## 5. Concluding remarks

The aim of this review was to evaluate the current state of the art in the coupling of methane for C<sub>2</sub> production by plasma alone and plasma-catalysis, with a focus on the effect of the reaction conditions and fixed parameters. The main parameters with strong influence in the plasma process alone and in the plasma-catalysis are compiled below:

PLASMA ALONE	PLASMA - CATALYSIS
<p>Type of discharge</p> <p>physical parameters (power, frequency, pulse duration, pressure, gap distance, temperature)</p> <p>Discharge volume/residence time</p> <p>Feed gas composition: noble gas or oxidant</p>	<p>Packing material: particle size, pore size, material shape, dielectric constant</p> <p>Catalyst: redox and acid-base properties, electrical conductivity</p> <p>Synergistic effects plasma-catalyst</p>
 <p>SPECIFIC ENERGY INPUT</p>	

Various types of plasma for methane conversion into higher hydrocarbons yield different performances in terms of conversion, energy cost and selectivity towards hydrocarbons. For this reason, it is important to have a clear understanding of the advantages and disadvantages of each type of discharge. Major advantages of cold plasma techniques are the low operating temperature, the low thermal inertia and the fast response to fluctuating or intermittent operating conditions. The specific energy input is the best indicator of the process efficiency, as it changes with each variable parameter. The advantage of glidarc, microwave and spark discharges is linked to their characteristics as they are warm and dense plasma. The pulsed nanodischarge approach seems promising as it results in high energy efficiency.

The addition of gases to the methane feed changes the reactivity of the system, which can have considerable effects on the methane conversion, carbon deposition or selectivities to final reaction products. The non-oxidative methane coupling is performed with additives like hydrogen, nitrogen or noble gases. Even though the additive gas can have positive effects on the methane conversion, the cost (especially for the noble gases) and the formation of undesired products (mostly in the case of nitrogen) must be considered. Hydrogen seems promising for methane conversion, but the product selectivities can be shifted only by a combined effect of hydrogen content in the feed and plasma reactor pressure. Concerning the oxidative coupling of methane, oxygen is considered effective for the activation of methane and the reduction of carbon contamination. However, excessive oxidation leads to the formation of carbon dioxide and a wide variety of oxygenated products that limit selectivity to  $C_2$ . The use of carbon dioxide as a milder oxidant may sometimes be preferable for the activation of methane, but it also leads to the production of syngas and oxygenated compounds. The plasma chemistry in the presence of an oxidant is quite complex and, until now, its understanding remains limited. Understanding the underlying plasma chemistry in the oxidative or non-oxidative coupling of methane is of great interest in the optimization of this technology, especially when the aim is to include a catalyst for the improvement of product yields.

Packing material into the discharge affects the electric field, the gas breakdown voltage and plasma behavior. It also modifies the electron density and electron energy distribution. Many factors, such as particle size, shape, structure, chemical nature and location (and hence the volume fraction of the packed material in the discharge area) may improve the overall processing performance compared to plasma or catalyst taken separately. These results are particularly interesting and future research should focus on this type of discharges in association with optimized catalytic phases. Dielectric constants and pore sizes contribute to the performance of the plasma by changing its electrical properties and propagation mode. The availability of plasma species inside the pore is of significant importance, as their interaction

with the surface might affect the morphology and work function of the catalyst, influencing its performance. Moreover, if the plasma species can exist inside the pores, it will increase the active surface of the catalyst that can participate in the reactions. The favored packing materials must have a low dielectric constant, high surface area, facile mass transport and homogeneous dispersion of active sites. The catalytic activity can be influenced by strong metal support interactions between the active catalyst component and the support. Novel design of efficient catalysts for the coupling of methane assisted by plasma requires deeper investigation of the surface effects such as oxygen vacancy, acid–base property, surface oxide reducibility and most importantly, how they influence and/or react with the plasma reactive species.

The synergism that originates from the complex plasma-catalyst interactions still represents a challenge of understanding. Plasma and catalyst characteristics and reactivities are interconnected. Plasma induces modifications in morphology, chemistry and surface work function, altering activity. Catalyst properties such as dielectric constant, acidity-basicity or structure affect plasma properties near the surface such as the electric-field distribution, surface charging and electron-energy distribution. Many efforts have been carried out to integrate plasma and catalysis in one step since it modifies selectivity to desired products, as well as energy efficiency. Moreover, the catalyst generates a wider variety of reaction products as compared to plasma alone.

Considering the current results from a cost perspective, a considerable advantage of the plasma alone process is that no catalyst is involved in the reaction therefore, the operation of the plasma reactor is stable and the process is easy to integrate. The challenges associated with catalyst utilization, such as catalyst activation, regeneration, poisoning and aging, consist in avoiding the disruption of the continuous operation. The process is still confronted to the formation of carbonaceous residue leading to the decrease of reactor performances and eventually to discharge extinction.

Reaching high energy efficiency is the biggest challenge to the industrialization of the plasma process. Although it is considered by many that the integration of plasma and catalysis can lead to a high energy efficiency, the critical selectivity/conversion limitations related to the experiments have led to the conclusion that, for the moment, the use of plasma-catalytic systems does not achieve favorable energy efficiencies as compared to the plasma process alone or thermal catalysis. In order to define appropriately the energy efficiency, its calculation should also be internationally standardized. Although various innovative strategies in catalyst synthesis, plasma reactor type and configuration have been employed in order to achieve oxidative or non-oxidative methane coupling with high and stable C<sub>2</sub> yield, the improvement achieved so far is not significant enough to take the process to an industrial and economically viable stage. It is still essential to accurately characterize and strengthen the understanding of the reaction mechanisms of plasma coupling with catalysis, before considering scaling up the process. The understanding of plasma-catalytic mechanisms occurring in such complex systems still requires the development of new approaches and techniques to provide insight into the associated fundamental phenomena and plasma-catalyst interaction. Answers to queries on the behavior of the plasma process and surface reaction should come from additional research (experimental and modeling) on the propagation of the discharge in the porosity of the material.

## References

- [1] Fernandez Palez A, Levi P. The Future of Petrochemicals 2018. <https://www.iea.org/reports/the-future-of-petrochemicals>.
- [2] Mynko O, Amghizar I, Brown DJ, Chen L, Marin GB, de Alvarenga RF, et al. Reducing CO<sub>2</sub> emissions of existing ethylene plants: Evaluation of different revamp strategies to reduce global CO<sub>2</sub> emission by 100 million tonnes. *Journal of Cleaner Production* 2022;362:132127. <https://doi.org/10.1016/j.jclepro.2022.132127>.
- [3] Cruellas A, Bakker JJ, van Sint Annaland M, Medrano JA, Gallucci F. Techno-economic analysis of oxidative coupling of methane: Current state of the art and future perspectives. *Ener Convers Manage* 2019;198:111789. <https://doi.org/10.1016/j.enconman.2019.111789>.
- [4] Alexiadis VI, Chaar M, van Veen A, Muhler M, Thybaut JW, Marin GB. Quantitative screening of an extended oxidative coupling of methane catalyst library. *Appl Catal B: Environ* 2016;199:252–9. <https://doi.org/10.1016/j.apcatb.2016.06.019>.
- [5] Ghose R, Hwang HT, Varma A. Oxidative coupling of methane using catalysts synthesized by solution combustion method: Catalyst optimization and kinetic studies. *Appl Catal A: Gen* 2014;472:39–46. <https://doi.org/10.1016/j.apcata.2013.12.004>.
- [6] Galadima A, Muraza O. Revisiting the oxidative coupling of methane to ethylene in the golden period of shale gas: A review. *J Ind Eng Chem* 2016;37:1–13. <https://doi.org/10.1016/j.jiec.2016.03.027>.
- [7] Zavyalova U, Holena M, Schlögl R, Baerns M. Statistical Analysis of Past Catalytic Data on Oxidative Methane Coupling for New Insights into the Composition of High-Performance Catalysts. *Chem Cat Chem* 2011;3:1935–47. <https://doi.org/10.1002/cctc.201100186>.
- [8] Schwach P, Pan X, Bao X. Direct Conversion of Methane to Value-Added Chemicals over Heterogeneous Catalysts: Challenges and Prospects. *Chem Rev* 2017;117:8497–520. <https://doi.org/10.1021/acs.chemrev.6b00715>.
- [9] Choudhary VR, Mulla SAR, Uphade BS. Oxidative coupling of methane over alkaline earth oxides deposited on commercial support precoated with rare earth oxides. *Fuel* 1999;78:427–37. [https://doi.org/10.1016/S0016-2361\(98\)00168-9](https://doi.org/10.1016/S0016-2361(98)00168-9).
- [10] Dinh DK, Lee DH, Song Y-H, Jo S, Kim K-T, Iqbal M, et al. Efficient methane-to-acetylene conversion using low-current arcs. *RSC Adv* 2019;9:32403–13. <https://doi.org/10.1039/C9RA05964D>.
- [11] Dipu AL, Ohbuchi S, Nishikawa Y, Iguchi S, Ogihara H, Yamanaka I. Direct Nonoxidative Conversion of Methane to Higher Hydrocarbons over Silica-Supported Nickel Phosphide Catalyst. *ACS Catal* 2020;10:375–9. <https://doi.org/10.1021/acscatal.9b03955>.
- [12] Guo X, Fang G, Li G, Ma H, Fan H, Yu L, et al. Direct, Nonoxidative Conversion of Methane to Ethylene, Aromatics, and Hydrogen. *Science* 2014;344:616–9. <https://doi.org/10.1126/science.1253150>.
- [13] Lee BJ, Hur YG, Kim DH, Lee SH, Lee K-Y. Non-oxidative aromatization and ethylene formation over Ga/HZSM-5 catalysts using a mixed feed of methane and ethane. *Fuel* 2019;253:449–59. <https://doi.org/10.1016/j.fuel.2019.05.014>.
- [14] Beloqui Redondo A, Troussard E, van Bokhoven JA. Non-oxidative methane conversion assisted by corona discharge. *Fuel Process Technol* 2012;104:265–70. <https://doi.org/10.1016/j.fuproc.2012.05.021>.
- [15] Meng X, Cui X, Rajan NP, Yu L, Deng D, Bao X. Direct Methane Conversion under Mild Condition by Thermo-, Electro-, or Photocatalysis. *Chem* 2019;5:2296–325. <https://doi.org/10.1016/j.chempr.2019.05.008>.



- [16] Bogaerts A, Tu X, Whitehead JC, Centi G, Lefferts L, Guaitella O, et al. The 2020 plasma catalysis roadmap. *J Phys D: Appl Phys* 2020;53:443001. <https://doi.org/10.1088/1361-6463/ab9048>.
- [17] Delikonstantis E, Scapinello M, Stefanidis GD. Process Modeling and Evaluation of Plasma-Assisted Ethylene Production from Methane. *Processes* 2019;7:68. <https://doi.org/10.3390/pr7020068>.
- [18] Nehra V, Kumar A, Dwivedi HK. Atmospheric Non-Thermal Plasma Sources. *Int J Eng* 2008;2:53.
- [19] Fridman A, Chirokov A, Gutsol A. Non-thermal atmospheric pressure discharges. *J Phys D: Appl Phys* 2005;38:R1–24. <https://doi.org/10.1088/0022-3727/38/2/R01>.
- [20] Lee DH, Song Y-H, Kim K-T, Lee J-O. Comparative Study of Methane Activation Process by Different Plasma Sources. *Plasma Chem Plasma Process* 2013;33:647–61. <https://doi.org/10.1007/s11090-013-9456-6>.
- [21] Scapinello M, Delikonstantis E, Stefanidis GD. The panorama of plasma-assisted non-oxidative methane reforming. *Chem Eng Process* 2017. <https://doi.org/10.1016/j.cep.2017.03.024>.
- [22] Liu C, Marafee A, Hill B, Xu G, Mallinson R, Lobban L. Oxidative Coupling of Methane with ac and dc Corona Discharges. *Ind Eng Chem Res* 1996;35:3295–301. <https://doi.org/10.1021/ie960138j>.
- [23] Liu C, Marafee A, Mallinson R, Lobban L. Methane conversion to higher hydrocarbons in a corona discharge over metal oxide catalysts with OH groups. *Appl Cat A: Gen* 1997;164:21–33. [https://doi.org/10.1016/S0926-860X\(97\)00154-3](https://doi.org/10.1016/S0926-860X(97)00154-3).
- [24] Zhu A, Gong W, Zhang X, Zhang B. Coupling of methane under pulse corona plasma (I): In the absence of oxygen. *Sc China Ser B-Chem* 2000;43:208–14. <https://doi.org/10.1007/BF03027312>.
- [25] Rahmati H, Ghorbanzadeh A. Parallel electrodes gliding plasma: Working principles and application in dry reforming of methane. *Energy* 2021;230:120753. <https://doi.org/10.1016/j.energy.2021.120753>.
- [26] Hu S, Wang B, Lv Y, Yan W. Conversion of Methane to C2 Hydrocarbons and Hydrogen Using a Gliding Arc Reactor. *Plasma Sci Technol* 2013;15:555–61. <https://doi.org/10.1088/1009-0630/15/6/13>.
- [27] Bo Z, Yan J, Li X, Chi Y, Cen K. Plasma assisted dry methane reforming using gliding arc gas discharge: Effect of feed gases proportion. *Int J Hydrog Energy* 2008;33:5545–53. <https://doi.org/10.1016/j.ijhydene.2008.05.101>.
- [28] Pourali N, Hessel V, Rebrov EV. The Effects of Pulse Shape on the Selectivity and Production Rate in Non-oxidative Coupling of Methane by a Micro-DBD Reactor. *Plasma Chem Plasma Process* 2022;42:619–40. <https://doi.org/10.1007/s11090-022-10242-6>.
- [29] Liu L, Das S, Zhang Z, Kawi S. Nonoxidative Coupling of Methane over Ceria-Supported Single-Atom Pt Catalysts in DBD Plasma. *ACS Appl Mater Interfaces* 2022;14:5363–75. <https://doi.org/10.1021/acsami.1c21550>.
- [30] García-Moncada N, van Rooij G, Cents T, Lefferts L. Catalyst-assisted DBD plasma for coupling of methane: Minimizing carbon-deposits by structured reactors. *Catalysis Today* 2021;369:210–20. <https://doi.org/10.1016/j.cattod.2020.04.028>.
- [31] Taheraslani M, Gardeniers H. Coupling of CH<sub>4</sub> to C<sub>2</sub> Hydrocarbons in a Packed Bed DBD Plasma Reactor: The Effect of Dielectric Constant and Porosity of the Packing. *Energies* 2020;13:468. <https://doi.org/10.3390/en13020468>.
- [32] Wang B, Yan W, Ge W, Duan X. Kinetic model of the methane conversion into higher hydrocarbons with a dielectric barrier discharge microplasma reactor. *Chem Eng J* 2013;234:354–60. <https://doi.org/10.1016/j.cej.2013.08.052>.

- [33] Nozaki T, Ağırallı A, Yuzawa S, Han Gardeniers JGE, Okazaki K. A single step methane conversion into synthetic fuels using microplasma reactor. *Chem Eng J* 2011;166:288–93. <https://doi.org/10.1016/j.cej.2010.08.001>.
- [34] Cho W, Baek Y, Moon S-K, Kim YC. Oxidative coupling of methane with microwave and RF plasma catalytic reaction over transitional metals loaded on ZSM-5. *Catal Today* 2002;74:207–23. [https://doi.org/10.1016/S0920-5861\(02\)00030-5](https://doi.org/10.1016/S0920-5861(02)00030-5).
- [35] Heintze M, Magureanu M, Kettlitz M. Mechanism of C2 hydrocarbon formation from methane in a pulsed microwave plasma. *J Appl Phys* 2002;92:7022–31. <https://doi.org/10.1063/1.1521518>.
- [36] Puliyalil H, Lašič Jurković D, Dasireddy VDBC, Likozar B. A review of plasma-assisted catalytic conversion of gaseous carbon dioxide and methane into value-added platform chemicals and fuels. *RSC Adv* 2018;8:27481–508. <https://doi.org/10.1039/C8RA03146K>.
- [37] Whitehead JC. Plasma-catalysis: the known knowns, the known unknowns and the unknown unknowns. *J Phys D: Appl Phys* 2016;49:243001. <https://doi.org/10.1088/0022-3727/49/24/243001>.
- [38] Zhang K, Mukhriza T, Liu X, Greco PP, Chiremba E. A study on CO2 and CH4 conversion to synthesis gas and higher hydrocarbons by the combination of catalysts and dielectric-barrier discharges. *Applied Catalysis A: General* 2015;502:138–49. <https://doi.org/10.1016/j.apcata.2015.06.002>.
- [39] Neyts EC, Ostrikov KK, Sunkara MK, Bogaerts A. Plasma Catalysis: Synergistic Effects at the Nanoscale. *Chem Rev* 2015;115:13408–46. <https://doi.org/10.1021/acs.chemrev.5b00362>.
- [40] Che F, Gray JT, Ha S, Kruse N, Scott SL, McEwen J-S. Elucidating the Roles of Electric Fields in Catalysis: A Perspective. *ACS Catal* 2018;8:5153–74. <https://doi.org/10.1021/acscatal.7b02899>.
- [41] Witvrouwen T, Paulussen S, Sels B. The Use of Non-Equilibrium Plasmas for the Synthesis of Heterogeneous Catalysts. *Plasma Processes Polym* 2012;9:750–60. <https://doi.org/10.1002/ppap.201200004>.
- [42] Eliasson B, Kogelschatz U. Nonequilibrium volume plasma chemical processing. *IEEE Trans Plasma Sci* 1991;19:1063–77. <https://doi.org/10.1109/27.125031>.
- [43] Indarto A, Choi J-W, Lee H, Song HK. Methane Conversion Using Dielectric Barrier Discharge: Comparison with Thermal Process and Catalyst Effects. *J Nat Gas Chem* 2006;15:87–92. [https://doi.org/10.1016/S1003-9953\(06\)60013-3](https://doi.org/10.1016/S1003-9953(06)60013-3).
- [44] Xu C, Tu X. Plasma-assisted methane conversion in an atmospheric pressure dielectric barrier discharge reactor. *J Ener Chem* 2013;22:420–5. [https://doi.org/10.1016/S2095-4956\(13\)60055-8](https://doi.org/10.1016/S2095-4956(13)60055-8).
- [45] Nozaki T, Hattori A, Okazaki K. Partial oxidation of methane using a microscale non-equilibrium plasma reactor. *Catal Today* 2004;98:607–16. <https://doi.org/10.1016/j.cattod.2004.09.053>.
- [46] Yang Y. Direct Non-oxidative Methane Conversion by Non-thermal Plasma: Experimental Study. *Plasma Chem Plasma Process* 2003;23:283.
- [47] Jo S, Hoon Lee D, Song Y-H. Product analysis of methane activation using noble gases in a non-thermal plasma. *Chem Eng Sci* 2015;130:101–8. <https://doi.org/10.1016/j.ces.2015.03.019>.
- [48] Scapinello M, Delikonstantis E, Stefanidis GD. A study on the reaction mechanism of non-oxidative methane coupling in a nanosecond pulsed discharge reactor using isotope analysis. *Chem Eng J* 2019;360:64–74. <https://doi.org/10.1016/j.cej.2018.11.161>.
- [49] De Bie C, Verheyde B, Martens T, van Dijk J, Paulussen S, Bogaerts A. Fluid Modeling of the Conversion of Methane into Higher Hydrocarbons in an Atmospheric Pressure

- Dielectric Barrier Discharge: Fluid Modeling of the Conversion of Methane. *Plasma Processes Polym* 2011;8:1033–58. <https://doi.org/10.1002/ppap.201100027>.
- [50] Shao T, Wang R, Zhang C, Yan P. Atmospheric-pressure pulsed discharges and plasmas: mechanism, characteristics and applications. *High Voltage* 2018;3:14–20. <https://doi.org/10.1049/hve.2016.0014>.
- [51] Kangjun W, Xiaosong L, Hui W, Chuan S, Yong X, Aimin Z. Oxygen-Free Conversion of Methane to Ethylene in a Plasma-Followed-by-Catalyst (PFC) Reactor. *Plasma Sci Technol* 2008;10:600–4. <https://doi.org/10.1088/1009-0630/10/5/15>.
- [52] Kado S, Urasaki K, Sekine Y, Fujimoto K, Nozaki T, Okazaki K. Reaction mechanism of methane activation using non-equilibrium pulsed discharge at room temperature. *Fuel* 2003;82:2291–7. [https://doi.org/10.1016/S0016-2361\(03\)00163-7](https://doi.org/10.1016/S0016-2361(03)00163-7).
- [53] Delikonstantis E, Scapinello M, Van Geenhoven O, Stefanidis GD. Nanosecond pulsed discharge-driven non-oxidative methane coupling in a plate-to-plate electrode configuration plasma reactor. *Chem Eng J* 2020;380:122477. <https://doi.org/10.1016/j.cej.2019.122477>.
- [54] Kirikov AV, Ryzhov VV, Suslov AI. Kinetics of free radicals in the plasma of a spark discharge in methane. *Tech Phys Lett* 1999;25:794–5. <https://doi.org/10.1134/1.1262638>.
- [55] Heijkers S, Aghaei M, Bogaerts A. Plasma-Based CH<sub>4</sub> Conversion into Higher Hydrocarbons and H<sub>2</sub>: Modeling to Reveal the Reaction Mechanisms of Different Plasma Sources. *J Phys Chem C* 2020;124:7016–30. <https://doi.org/10.1021/acs.jpcc.0c00082>.
- [56] Saleem F, Kennedy J, Dahiru UH, Zhang K, Harvey A. Methane conversion to H<sub>2</sub> and higher hydrocarbons using non-thermal plasma dielectric barrier discharge reactor. *Chem Eng Process* 2019;142:107557. <https://doi.org/10.1016/j.cep.2019.107557>.
- [57] Wang B, Yan W, Ge W, Duan X. Methane conversion into higher hydrocarbons with dielectric barrier discharge micro-plasma reactor. *J Ener Chem* 2013;22:876–82. [https://doi.org/10.1016/S2095-4956\(14\)60267-9](https://doi.org/10.1016/S2095-4956(14)60267-9).
- [58] Indarto A, Choi J-W, Lee H, Song HK. Methane Conversion Using Dielectric Barrier Discharge: Comparison with Thermal Process and Catalyst Effects. *Journal of Natural Gas Chemistry* 2006;15:87–92. [https://doi.org/10.1016/S1003-9953\(06\)60013-3](https://doi.org/10.1016/S1003-9953(06)60013-3).
- [59] Zhang X, Wang B, Liu Y, Xu G. Conversion of Methane by Steam Reforming Using Dielectric-barrier Discharge. *Chinese Chem Eng* 2009;17:625–9. [https://doi.org/10.1016/S1004-9541\(08\)60254-2](https://doi.org/10.1016/S1004-9541(08)60254-2).
- [60] Scapinello M, Delikonstantis E, Stefanidis GD. Direct methane-to-ethylene conversion in a nanosecond pulsed discharge. *Fuel* 2018;222:705–10. <https://doi.org/10.1016/j.fuel.2018.03.017>.
- [61] Li X-S, Zhu A-M, Wang K-J, Xu Y, Song Z-M. Methane conversion to C<sub>2</sub> hydrocarbons and hydrogen in atmospheric non-thermal plasmas generated by different electric discharge techniques. *Catal Today* 2004;98:617–24. <https://doi.org/10.1016/j.cattod.2004.09.048>.
- [62] Kado S, Sekine Y, Fujimoto K. Direct synthesis of acetylene from methane by direct current pulse discharge. *Chem Commun* 1999:2485–6. <https://doi.org/10.1039/a906914c>.
- [63] Lotfalipour R, Ghorbanzadeh AM, Mahdian A. Methane conversion by repetitive nanosecond pulsed plasma. *J Phys D: Appl Phys* 2014;47:365201. <https://doi.org/10.1088/0022-3727/47/36/365201>.
- [64] Fridman A. *Plasma Chemistry*. Cambridge: Cambridge University Press; 2008. <https://doi.org/10.1017/CBO9780511546075>.
- [65] Liu SY, Mei DH, Shen Z, Tu X. Nonoxidative Conversion of Methane in a Dielectric Barrier Discharge Reactor: Prediction of Reaction Performance Based on Neural

- Network Model. *J Phys Chem C* 2014;118:10686–93. <https://doi.org/10.1021/jp502557s>.
- [66] Jeong H-K, Kim S-C, Han C, Lee H, Song HK, Na B-K. Conversion of methane to higher hydrocarbons in pulsed DC barrier discharge at atmospheric pressure. *Korean J Chem Eng* 2001;18:196–201. <https://doi.org/10.1007/BF02698459>.
- [67] Tarverdi MSH, Mortazavi Y, Khodadadi AA, Mohajerzadeh S. Synergetic Effects of Plasma, Temperature and Diluant on Nonoxidative Conversion of Methane to C<sub>2</sub>+ Hydrocarbons in a Dielectric Barrier Discharge Reactor. *Iranian Journal of Chemistry & Chemical Engineering* 2005;24:63–71.
- [68] Zhang X, Cha MS. Partial oxidation of methane in a temperature-controlled dielectric barrier discharge reactor. *P Combust Inst* 2015;35:3447–54. <https://doi.org/10.1016/j.proci.2014.05.089>.
- [69] Zhang X, Cha MS. Electron-induced dry reforming of methane in a temperature-controlled dielectric barrier discharge reactor. *J Phys D: Appl Phys* 2013;46:415205. <https://doi.org/10.1088/0022-3727/46/41/415205>.
- [70] Liu J-L, Snoeckx R, Cha MS. Steam reforming of methane in a temperature-controlled dielectric barrier discharge reactor: the role of electron-induced chemistry versus thermochemistry. *J Phys D: Appl Phys* 2018;51:385201. <https://doi.org/10.1088/1361-6463/aad7e7>.
- [71] Ravasio S, Cavallotti C. Analysis of reactivity and energy efficiency of methane conversion through non thermal plasmas. *Chem Eng Sci* 2012;84:580–90. <https://doi.org/10.1016/j.ces.2012.09.012>.
- [72] Abhijit Majumdar, Jürgen F. Behnke and, Hippler R, and KM, Schneider R. Chemical Reaction Studies in CH<sub>4</sub>/Ar and CH<sub>4</sub>/N<sub>2</sub> Gas Mixtures of a Dielectric Barrier Discharge. ACS Publications 2005. <https://doi.org/10.1021/jp053588a>.
- [73] Snoeckx R, Setareh M, Aerts R, Simon P, Maghari A, Bogaerts A. Influence of N<sub>2</sub> concentration in a CH<sub>4</sub>/N<sub>2</sub> dielectric barrier discharge used for CH<sub>4</sub> conversion into H<sub>2</sub>. *Int J Hydrog Energy* 2013;38:16098–120. <https://doi.org/10.1016/j.ijhydene.2013.09.136>.
- [74] Bai X, Tiwari S, Robinson B, Killmer C, Li L, Hu J. Microwave catalytic synthesis of ammonia from methane and nitrogen. *Catal Sci Technol* 2018;8:6302–5. <https://doi.org/10.1039/C8CY01355A>.
- [75] Kado S. Direct conversion of methane to acetylene or syngas at room temperature using non-equilibrium pulsed discharge. *Fuel* 2003;82:1377–85. [https://doi.org/10.1016/S0016-2361\(03\)00038-3](https://doi.org/10.1016/S0016-2361(03)00038-3).
- [76] Bin D, Xiu-ling Z, Wei-min G, Ren H. Effects of Hydrogen on the Methane Coupling under Non-Equilibrium Plasma. *Plasma Sci Technol* 2001;3:637–9. <https://doi.org/10.1088/1009-0630/3/1/007>.
- [77] Shen C, Sun D, Yang H. Methane coupling in microwave plasma under atmospheric pressure. *J Nat Gas Chem* 2011;20:449–56. [https://doi.org/10.1016/S1003-9953\(10\)60209-5](https://doi.org/10.1016/S1003-9953(10)60209-5).
- [78] Maitre P-A, Long J, Bieniek MS, Bannerman MN, Kechagiopoulos PN. Investigating the effects of helium, argon and hydrogen co-feeding on the non-oxidative coupling of methane in a dielectric barrier discharge reactor. *Chem Eng Sci* 2022;259:117731. <https://doi.org/10.1016/j.ces.2022.117731>.
- [79] Goujard V, Tatibouët J-M, Batiot-Dupeyrat C. Carbon Dioxide Reforming of Methane Using a Dielectric Barrier Discharge Reactor: Effect of Helium Dilution and Kinetic Model. *Plasma Chem Plasma Process* 2011;31:315–25. <https://doi.org/10.1007/s11090-010-9283-y>.

- [80] Eliasson B, Hirth M, Kogelschatz U. Ozone synthesis from oxygen in dielectric barrier discharges. *J Phys D: Appl Phys* 1987;20:1421–37. <https://doi.org/10.1088/0022-3727/20/11/010>.
- [81] Taylor KJ, Tynan GR. Control of dissociation by varying oxygen pressure in noble gas admixtures for plasma processing. *J Vac Sci Technol* 2005;23:643–50. <https://doi.org/10.1116/1.1931682>.
- [82] Zhou J, Zhou J, Xu Y, Yan B, Yu X. Control of methane plasma oxidative pathways by altering the contribution of oxygen species. *Fuel* 2021;284:118944. <https://doi.org/10.1016/j.fuel.2020.118944>.
- [83] Miao Y, Kreider P, Reddick I, Pommerenck J, Collin R, AuYeung N, et al. Methane Coupling to Ethylene and Longer-Chain Hydrocarbons by Low-Energy Electrical Discharge in Microstructured Reactors. *Ind Eng Chem Res* 2021;60:6950–8. <https://doi.org/10.1021/acs.iecr.0c05984>.
- [84] Aghamir FM, Matin NS, Jalili AH, Esfarayeni MH, Khodagholi MA, Ahmadi R. Conversion of methane to methanol in an ac dielectric barrier discharge. *Plasma Sources Sci Technol* 2004;13:707–11. <https://doi.org/10.1088/0963-0252/13/4/021>.
- [85] Istadi, Amin NAS. Co-generation of synthesis gas and C<sub>2</sub>+ hydrocarbons from methane and carbon dioxide in a hybrid catalytic-plasma reactor: A review. *Fuel* 2006;85:577–92. <https://doi.org/10.1016/j.fuel.2005.09.002>.
- [86] Liu S, Winter LR, Chen JG. Review of Plasma-Assisted Catalysis for Selective Generation of Oxygenates from CO<sub>2</sub> and CH<sub>4</sub>. *ACS Catal* 2020;10:2855–71. <https://doi.org/10.1021/acscatal.9b04811>.
- [87] Khoja AH, Tahir M, Amin NAS. Recent developments in non-thermal catalytic DBD plasma reactor for dry reforming of methane. *Ener Convers Manage* 2019;183:529–60. <https://doi.org/10.1016/j.enconman.2018.12.112>.
- [88] Ozkan A, Dufour T, Arnoult G, De Keyzer P, Bogaerts A, Reniers F. CO<sub>2</sub>–CH<sub>4</sub> conversion and syngas formation at atmospheric pressure using a multi-electrode dielectric barrier discharge. *J CO<sub>2</sub> Utiliz* 2015;9:74–81. <https://doi.org/10.1016/j.jcou.2015.01.002>.
- [89] Pokrovskiy G. Dissociation of carbon dioxide in pulsed plasma at high electric fields: role of energy exchange with electronically excited species. PhD thesis. Institut Polytechnique de Paris, 2021.
- [90] Fox JL. CO<sub>2</sub>+ dissociative recombination: A source of thermal and nonthermal C on Mars. *J Geophys Res-Space* 2004;109. <https://doi.org/10.1029/2004JA010514>.
- [91] Seiersen K, Khalili A, Heber O, Jensen M, Nielsen I, Pedersen H, et al. Dissociative recombination of the cation and dication of CO<sub>2</sub>. *Phys Rev A* 2003;68:022708–022708. <https://doi.org/10.1103/PhysRevA.68.022708>.
- [92] Janeco A, Pinhão NR, Guerra V. Electron Kinetics in He/CH<sub>4</sub>/CO<sub>2</sub> Mixtures Used for Methane Conversion. *J Phys Chem C* 2015;119:109–20. <https://doi.org/10.1021/jp509843e>.
- [93] De Bie C, van Dijk J, Bogaerts A. The Dominant Pathways for the Conversion of Methane into Oxygenates and Syngas in an Atmospheric Pressure Dielectric Barrier Discharge. *J Phys Chem C* 2015;119:22331–50. <https://doi.org/10.1021/acs.jpcc.5b06515>.
- [94] Liu C-J, Xue B, Eliasson B, He F, Li Y, Xu G-H. Methane Conversion to Higher Hydrocarbons in the Presence of Carbon Dioxide Using Dielectric-Barrier Discharge Plasmas. *Plasma Chem Plasma Process* 2001;21:301–10. <https://doi.org/10.1023/A:1011098824117>.
- [95] Lee H, Lee C-H, Choi J-W, Song HK. The Effect of the Electric Pulse Polarity on CO<sub>2</sub> Reforming of CH<sub>4</sub> Using Dielectric Barrier Discharge. *Energy Fuels* 2007;21:23–9. <https://doi.org/10.1021/ef060115+>.

- [96] Mei D, Zhang P, Duan G, Liu S, Zhou Y, Fang Z, et al. CH<sub>4</sub> reforming with CO<sub>2</sub> using a nanosecond pulsed dielectric barrier discharge plasma. *J CO<sub>2</sub> Utiliz* 2022;62:102073. <https://doi.org/10.1016/j.jcou.2022.102073>.
- [97] Berkowitz J, Ellison GB, Gutman D. Three methods to measure RH bond energies. *J Phys Chem* 1994;98:2744–65. <https://doi.org/10.1021/j100062a009>.
- [98] Mordaunt DH, Ashfold MNR. Near ultraviolet photolysis of C<sub>2</sub>H<sub>2</sub>: A precise determination of D<sub>0</sub>(HCC–H). *J Chem Phys* 1994;101:2630–1. <https://doi.org/10.1063/1.467635>.
- [99] Uytendhouwen Y, Hereijgers J, Breugelmans T, Cool P, Bogaerts A. How gas flow design can influence the performance of a DBD plasma reactor for dry reforming of methane. *Chem Eng J* 2021;405:126618. <https://doi.org/10.1016/j.cej.2020.126618>.
- [100] Pham MH, Goujard V, Tatibouët JM, Batiot-Dupeyrat C. Activation of methane and carbon dioxide in a dielectric-barrier discharge-plasma reactor to produce hydrocarbons—Influence of La<sub>2</sub>O<sub>3</sub>/γ-Al<sub>2</sub>O<sub>3</sub> catalyst. *Catal Today* 2011;171:67–71. <https://doi.org/10.1016/j.cattod.2011.03.015>.
- [101] Zeng Y, Zhu X, Mei D, Ashford B, Tu X. Plasma-catalytic dry reforming of methane over γ-Al<sub>2</sub>O<sub>3</sub> supported metal catalysts. *Catal Today* 2015;256:80–7. <https://doi.org/10.1016/j.cattod.2015.02.007>.
- [102] Zhang X, Dai B, Zhu A, Gong W, Liu C. The simultaneous activation of methane and carbon dioxide to C<sub>2</sub> hydrocarbons under pulse corona plasma over La<sub>2</sub>O<sub>3</sub>/γ-Al<sub>2</sub>O<sub>3</sub> catalyst. *Catal Today* 2002:5.
- [103] George A, Shen B, Craven M, Wang Y, Kang D, Wu C, et al. A Review of Non-Thermal Plasma Technology: A novel solution for CO<sub>2</sub> conversion and utilization. *Renew Sustain Energy Rev* 2021;135:109702. <https://doi.org/10.1016/j.rser.2020.109702>.
- [104] Pinhão N, Moura A, Branco JB, Neves J. Influence of gas expansion on process parameters in non-thermal plasma plug-flow reactors: A study applied to dry reforming of methane. *Int J Hydrog Energy* 2016;41:9245–55. <https://doi.org/10.1016/j.ijhydene.2016.04.148>.
- [105] Krawczyk K, Młotek M, Ulejczyk B, Schmidt-Szałowski K. Methane conversion with carbon dioxide in plasma-catalytic system. *Fuel* 2014;117:608–17. <https://doi.org/10.1016/j.fuel.2013.08.068>.
- [106] Tu X, Whitehead JC. Plasma-catalytic dry reforming of methane in an atmospheric dielectric barrier discharge: Understanding the synergistic effect at low temperature. *Appl Catal B: Environ* 2012;125:439–48. <https://doi.org/10.1016/j.apcatb.2012.06.006>.
- [107] Górska A, Krawczyk K, Jodzis S, Schmidt-Szałowski K. Non-oxidative methane coupling using Cu/ZnO/Al<sub>2</sub>O<sub>3</sub> catalyst in DBD. *Fuel* 2011;90:1946–52. <https://doi.org/10.1016/j.fuel.2010.12.023>.
- [108] Jo S, Hoon Lee D, Seok Kang W, Song Y-H. Effect of packing material on methane activation in a dielectric barrier discharge reactor. *Phys Plasmas* 2013;20:123507. <https://doi.org/10.1063/1.4843875>.
- [109] Kim J, Jeoung J, Jeon J, Kim J, Mok YS, Ha K-S. Effects of dielectric particles on non-oxidative coupling of methane in a dielectric barrier discharge plasma reactor. *Chem Eng J* 2019;377:119896. <https://doi.org/10.1016/j.cej.2018.09.057>.
- [110] Tu X, Gallon HJ, Twigg MV, Gorry PA, Whitehead JC. Dry reforming of methane over a Ni/Al<sub>2</sub>O<sub>3</sub> catalyst in a coaxial dielectric barrier discharge reactor. *J Phys D: Appl Phys* 2011;44:274007. <https://doi.org/10.1088/0022-3727/44/27/274007>.
- [111] Gallon HJ, Tu X, Whitehead JC. Effects of Reactor Packing Materials on H<sub>2</sub> Production by CO<sub>2</sub> Reforming of CH<sub>4</sub> in a Dielectric Barrier Discharge. *Plasma Process Polym* 2012;9:90–7. <https://doi.org/10.1002/ppap.201100130>.
- [112] Zhang Q-Z, Bogaerts A. Propagation of a plasma streamer in catalyst pores. *Plasma Sources Sci Technol* 2018;27:035009. <https://doi.org/10.1088/1361-6595/aab47a>.

- [113] Zhang Y-R, Van Laer K, Neyts EC, Bogaerts A. Can plasma be formed in catalyst pores? A modeling investigation. *Appl Catal B: Environ* 2016;185:56–67. <https://doi.org/10.1016/j.apcatb.2015.12.009>.
- [114] Zhang Y-R, Neyts EC, Bogaerts A. Influence of the Material Dielectric Constant on Plasma Generation inside Catalyst Pores. *J Phys Chem C* 2016;120:25923–34. <https://doi.org/10.1021/acs.jpcc.6b09038>.
- [115] Butterworth T, Elder R, Allen R. Effects of particle size on CO<sub>2</sub> reduction and discharge characteristics in a packed bed plasma reactor. *Chem Eng J* 2016;293:55–67. <https://doi.org/10.1016/j.cej.2016.02.047>.
- [116] Kasinathan P, Park S, Choi WC, Hwang YK, Chang J-S, Park Y-K. Plasma-Enhanced Methane Direct Conversion over Particle-Size Adjusted MO<sub>x</sub>/Al<sub>2</sub>O<sub>3</sub> (M = Ti and Mg) Catalysts. *Plasma Chem Plasma Process* 2014;34:1317–30. <https://doi.org/10.1007/s11090-014-9574-9>.
- [117] Bouchoul N, Fourré E, Tatibouët J-M, Batiot-Dupeyrat C. Plasma-Catalytic Dry Reforming of CH<sub>4</sub> over Calcium Oxide: Catalyst Structural and Textural Modifications. *Plasma Chem Plasma Process* 2019;39:713–27. <https://doi.org/10.1007/s11090-019-09966-9>.
- [118] Bouchoul N, Touati H, Fourré E, Clacens J-M, Batonneau-Gener I, Batiot-Dupeyrat C. Plasma-catalysis coupling for CH<sub>4</sub> and CO<sub>2</sub> conversion over mesoporous macroporous Al<sub>2</sub>O<sub>3</sub>: Influence of the physico-chemical properties. *Appl Catal B: Environ* 2021;295:120262. <https://doi.org/10.1016/j.apcatb.2021.120262>.
- [119] Zhang Q-Z, Wang W-Z, Bogaerts A. Importance of surface charging during plasma streamer propagation in catalyst pores. *Plasma Sources Sci Technol* 2018;27:065009. <https://doi.org/10.1088/1361-6595/aaca6d>.
- [120] Bouchoul N, Fourré E, Duarte A, Tanchoux N, Louste C, Batiot-Dupeyrat C. Plasma-metal oxides coupling for CH<sub>4</sub>-CO<sub>2</sub> transformation into syngas and/or hydrocarbons, oxygenates. *Catal Today* 2021;369:62–8. <https://doi.org/10.1016/j.cattod.2020.06.058>.
- [121] Nizio M, Benrabbah R, Krzak M, Debek R, Motak M, Cavadias S, et al. Low temperature hybrid plasma-catalytic methanation over Ni-Ce-Zr hydrotalcite-derived catalysts. *Catal Comm* 2016;83:14–7. <https://doi.org/10.1016/j.catcom.2016.04.023>.
- [122] Rane VH, Chaudhari ST, Choudhary VR. Influence of alkali metal doping on surface properties and catalytic activity/selectivity of CaO catalysts in oxidative coupling of methane. *Journal of Natural Gas Chemistry* 2008;17:313–20. [https://doi.org/10.1016/S1003-9953\(09\)60001-3](https://doi.org/10.1016/S1003-9953(09)60001-3).
- [123] Sheng H, Schreiner EP, Zheng W, Lobo RF. Non-oxidative Coupling of Methane to Ethylene Using Mo<sub>2</sub>C/[B]ZSM-5. *Chem Phys Chem* 2018;19:504–11. <https://doi.org/10.1002/cphc.201701001>.
- [124] Choudhary VR, Mulla SAR, Uphade BS. Oxidative Coupling of Methane over Supported La<sub>2</sub>O<sub>3</sub> and La-Promoted MgO Catalysts: Influence of Catalyst–Support Interactions. *Ind Eng Chem Res* 1997;36:2096–100. <https://doi.org/10.1021/ie960318t>.
- [125] Yildiz M, Aksu Y, Simon U, Kailasam K, Goerke O, Rosowski F, et al. Enhanced catalytic performance of Mn<sub>x</sub>O<sub>y</sub>–Na<sub>2</sub>WO<sub>4</sub>/SiO<sub>2</sub> for the oxidative coupling of methane using an ordered mesoporous silica support. *Chem Comm* 2014;50:14440–2. <https://doi.org/10.1039/C4CC06561A>.
- [126] Wang H, Schmack R, Paul B, Albrecht M, Sokolov S, Rümmler S, et al. Porous silicon carbide as a support for Mn/Na/W/SiC catalyst in the oxidative coupling of methane. *Applied Catalysis A: General* 2017;537:33–9. <https://doi.org/10.1016/j.apcata.2017.02.018>.
- [127] Borkó L, Guczi L. Non-oxidative methane transformations into higher hydrocarbons over bimetallic Pt–Co catalysts supported on Al<sub>2</sub>O<sub>3</sub> and NaY. *Topics Cata* 2006;39:35–43. <https://doi.org/10.1007/s11244-006-0035-4>.

- [128] Andersen JA, Christensen JM, Østberg M, Bogaerts A, Jensen AD. Plasma-catalytic dry reforming of methane: Screening of catalytic materials in a coaxial packed-bed DBD reactor. *Chem Eng J* 2020;397:125519. <https://doi.org/10.1016/j.cej.2020.125519>.
- [129] Gadzhieva NN. Methane Adsorption and Plasma-Assisted Catalytic Conversion on the Surface of  $\gamma$ -Alumina. *High Ener Chem+* 2003;37:38–43.
- [130] Song HK, Choi J-W, Yue SH, Lee H, Na B-K. Synthesis gas production via dielectric barrier discharge over Ni/ $\gamma$ -Al<sub>2</sub>O<sub>3</sub> catalyst. *Catal Today* 2004;89:27–33. <https://doi.org/10.1016/j.cattod.2003.11.009>.
- [131] Młotek M, Sentek J, Krawczyk K, Schmidt-Szałowski K. The hybrid plasma–catalytic process for non-oxidative methane coupling to ethylene and ethane. *Applied Catalysis A: General* 2009;366:232–41. <https://doi.org/10.1016/j.apcata.2009.06.043>.
- [132] Aitugan AN, Tanirbergenova SK, Tileuberdi Y, Ongarbayev YK, Mansurov ZA. Catalysts for hydrocarbon hydrogenation processes. *ГОРЕНИЕ И ПЛАЗМОХИМИИ (Combustion and Plasma Chemistry)* 2019;17:57–64. <https://doi.org/10.18321/cpc278>.
- [133] Jo S, Kim T, Lee DH, Kang WS, Song Y-H. Effect of the Electric Conductivity of a Catalyst on Methane Activation in a Dielectric Barrier Discharge Reactor. *Plasma Chem Plasma Process* 2014;34:175–86. <https://doi.org/10.1007/s11090-013-9505-1>.
- [134] Taheraslani M, Gardeniers H. Plasma Catalytic Conversion of CH<sub>4</sub> to Alkanes, Olefins and H<sub>2</sub> in a Packed Bed DBD Reactor. *Processes* 2020;8:774. <https://doi.org/10.3390/pr8070774>.
- [135] Julbe A, Drobek M. Zeolite X: Type. In: Drioli E, Giorno L, editors. *Encyclopedia of Membranes*, Berlin, Heidelberg: Springer; 2015, p. 1–2. [https://doi.org/10.1007/978-3-642-40872-4\\_607-1](https://doi.org/10.1007/978-3-642-40872-4_607-1).
- [136] Julbe A, Drobek M. Zeolite Y: Type. In: Drioli E, Giorno L, editors. *Encyclopedia of Membranes*, Berlin, Heidelberg: Springer; 2015, p. 2060–1. [https://doi.org/10.1007/978-3-642-40872-4\\_608-1](https://doi.org/10.1007/978-3-642-40872-4_608-1).
- [137] Ayodele OB. Resolving one of the holy grails of catalysis: Direct nonoxidative methane conversion to ethylene over plasma-assisted atomically dispersed Pt catalyst. *Int J Hydrog Energy* 2022;47:41527–69. <https://doi.org/10.1016/j.ijhydene.2021.12.200>.
- [138] Liu C, Mallinson R, Lobban L. Comparative investigations on plasma catalytic methane conversion to higher hydrocarbons over zeolites. *Appl Cat A: Gen* 1999;178:17–27. [https://doi.org/10.1016/S0926-860X\(98\)00281-6](https://doi.org/10.1016/S0926-860X(98)00281-6).
- [139] Eliasson B, Liu C, Kogelschatz U. Direct Conversion of Methane and Carbon Dioxide to Higher Hydrocarbons Using Catalytic Dielectric-Barrier Discharges with Zeolites. *Ind Eng Chem Res* 2000;39:1221–7. <https://doi.org/10.1021/ie990804r>.
- [140] Chawdhury P, Bhargavi KVSS, Subrahmanyam Ch. Enhanced synergy by plasma reduced Pd nanoparticles on in-plasma catalytic methane conversion to liquid oxygenates. *Catal Comm* 2020;147:106139. <https://doi.org/10.1016/j.catcom.2020.106139>.
- [141] Wang H, Zhao B, Qin L, Wang Y, Yu F, Han J. Non-thermal plasma-enhanced dry reforming of methane and CO<sub>2</sub> over Ce-promoted Ni/C catalysts. *Molecular Catal* 2020;485:110821. <https://doi.org/10.1016/j.mcat.2020.110821>.
- [142] Hu X, Liu Y, Dou L, Zhang C, Zhang S, Gao Y, et al. Plasma enhanced anti-coking performance of Pd/CeO<sub>2</sub> catalysts for the conversion of methane. *Sustain Ener Fuels* 2022;6:98–109. <https://doi.org/10.1039/D1SE01441B>.
- [143] Delikonstantis E, Scapinello M, Stefanidis GD. Low energy cost conversion of methane to ethylene in a hybrid plasma-catalytic reactor system. *Fuel Process Technol* 2018;176:33–42. <https://doi.org/10.1016/j.fuproc.2018.03.011>.
- [144] Wang B, Guan HM. Highly Efficient Conversion of Methane to Olefins via a Recycle-Plasma-Catalyst Reactor. *Catal Lett* 2016;146:2193–9. <https://doi.org/10.1007/s10562-016-1846-y>.



- [145] Wang K, Li X, Zhu A. A Green Process for High-Concentration Ethylene and Hydrogen Production from Methane in a Plasma-Followed-by-Catalyst Reactor. *Plasma Sci Technol* 2011;13:77–81. <https://doi.org/10.1088/1009-0630/13/1/16>.
- [146] Kado S, Sekine Y, Urasaki K, Okazaki K, Nozaki T. High performance methane conversion into valuable products with spark discharge at room temperature. *Studies in Surface Science and Catalysis* 2004;147:577–82. [https://doi.org/10.1016/S0167-2991\(04\)80114-9](https://doi.org/10.1016/S0167-2991(04)80114-9).
- [147] Gordon CL, Lobban LL, Mallinson RG. Ethylene production using a Pd and Ag–Pd–Y-zeolite catalyst in a DC plasma reactor. *Catalysis Today* 2003;84:51–7. [https://doi.org/10.1016/S0920-5861\(03\)00300-6](https://doi.org/10.1016/S0920-5861(03)00300-6).